Conceptual study on the energy independence of fuel cell cogeneration systems using solar energy

May 2016

Jorge Eduardo Lamas De Anda

Index

Abbreviations

AC	Alternating Current
APF	Annual Performance Factor
ACH	Absorption Chiller-Heater
BARON	Branch and Reduce Optimization Navigator
CAES	Compressed Air Energy Storage
COG	Coke-Oven Gas
COP	Coefficient of Performance
DC	Direct Current
DER	Distributed Energy Resources
ELZ	Electrolyzer
FIT	Feed-in Tariff
FSR	Fuel Savings Ratio
GAMS	General Algebraic Modeling System
HC	Heat Collector
HEX	Heat Exchanger
HP	Heat Pump
HPWH	Heat Pump Water Heater
LHV	Lower Heating Value
LPG	Liquefied Petroleum Gas
MINLP	Mixed Integer Nonlinear Programming
MINOS	Modular In-core Nonlinear Optimization System
PEFC	Polymer Electrolyte Fuel Cell
PHS	Pumped Hydro Storage
PV	Photovoltaics
SMR	Steam Methane Reforming
SOC	State of Charge
SOFC	Solid Oxide Fuel Cell

Chapter 1. Introduction

1.1 Introduction

With the developments in Distributed Energy Resources (DER) during recent years, the implementation of micro-grids and stand alone energy systems with high independence from the main power grid is becoming a reality. From single households to large communities in isolated areas, DER are regarded as an alternative to the current energy infrastructure that relies on combustion of fossil fuels with high pollutant emissions and large distribution losses. As the scale of micro-grids increases, hydrogen fuel offers a means for energy storage and external energy supply that gives the community flexibility in their energy demands and improved energy security.

This chapter presents a detailed background of the current situation regarding energy supply utilizing DER and explains the need to continue research in this field. Section 1.2 addresses the situation of energy supply in isolated areas and the growing efforts to design efficient and reliable energy supply systems with high energy independence. In Section 1.3, the author's motivation to pursue research in this area and write the present thesis is expressed, followed by a description of the scale and objectives of this research, in Section 1.4. Finally, an outline of the chapters of this thesis is given in Section 1.5

1.2 Background

1.2.1 Energy supply through Distributed Energy Resources

Access to sustainable energy is essential for human development and it has become a priority sector for investments. For decades, the energy industry has relied on large scale power plants where electricity is mass produced at relatively low costs. Although this method has been effective, its weaknesses are becoming apparent now more than ever. The current power transmission method through nation-wide grids greatly separates the consumption and generation points, resulting in large energy losses. The grid is also vulnerable to technical faults, human errors and natural disasters that can cause large-scale blackouts that can last from minutes to several days with significant negative impacts on the affected communities. Furthermore, CO_2, particulate matter and other greenhouse gas emissions resulting from fossil fuel combustion in large scale power plants pose a great risk to the environment and human health. After the Great Fukushima earthquake in Japan in 2011, several nuclear power plants around the globe were shut down, resulting in an increased load on fossil fuel based power plants, exacerbating pollutant emissions and exposing the risks of the conventional energy supply systems.

In an effort to reduce the dependence on fossil fuels for power generation, the penetration of renewable energies has seen a significant boost in recent years. These technologies, albeit having poor energy density and large output fluctuations compared to large power plants, they can be efficiently implemented as DER [1, 2]. The installation of renewable energy systems, in particular wind turbines and solar photovoltaics (PV), has been rapidly increasing during the last decade [3]. Together with other DER, renewable energies can offer a reliable power supply system with low pollutant emissions, minimal energy losses, high power quality and resilience against failures of the main power grid.

Distributed energy systems employ several small-scale (1 kW to 100 MW) power generation and storage systems to generate electricity on-site, reducing transmission losses due to transmission and distribution. In addition to electricity, cogeneration and multi-generation technologies that can simultaneously generate electricity, hot water, heating and cooling, or fuel are also available [4]. Although initial costs for distributed generation systems tend to be high, their advantages can be clearly seen in other factors such as high generation efficiency, low carbon dioxide emissions, increased fossil fuel independence, and impacts on society including improved health and economic growth. Optimization criteria using these factors are being researched to determine whether the impact of implementing distributed systems is significant [5].

Distributed energy systems using renewable energies, in particular solar, wind and micro-hydro, have the capacity to benefit remote areas as well. There are several agricultural applications for renewable energies, including but not limited to irrigation, greenhouse ventilation, refrigeration, grain threshing and milling, food processing and storage, as well as electricity for radio, television and telecommunications [6]. Energy demand patterns for rural areas are generally different from those for urban and suburban areas; therefore the approach to installing distributed energy systems presents different challenges. Areas that previously had no access to electricity may rapidly increase their energy demands after the electric supply has been installed. A study by Pereira *et al.* explains the impacts of the "2003 national rural electrification project" in Brazil [7]. Energy consumption per capita for households that were not part of the electrification program decreased from 6.91 to 5.00 GJ per year after the program. This decrease was attributed to changes in energy consumption behavior. In contrast, energy consumption for electrified households increased from 5.16 to 6.19 GJ per year after the program. When electricity is supplied to rural areas by expanding the power network, an increase in energy demand may be met without the need to increase the installed capacity. However, if distributed energy systems are implemented instead, it is important to consider future energy demand growths, and allow room for increasing the generation capacity.

1.2.2 Energy supply in isolated areas

The International Energy Agency [8] estimates that about 1.3 billion people still lack access to electricity, and 2.7 billion people lack alternatives to biomass for cooking. A stable energy supply for industries, hospitals and schools, can greatly contribute to economic growth, improved health and education. Statistics show a correlation between increasing commercial energy consumption in several countries, with increased average life expectancy, school enrollment ratio, underweight children, and population with access to clean water. Several studies have been conducted regarding the impact of electricity availability in rural areas [9-12]. Both in developed and developing countries, electrification of rural areas has been linked to a significant increase in socio-economic levels. Expansion of the main power network (*i.e.*, the power network that interconnects large-scale power generating stations to distribute electricity throughout the nation) allows the rural population to rely more on electric appliances that reduce manual labor and make life more comfortable. Thus, increased electrification is reflected in increased energy consumption per capita.

Expansion of the main power network is generally the cheapest means of electrification. A study on an isolated island in India assessed the difference in cost of electricity by supplying the island with power from the existing network, and with renewable energies [13]. The study area considered a peak load of 530 kW, where power consumption per capita is 0.46 kWh/day. The study reveals that a PV-biomass stand-alone system would produce the highest cost of electricity for this area, unless policies such as net metering and feed-in tariffs are implemented. However, not all isolated areas respond the same way to distributed energy generation. Szabó *et al.* [14] used spatial mapping to compare costs between different energy generation technologies in the African continent. In this study, costs of connection to the network, installation of solar PV, and generation by diesel engines, including fuel transport, are calculated for the African continent. The number of people that can be supplied with each system is then estimated, with regard to their ability to pay a certain rate for electricity. The study finds that when people can afford to pay 0.05 EUR[1] (6.18 JPY) more per kilowatt-hour of electricity, the amount of people that can be supplied with PV increases dramatically, while for diesel generation it remains the same, and for network connection it actually decreases. These results suggest that in some cases, distributed energy generation systems show lower electricity costs compared to extension of the main power network. Hence, deciding which areas should be connected to the main power network and which should use distributed energy systems, can help optimize the consumption of resources.

However, there is a vast amount of populated areas surrounded by unsuitable terrain that complicates extending the main power network. Archipelago countries, such as Japan, Indonesia and The Philippines, face the problem of extending their power networks over the sea to reach populated

[1] All currency exchange in 2016 JPY (1 EUR = 123.56 JPY)

islands. Forests and mountainous regions often require terrain conditioning, which can rapidly escalate the costs of extending the power network. Furthermore, plans to extend the power network may be hindered over the presence of national reserves and wildlife sanctuaries, where construction activities are restricted. As a result, extending the main power network to isolated areas sometimes requires vast resources that may not be deemed justifiable. For such areas, energy is often supplied through small- or medium-scale diesel or fuel oil generators, which require low initial investment and are easy to scale up as the electric demands increase.

Despite the increasing global demand for fossil fuels, their use is being discouraged over concerns of air and water pollution, environmental changes, and global climate change. There is also uncertainty about coal and natural gas reserves, and whether they can meet global energy demands. The coal reserves are estimated to be largest, and are expected to last for 200 years more, at consumption rates of 2006 [15]. In contrast, oil and natural gas are expected to last for only 40 and 70 years, respectively. These numbers could decrease drastically if global demands increase faster than expected. As reserves decrease, energy security could become vulnerable for countries that rely on fossil fuel imports, including developing countries that are rapidly increasing their energy consumption [16]. Furthermore, oil prices are rapidly increasing as the reservoirs become more difficult to access and require more complex technology (Fig. 1.1). These rising prices will either result in expensive energy infrastructures, or an increased demand for coal and natural gas to supply current thermal power plants.

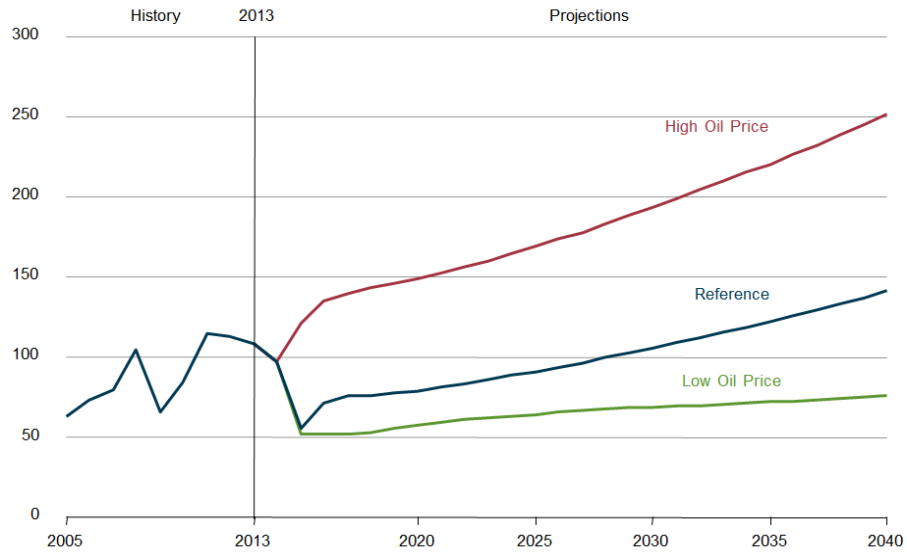

Figure 1.1 North Sea Brent crude oil spot prices in four cases, 2005-2040. Vertical axis units are 2013 US dollars per barrel [17].

Currently Japan has achieved close to 100% of electrification rate in populated islands mainly through the use of electric generators using fuel oil. Figure 1.2 shows the power generation and

distribution network of the Kyushu region, in the south of Japan. Although renewable energy systems have been implemented in the islands with the resources to do so, fossil fuel dependence remains higher than 90%. Due to the lack of other options for energy supply, communities in these islands require a constant supply of fuel, which results in highly increased costs and additional consumption of resources related to transport and handling. The cost of electricity in Japanese islands using fuel oil generators can increase more than double compared to electricity from the power network [18]. Furthermore, above 80% of Japanese oil products are imported from the Middle East, which has an impact on their carbon footprint and insecurity issues related to political conflicts in the area.

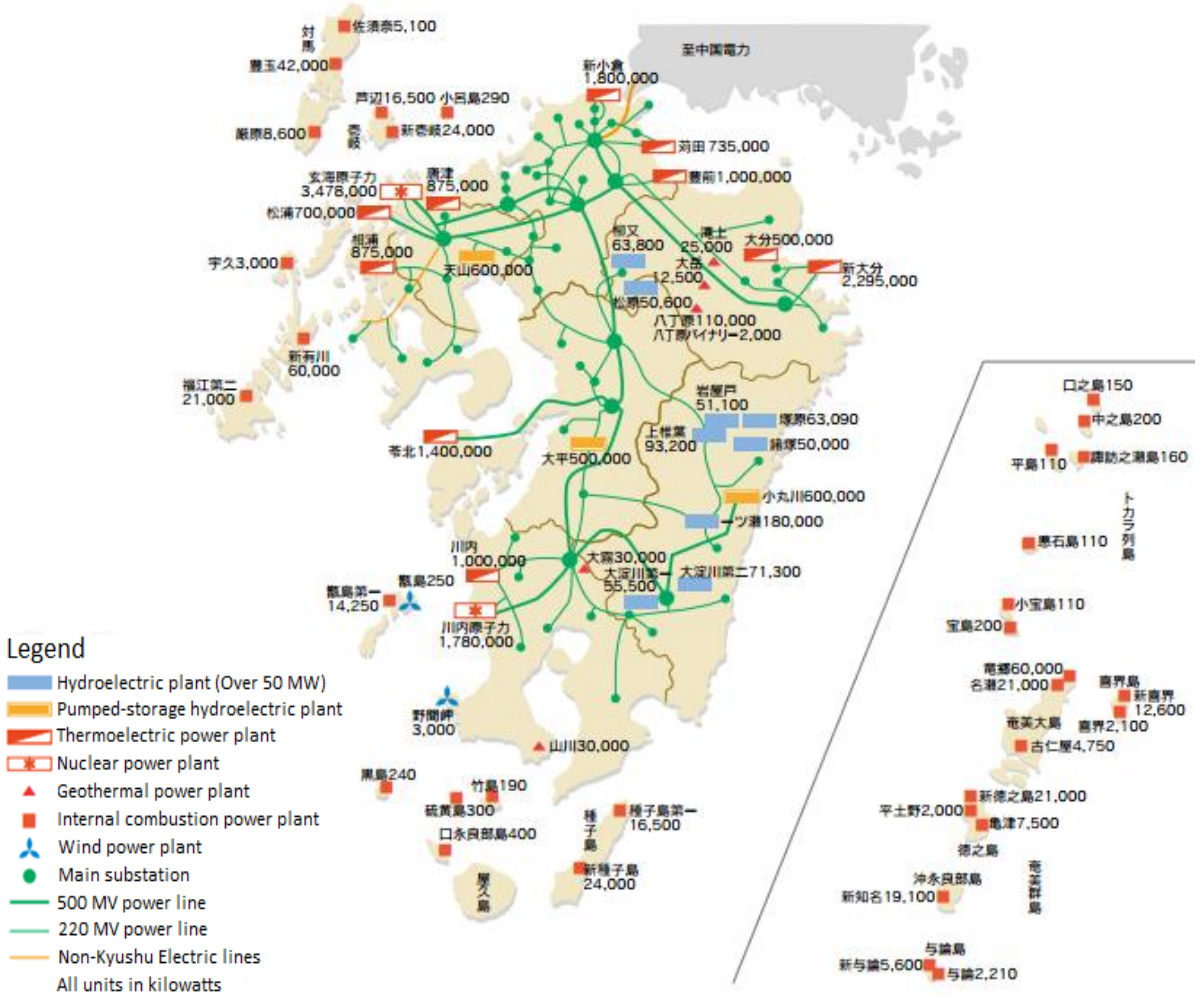

Figure 1.2. Map of the Kyushu region, Japan, showing the distribution of power plants and distribution lines in the main island and neighboring islands belonging to prefectures in this region. Nuclear power plants are now inactive [18].

Unlike the main power grid, isolated areas do not have the freedom to modify their share of energy sources to minimize costs, thus the impact of oil availability and its volatile price has the strongest impact in these areas. Furthermore, energy supply must remain constant in order to maximize its cost-benefit, since electrification shows a reduced impact in areas where a consistent

supply of fuel cannot be guaranteed. If power cuts are frequent, stored reserves of alternative energy sources, such as candles for lighting and firewood for heating, appear to be more useful than their electric counterparts [19]. Therefore, a different approach to the electrification of isolated areas should be considered.

1.2.3 Isolated Grids

With the advances in distributed power generation technologies, power supply becomes possible without integration to the national power network. This is especially important for isolated areas (as discussed in the introduction), where extension of the main power network is not always economically or technologically feasible. In order to design a micro-grid that can supply all energy demands during the year, the capacity of components would most likely tend to increase. Although this is expected to have higher investment costs, a comparison for the long term may favor the use of micro-grids, since the costs would escalate in the same manner if the main power network is to be extended through unfavorable terrain. Energy consumption using the power network would increase as well since higher electric losses exist when long power lines are used. For on-site generation using conventional engines, fuel transportation costs and future oil prices also need to be taken into account. For isolated areas where energy demand and fuel consumption patterns are different from those in urban areas, a corresponding analysis is required.

As previously discussed, provision of a sustainable power supply in isolated areas is a persistent issue. Expansion of the main power network is not always possible, and constant demand for fossil fuels for diesel generators has negative impacts on the environment and the economy. The low availability of oil products in the near future also poses a threat to energy security in isolated areas. With the advances in micro-grids using renewable energies, the viability for isolated micro-grids for remote and rural areas increases. Efficient energy storage systems in these areas play a major role compared to network-connected distributed energy systems. Considering the future potential of these technologies, some countries have begun implementing energy independent power supply systems in remote areas.

Nayar *et al.* [20] present a study on an isolated micro-grid for three islands in the Republic of Maldives using a 2.5 kWp solar PV system and 24 wind turbines each with a rated capacity of 1.8 kW, where a 30 kW diesel generator is considered for backup power. Using electronics and control technology to schedule the operation of the diesel generator, this system has been operating for over a decade with satisfactory results. In contrast, a study by Himria *et al.* [21] on a remote area in Algeria analyzed another wind-diesel hybrid system (600 kW wind turbine, and a 500 kW diesel generator), but found that the economic feasibility of the isolated grid was heavily limited by the price of fuel, as

well as the wind speeds in the area. Moharil and Kulkarni [22] analyzed an isolated micro-grid using only a 25 kWp solar PV system in Sagardeep Island, India, a rural community with severe energy shortages. The community at Sagardeep used to obtain electricity from a diesel generator, although a shortage of fuel only allowed for energy production for a few hours a day and only for selected customers. However, the increasing price of oil made it difficult to sustain this system. In response, 17 solar PV panel systems were installed over a period of ten years, together with energy meters to monitor individual electric consumption. This system was deemed successful, as education, working hours, entertainment for human recreation, and residential commodities were all improved thanks to the availability of electricity. Thiam [23] presents a summary of micro-grids in Senegal. The performance of diesel generators, wind turbines, and solar PV are compared against each other for three remote areas in Senegal with energy demands between 7.77 and 13.05 kW/day. In this case, diesel generators presented the highest levelized electricity cost, over seven times the levelized cost of solar power in the worst case. In this study the impact of fuel transport and distribution costs on energy supply in remote areas can be clearly seen. Although wind power in this case was not as competitive as solar, the results depended greatly on the wind speeds available for the area. Higher wind speeds are expected to increase power generation and thus improve the competitiveness of wind systems. Regardless, both solar and wind power systems were well above the diesel system.

Sen *et al.* [24] analyzed the possibility of co- and tri-generation in remote areas in India using biomass. Utilizing biomass it is possible to generate electricity, heat for refrigeration or food processing, and distilled water. The main complications with tri-generation is that it has conventionally been used for large-scale industries, where installed capacity is over one megawatt, and scaling it down to lower capacity systems faces technical difficulties. However, successful implementation of these systems is expected to have a positive impact on society by creating microindustries in rural areas and thus increasing economic activity. Kumaravel and Ashok [25] present an off-grid model for a micro-grid in an isolated area in West India. Several configurations for micro-grids are compared, and the authors conclude that for this area, a 22 kW solar PV/biomass/hydropower micro-grid can achieve competitive costs and higher performance than the conventional system used in this area: diesel and hydroelectric generators. In order to further minimize the investment costs, design optimization models are under development. Morais *et al.* [26] present an optimization model to minimize capital costs for a 630 W isolated micro-grid in Budapest. The model is able to schedule the operation of batteries for energy storage and fuel cells for backup power, depending on the availability of wind and solar resources for power generation. A similar model is presented by Kyriakarakos *et al.* [27] for a small island in the Aegean Sea, in Greece. This model incorporates poly-generation of power, purified water, and fuel for a 10 kWh/day local consumption. A detailed economic analysis is presented as well, including a forecast of future oil prices. The study concludes that such system is feasible with minimal financial risk.

Domenech *et al.* [28] analyzed the social factors in the implementation of a micro-grid in a remote area in Peru, using renewable energies. This micro-grid was installed over the course of a year, starting with wind power systems, followed by a micro-hydro power plant, a solar PV farm, and finalizing with individual PV systems. This implementation in stages was due to the varied energy demand patterns across the community, and the different power output profiles of each renewable energy source. Rechargeable batteries were installed for energy storage. The community of Alto Peru, where the micro-grid was installed, had diverse reactions to this micro-grid, regarding power reliability and excessive power consumption by certain users. Therefore, the people relied heavily on technicians for repair, maintenance, and installation of power meters for example. The results of this study reveal the differences of implementing micro-grids between isolated areas and areas that have access to the main power network. In isolated areas, local participation plays a key role in the successful implementation as they get to decide where power is needed most and who has the potential to benefit more from the energy supply.

1.3 Motivation

A majority of studies regarding energy supply using DER systems are done under two assumptions that are important to notice. The first assumption is that DER systems with access to the grid are able to freely consume power from the grid and feed surplus power back into it as needed. If systems that are designed under this assumption became widely implemented, the power quality of the existing power grid would be challenged by the frequent voltage fluctuations that DER systems would create. A common example is seen in solar PV and battery systems. If the batteries cannot be recharged due to prolonged bad weather, the base load as well as the power peak would revert back to those before implementation of DER systems. In this case, large scale power plants would be forced to operate normally at low capacity when solar power is available, while retaining their original capacity just in case the community's electric storage is short, lest there be a brownout.

The second assumption is that stand-alone DER systems will not be subject to large demand variations during the following years after installation. Several studies show grid independent systems for which an energy storage system is designed according to the initial conditions. Under this assumption, the system can function with optimum efficiency and smart use of their energy reserves. However, investing in the energy infrastructure of isolated areas is expected to increase their economic sector, which is usually reflected in higher energy demands. If the energy storage system is not designed with the possibility of future growth, these communities will most likely return to using fossil fuels for backup power, if not as their main source of energy.

Therefore, there is a need to design DER systems with high grid independence, which can respond to long term changes in load without the need to redesign them. Hydrogen fuel cells appear to be the optimum technology for this task. Hydrogen can act as a method of energy storage through the use of water electrolyzers, which generate useful fuel using electricity. But hydrogen may also be generated through reformation of hydrocarbons, offering an external energy input channel for times when stored hydrogen is not enough to meet the energy demands. This thesis focuses on the design of energy supply systems with high independence from the main power grid, utilizing fuel cells as primary energy generators and solar energy systems as secondary energy inputs, with hydrogen as both the fuel source and main storage system.

1.4 Research scale and objectives of the thesis

In this thesis, the level of independence for DER based systems utilizing hydrogen fuel is analyzed over two main scales. The first one is residential systems that have a stable infrastructure to provide the needed fuel but seek independence from the grid in order to avoid affecting its power quality. The second one is small to medium communities without access to the main power grid, who require a sustainable source of hydrogen fuel that can keep up with the economic and social growth of the community.

The main objective of this thesis is to design efficient and reliable DER systems with high level of energy independence, which are not bound to limited reserves of stored energy. The performance of these systems is compared to their current alternatives, in terms of cost and energy independence. Independence from the grid is favored for residential scale systems, although fuel dependence is expected. For community scale systems, the complete independence from the grid is a given, thus independence from external fuel input is sought. The long term objective of this thesis is to set the groundwork for future grid independent DER systems, considering the effects and benefits of their widespread implementation on social development and preservation of the existing infrastructure.

1.5 Outline of the thesis

This thesis is divided in eight chapters. Chapter 1 gives a substantial introduction on the current situation of energy supply using DER systems and the current approaches for energy supply in isolated areas. The operation characteristics of existing DER technologies are explained in Chapter 2 and their integration into cogeneration systems is discussed in Chapter 3, including novel approaches involving hydrogen energy storage in both residential and community scale systems. Chapter 4 presents an introduction to mathematical optimization, followed by the development of an

optimization model for micro-grids without access to the main power grid. The analyses carried out using this optimization model are explained in Chapter 5. In Chapter 6, hydrogen supply channels are presented as a method to supply fuel to independent micro-grids, and in Chapter 7 the viability of the optimized micro-grid using these hydrogen fuel channels is analyzed for Japanese islands. The contributions of this thesis are summarized in Chapter 8.

1.6 Conclusions

In this chapter, a background of Distributed Energy Resources (DER), micro-grids and power supply in isolated areas has been presented. DER are regarded as a viable method for energy supply that can reduce the vulnerability of the main power grid and supply energy to areas with limited access to conventional fuel resources. Although DER have been successfully implemented in numerous places, there is still no effective solution for independent operation of these technologies. This chapter summarizes the reasons for the need of research regarding energy independence of DER based systems, and explains the objectives of this thesis.

1.7 References

[1] Shinji, T., Sekine, T., Akisawa, A., Kashiwagi, T., Fujita, G. and Matsubara, M. (2008). Reduction of power fluctuation by distributed generation in micro grid. *Electrical Engineering in Japan*, 163 (2), 22-9.

[2] Steimer, P.K. (2010). Enabled by high power electronics-Energy efficiency, renewables and smart grids. *In Proceedings of the International Power Electronics Conference (IPEC), Sapporo, 2010*, 11-5.

[3] International Renewable Energy Agency. (2014). Global annual new installed capacity of solar PV and wind, 2000-2011. *Renewable Energy Costs, Technologies and Markets*.

[4] Chicco, G. and Pierluigi M. (2009). Distributed multi-generation: A comprehensive view. *Renewable and Sustainable Energy Reviews*, 13: 535-51.

[5] Østergaard , P.A. (2009). Reviewing optimisation criteria for energy systems analyses of renewable energy integration. *Energy,* 34, 1236-45.

[6] Weingart, J. and Giovannucci, D. (2004). Rural (Renewable) Energy: A Practical Primer for Productive Applications. *World Bank Group*.

[7] Pereira, M.G., Vasconcelos Freitas, M.A. and Fidelis da Silva, N. (2010). Rural electrification and energy poverty: Empirical evidences from Brazil. *Renewable and Sustainable Energy Reviews,* 14, 1229-40.

[8] International Energy Agency. (2015). *World Energy Outlook 2015,* Paris: OECD Publishing.

[9] Reiche, K., Covarrubias, A. and Martinot, E. (2000). Expanding electricity access to remote areas: off-grid rural electrification in developing countries. *WorldPower 2000,* 52-60.

[10] Kanagawa, M. and Nakata, T. (2007). Analysis of the energy access improvement and its socio-economic impacts in rural areas of developing countries. *Ecological Economics,* 62, 319-29.

[11] Gómez, M.F. and Silveira, S. (2010). Rural electrification of the Brazilian Amazon - Achievements and lessons. *Energy Policy,* 38, 6251-60.

[12] Van Gevelt, T. (2014). Rural electrification and development in South Korea. *Energy for Sustainable Development,* 23, 179-87.

[13] Karki, S., Mann, M.D. and Salehfar, H. (2008). Environmental Implications of Renewable Distributed Generation Technologies in Rural Electrification. *Energy Sources, Part B: Economics, Planning, and Policy,* 3 (2), 186-95.

[14] Szabó, S., Bódis, K., Huld, T. and Moner-Girona, M. (2011). Energy solutions in rural Africa: mapping electrification costs of distributed solar and diesel generation versus grid extension. *Environmental Research Letters,* 6 (3), 34002.

[15] Shafiee, S. and Topal, E. (2009). When will fossil fuel reserves be diminished? *Energy Policy,* 37, 181-9.

[16] Lior, N. (2008). Energy resources and use: The present situation and possible paths to the future. *Energy,* 33, 842-57.

[17] EIA. (2015). Annual energy outlook 2015. *US Energy Information Administration.*

[18] Kyushu Electric Power Co. Inc. (2013). *Kyushu electric data-book 2013.* Retrieved May 1, 2016 from http://www.kyuden.co.jp/library/pdf/company/data_book/data_book_2013.pdf

[19] Davis, M. (1998). Rural household energy consumption- the effects of access to electricity-evidence from South Africa. *Energy Policy,* 26 (3), 207-17.

[20] Nayar, C., Tang, M. and Suponthana, W. (2008). Wind/PV/Diesel Micro Grid System implemented in Remote Islands in the Republic of Maldives. *In Proceedings of the IEEE International Conference on Sustainable Energy Technologies (ICSET), Singapore, 2008*, 1076-80.

[21] Himria, Y., Boudghene Stamboulib, A., Draouic, B. and Himri, S. (2008). Techno-economical study of hybrid power system for a remote village in Algeria. *Energy,* 33, 1128-36.

[22] Moharil, R.M. and Kulkarni, P.S. (2009). A case study of solar photovoltaic power system at Sagardeep Island, India. *Renewable and Sustainable Energy Reviews*, 13, 673-81.

[23] Thiam, D.R. (2010). Renewable decentralized in developing countries: Appraisal from microgrids project in Senegal. *Renewable Energy,* 35, 1615-23.

[24] Sen, P.K., Vasudevan, P., Singh, S.M. and Davies, P. (2011). Sustainable rural micro-enterprises through co- and tri-generation: review of concepts. *Journal of Scientific and Industrial Research,* 70, 683-7.

[25] Kumaravel, S. and Ashok, S. (2012). An Optimal Stand-Alone Biomass/Solar-PV/Pico-Hydel Hybrid Energy System for Remote Rural Area Electrification of Isolated Village in Western-Ghats Region of India. *International Journal of Green Energy,* 9, 398-408.

[26] Morais, H., Kadar, P., Faria, P., Vale, Z.A. and Khodr, H.M. (2010). Optimal scheduling of a renewable micro-grid in an isolated load area using mixed-integer linear programming. *Renewable Energy,* 35, 151-6.

[27] Kyriakarakos, G., Dounis, A.I., Rozakis, S., Arvanitis, K.G. and Papadakis, G. (2011). Polygeneration microgrids: A viable solution in remote areas for supplying power, potable water and hydrogen as transportation fuel. *Applied Energy,* 88, 4517-26.

[28] Domenech, B., Ferrer-Martí, L., Lillo, P., Pastor, R. and Chiroque, J. (2014). A community electrification project: Combination of microgrids and household systems fed by wind, PV or micro-hydro energies according to micro-scale resource evaluation and social constraints. *Energy for Sustainable Development,* 23, 275-85.

Chapter 2. Distributed Energy Resources

2.1 Introduction

This chapter contains an outline of the characteristics and operating principles of commonly used DER technologies. One of the benefits from the different availability of DER is that the disadvantages that each technology presents can be offset through the smart combination of other technologies that can compensate with their individual advantages. First, renewable energies regarded as DER are addressed in Section 2.2, focusing on solar and wind energy. Section 2.3 gives a detailed introduction to the available fuel cell types and their operating principles. Exhaust heat recovery strategies are discussed in Section 2.4, in particular heat exchangers and heat driven absorption refrigerators, in particular absorption chiller-heaters. Lastly, current energy storage technologies are discussed in Section 2.5, followed by an overview on the future of hydrogen energy storage. Since the objective of this thesis is to maximize energy independence through the minimization of fossil fuel consumption, DER technologies that involve internal combustion of hydrocarbons are not included in this study.

2.2 Renewable energies

Renewable energies have been regarded as the staple in DER systems. When the current energy infrastructure based on large centralized thermal power plants and grid power transmission was established, renewable energies were unable to compete in scale. Until now, the most widely implemented form of renewable energy is hydroelectric power, particularly in large dams. Unfortunately, water resources are not always available and their utilization needs to taken into account the effects that it will have on the surrounding environment. These reasons generate debate as to considering hydroelectric power as DER, since by nature it needs to be centralized around the existing water resources. Nevertheless, one should make the most out of them when available, even in minimal scale [1]. Another renewable energy source that provides a valuable addition when available is geothermal energy. This resource can be roughly divided into two types: underground steam, which can come either from natural underground water sources or pumped water into underground hot rocks, and ground heat sources, which utilize the nearly constant temperature of shallow ground as a heat source or sink. Underground steam resources are also difficult to classify as DER since not all areas have direct access to it. In contrast, ground source heat pumps can be installed almost everywhere with relative ease. Lastly, the most widely spread renewable energy systems are wind and solar energy. They take advantage of the fact that the resources are available nearly everywhere, and the technologies to extract useful energy from them have very flexible requirements.

For solar energy, two conversion technologies are commercially available from small watt scale units to large megawatt systems: photovoltaics (PV) and heat collectors (HC). Solar PV have had large success as DER for urban power generation thanks to their relatively small size and their lack of moving components, which reduce maintenance work and produce no noise. Residential PV systems have found a place in many rooftops which has reduced the need to reserve land area for their installation. Their modular structure also allows them to be installed without significant changes on the existing infrastructure. Solar PV technologies can be divided according to their manufacturing method into four main types: monocrystalline silicon cells, polycrystalline silicon cells, thick-film silicon cells and amorphous silicon cells. Monocrystalline cells offer the highest efficiency, and in consequence the highest costs. For situations where maximum power output per area unit is critical, this type of cell is the best option. However, residential PV systems often utilize polycrystalline cell PV panels, which although having a slightly lower efficiency, their costs are lower. If area is not a constraint, larger polycrystalline cell panels can be installed to produce the needed power output.

The operation of solar PV cells can be described as follows. The equivalent circuit of a PV cell can be seen in Fig. 2.1. The equations that govern this circuit are given in Eq. (2.1)-(2.5). The output current of the cell I is equal to the light generated current I_{ph} minus the diode current I_D minus the shunt leakage current I_{sh}. The open circuit voltage U_{oc} is equal to terminal voltage U plus the voltage seen in the series resistance R_s. To calculate the value of these currents, the intrinsic component characteristics are needed. The variables in Eq. (2.1)-(2.5) are as follows: q is the electron charge of $1.9\text{x}10^{-19}$ C, A_{cf} is the curve fitting constant of the diode, K_B is the Boltzmann constant, $1.38\text{x}10^{-23}$ J/K, T is the cell temperature, I_{os} is the reverse saturation current, B is the ideality factor of the p-n junction, G is the solar irradiation in W/m^2, I_{SCR} is the short circuit current at 298.15 K and solar irradiation of 1000 W/m^2, K_I is the short circuit current temperature coefficient at I_{SCR}, E_{GO} is the band gap for silicon, T_r is the reference temperature of 301.18 K, and I_{or} is the cell saturation current at T_r.

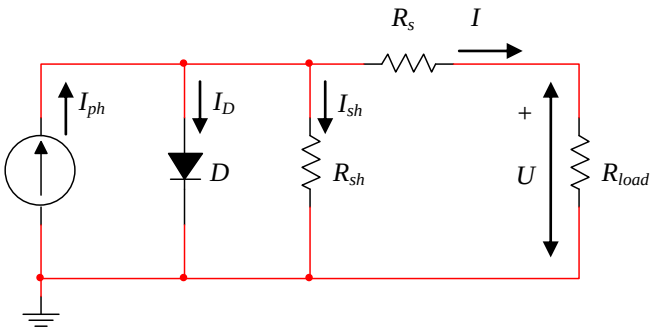

Figure 2.1. Equivalent circuit of a solar PV cell.

$$I = I_{ph} - I_D - I_{sh} \tag{2.1}$$

$$U_{oc} = U + IR_s \tag{2.2}$$

$$I_D = I_{os}\left[exp\frac{qU_{oc}}{A_{cf}K_BT} - 1\right] \tag{2.3}$$

$$I_{ph} = \frac{G}{100}[I_{SCR} + K_I(T - 25)] \tag{2.4}$$

$$I_{os} = I_{or}\left(\frac{T}{T_r}\right)^3 exp\left[\frac{qE_{GO}}{BK_B}\left(\frac{1}{T_r} - \frac{1}{T}\right)\right] \tag{2.5}$$

For commercial PV systems, a simplified formula that groups the intrinsic values of the internal components of the cells is given by Eq. (2.6) [2]. In this equation, the output power W_{PV} is calculated with respect to the solar irradiation and the panel's surface temperature. Here, P_{cap} is the peak installed capacity of the system, G is solar irradiation, K_{pa} is the correction factor for electric losses, K_{pm} is the load matching correction factor, η_{inv} is the DC to AC inverter's efficiency, α_{Pmax} is the temperature coefficient, T_{av} is the monthly average surface temperature in °C, and G_s is the solar irradiation intensity in standard conditions. The indexes *h* and *m* represent hour and month, respectively.

$$W_{PV(h,m)} = P_{cap} \cdot G_{(h,m)} \cdot K_{pa} \cdot K_{pm} \cdot \eta_{inv} \cdot \left[1 - \alpha_{Pmax}\left(T_{av(m)} - 25\right)/100\right] \cdot G_s^{-1} \tag{2.6}$$

Solar heat collectors (HC) provide a different method for converting solar energy into useful energy. Concentrated solar power systems redirect a large amount of solar energy into a fluid, which when heated can be utilized as the working fluid for a turbine to produce electricity. These systems although efficient in large scales, are less suitable as small scale DER due to their space requirements. Instead of electricity, solar HC can be utilized to effectively produce hot water for residential use, reducing the need for natural gas used in conventional gas water boilers. These systems are commercially available at capacities suitable for residential use, but in the same way as solar PV, they occupy a small area and are easy to integrate into the current infrastructure, allowing them to be installed in larger quantities if the hot water demands require so.

Solar HC for residential hot water use are available in two main configurations. Evacuated tube collectors consist of a series of insulated tubes that contain heat transfer fins connected to heat pipes, through which solar energy in the form of heat is transmitted into water. Panel collectors on the other hand, consist of an insulated case containing a collector plate on which heat pipes are placed. Heat from solar irradiation is transmitted through the plate onto the heat pipes and finally into the water. Panel collectors can utilize either a glass cover (glazed) or not (unglazed), depending on the heating purpose. The importance of the glass cover is that it represents an increase in cost, which should be avoided if possible. Unglazed panels can operate properly with small to moderate heating applications, and are thus generally utilized for pool heating. For residential use however, higher water temperature

is required and therefore glazed panels are the common choice. Hot water storage from the solar HC is included in some systems, but a separate storage tank may be installed instead.

Wind turbines rely on the basic turbine principle where a fast moving flow of air is used to power a rotor. Their main parts include turbine blades, a rotor, a generator and a coupling device. It is common now to find systems that incorporate sensors and electronic controls to change the direction of the rotor and the pitch of the blades in order to maximize generation efficiency or as a safety measure during maintenance work. The generator produces an electric output as aerodynamic forces cause the blades to turn the rotor, which powers the generator. Actual power output from wind turbines is directly related to the available wind speed, while rated power output depends on the swept area of the rotor disk. Larger swept area is usually accompanied by increased tower height. For installation of wind turbines it is also recommended that there are no structures in front that can block the flow of air, which roughly implies that the tower height be at least twice the size of the largest structure. Wind turbines also need to be spaced from 3-10 rotor diameters between them to allow adequate flow of wind and reduce the effect that wind wakes have on downstream turbines. Because of these requirements, large wind farms are usually in unpopulated areas where obstacle and space restrictions are fewer.

2.3 Fuel cells

Fuel cells are predicted to be the optimum distributed generation alternative during following years. Fuel cells operate on an electrochemical process at relatively low temperatures, which as opposed to combustion of hydrocarbons, generates no soot, particulate matter, nitrous oxides, and produce energy in the form of electricity without the need for an additional electric generator. Fuel cells also have no moving parts, which decreases the need for maintenance and requires no lubrication, in addition to operating with minimal noise. On the downside, fuel cells operate on hydrogen fuel (with a few exceptions that will be addressed promptly) which is a resource that is not naturally found in its pure form. Fuel cells also require a more complex technology than engines and turbines, which is to this day relatively expensive. Nevertheless, fuel cells have already seen their way into the energy market, not only in residential applications but in the commercial and transport sectors as well.

The basic components of a fuel cell are an electrolyte, a cathode and an anode. There are six types of fuel cells available, differentiated mainly by the material utilized for the electrolyte. Detailed description of these systems can be found in the literature [3]. The most commonly found types of fuel cells are currently Polymer Electrolyte Fuel Cells (PEFC) and Solid Oxide Fuel Cells (SOFC). The operation diagram of a PEFC is show in Fig. 2.2. In a PEFC, hydrogen fuel is fed into the anode side of the cell stack and oxygen is fed through the cathode. The anode acts as a catalyst, dissociating

hydrogen molecules into hydrogen ions, which flow through the electrolyte, and a continuous current of electrons between the electrodes. This current represents the useful energy generated by fuel cells. In the cathode side, the electrons are recombined and as hydrogen ions react with the oxygen, water is formed. The electrolyte used in PEFC is a polymer membrane that allows the conduction exclusively of protons, while remaining impermeable to oxygen and hydrogen. This electrolyte becomes active at temperatures of around 80 °C, which defines the operating range of the fuel cell system. The electrodes in PEFC are generally made of platinum or platinum alloys, which are highly sensitive to contaminants. Because of this, PEFC systems require a hydrogen fuel supply of high purity.

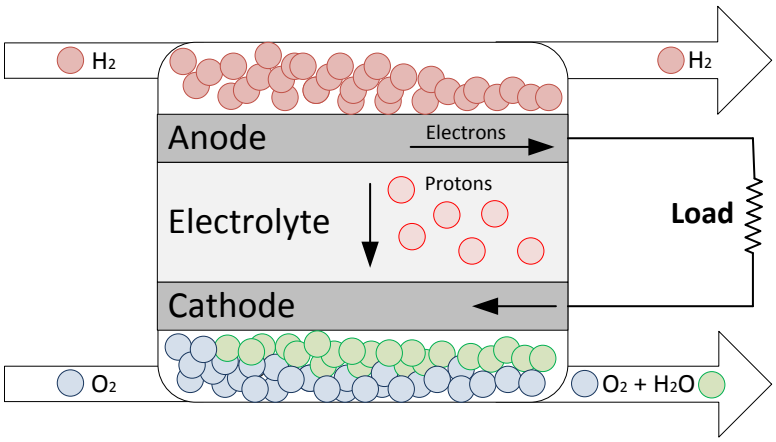

Figure 2.2. Schematic of fuel cell operation in a PEFC.

SOFC systems utilize a ceramic or solid oxide electrolyte that, unlike the electrolyte in PEFCs, allows the flow of negative oxygen ions. Therefore, the oxidation reaction in SOFCs occurs on the anode side of the cell stack. The electrolyte used in SOFCs activates at temperatures between 500 and 1000 °C, which differentiates them from PEFC in several ways. Reaction rates are favored at such high temperatures and thus SOFCs can achieve satisfactory reaction rates using nickel based catalysts instead of the platinum utilized in PEFCs. Nickel is much more inexpensive than platinum and does not present poisoning problems due to carbon monoxide. On the other hand, SOFCs require longer startup times to reach the operating temperature and present slower response times than PEFC systems. This short response time, along its low operating temperature, make PEFCs the preferred type of fuel cell for automotive applications, but for residential and commercial power applications where constant load operation is common, both PEFC and SOFC systems have competitive advantages.

Fuel cells operate on an electrical process, and thus extracted power is a function of the voltage and current delivered by the cell stack. The stack current I_{cell} depends linearly on the molar flow of hydrogen electrons $\dot{n}_{H2}$, and is calculated with Eq. (2.7), where F is the Faraday constant (96,485 C/mol).

$$I_{cell} = -2\dot{n}_{H2} \cdot F \tag{2.7}$$

The potential of an ion charge across a membrane is called the Nernst Voltage. The Nernst Voltage V_N in the cell is a function of both the stack temperature T and the partial pressures in the anode and cathode, and it is calculated with Eq. (2.8), where E^o is the Nernst voltage at standard pressure, R is the ideal gas constant (8.314 J/mol·K), and P_i are the partial pressures of each component in the reaction. The power in the oxygen pressure corresponds to the number of oxygen moles that take part in the reaction.

$$V_N = E^o - \frac{R \cdot T}{2F} \ln\left(\frac{P_{H2} \cdot {P_{O2}}^{1/2}}{P_{H2O}}\right) \tag{2.8}$$

Ideally, one would expect that all of the input fuel will react in order to extract the highest possible amount of power. However, as reactions in the cell take place and protons flow to the cathode side, fuel concentration in the anode will decrease which will cause the partial pressure near the outlet of the anode to be smaller. From Eq. (2.8) it is evident that as the partial pressure in the anode decreases to zero, the equation does not hold. Therefore in order to maintain the power output from the cell, a fuel utilization factor U_f less than 100% needs to be specified to determine the fraction of the fuel that will react in the cell, while the remaining fuel is allowed to exit the anode without reacting. Figure 2.3 shows calculated Nernst voltage as a function of fuel utilization at different inlet pressures [4]. Here we see that above U_f values of 90%, Nernst voltage drops dramatically. In practice, utilization factors of 80-85% are often considered.

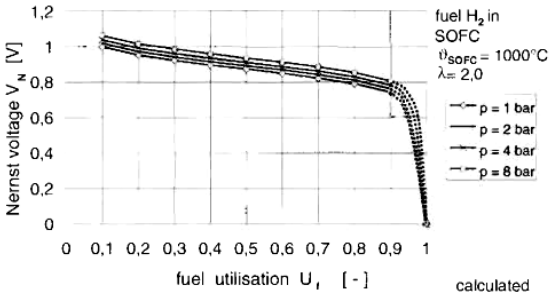

Figure 2.3. Calculated Nernst voltage V_N as a function of fuel utilization U_f [4].

Equation (2.8) also implies that the Nernst voltage and thus the power output from the cell decreases at higher temperatures. While this is true for the stated equation, irreversibilities need to be taken into account to obtain the actual output of the cell stack. Irreversibilities include ohmic, activation and mass transport losses. The operating voltage of the fuel cell system can be then calculated as the Nernst voltage minus voltage losses, as shown in Eq. (2.9).

$$V = V_N - \Delta V_{ohm} - \Delta V_{act} - \Delta V_{trans} \tag{2.9}$$

Ohmic losses represent the electrical resistance of the electrodes and the resistance to the flow of protons through the electrolyte. The voltage drop ΔV_{ohm} observed here is a function of the current density i given in mA/cm^2 and is calculated with Eq. (2.10), where r is the area specific resistance given in kΩ/cm^2.

$$\Delta V_{ohm} = ir \tag{2.10}$$

Activation losses are related to the overpotential seen at the electrodes' interface. The overpotential indicates the amount of energy that is required in practice to drive an electrolytic reaction, and it is parameter that is experimentally determined. The overpotential ΔV_{act} is given by Eq. (2.11), where α is the charge transfer coefficient, which depends on the reaction that is taking place and the material of the electrode. Here, i_0 is called the exchange current density and this value has been experimentally observed to have a much higher impact on the overpotential than the temperature. For the platinum electrodes utilized PEFCs, the value of i_0 is around 0.1 mA/cm. For SOFCs using nickel electrodes on the other hand, the exchange current obtained is around 10 mA/cm.

$$\Delta V_{act} = \frac{RT}{2\alpha F} \ln\left(\frac{i}{i_0}\right) \tag{2.11}$$

The voltage losses associated with mass transport ΔV_{trans} represent the decreased concentration of reactants over the electrodes as the oxygen and hydrogen are transformed into water molecules. This phenomenon was illustrated before with the definition of the fuel utilization factor. Mass transport losses are thus a function of partial pressures across the electrode length. These losses may also be approximated as a function of operating current, as given in Eq. (2.12), where m and n are experimental constants.

$$\Delta V_{trans} = m \exp(ni) \tag{2.12}$$

Equation (2.9) can then be rewritten as (2.13). From this equation it is evident that although Nernst voltage becomes lower at higher temperatures, the actual operating voltage depends largely on material and design parameters. In reality, SOFC systems have shown higher electric efficiencies than the lower temperature PEFC systems as shown in Fig. 2.4. It is worth noting though, that SOFC efficiency starts decreasing rapidly at lower loads unlike PEFCs, where there is little variation in electric efficiency over the operating load range.

$$V = V_N - ir - \frac{RT}{2\alpha F} \ln\left(\frac{i}{i_0}\right) + m \exp(ni) \tag{2.13}$$

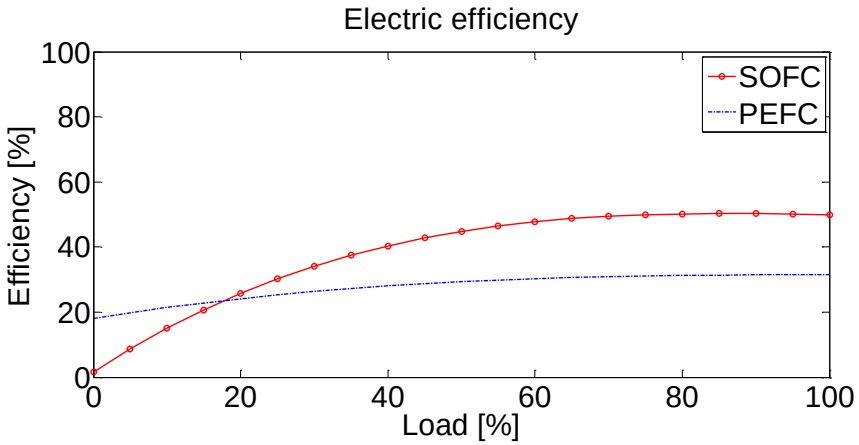

Figure 2.4. Electric efficiencies at varying operating loads for SOFC and PEFC systems.

2.4 Exhaust heat recovery

2.4.1 Heat exchangers

With fuel cells, as well as with internal combustion engines that are not discussed here, the heat content available in exhaust gases presents a valuable source of energy that can be recovered in order to maximize the extracted energy from input fuels. After undergoing the processes and reactions described in Section 2.3, the exhaust gases from fuel cells are mainly composed of a mixture of air and water steam at high temperatures. These gases are regarded as a quality heat source that may be easily converted in other types of thermal energy for human consumption, such as hot water and air conditioning. Such systems can accept several forms of thermal energy, including that obtained from renewable energies. For hot water production, heat exchangers (HEX) provide the simplest and most effective method for energy transfer.

Basic HEX operation consists of two fluid streams that exchange heat without mixing. Figure 2.6 shows a schematic of a direct-contact HEX, composed of two concentric tubes [5]. A Fluid B of high temperature T_{B1} enters the external tube, while Fluid A of low temperature T_{A1} enters the inner tube. Fluid A absorbs heat from Fluid B as it travels through the tube, leaving the heat exchanger at a higher temperature T_{A2}, while the temperature T_{B1} drops according to the amount of heat transferred. Heat transfer rate is dependent on the heat transfer area of the pipe, thus longer tubes can be used to increase the amount of heat transferred, and in consequence the final temperature of Fluid A, if the application requires so. Heat exchangers are generally insulated to avoid heat transfer to the environment, and are usually considered to involve no work interactions or kinetic and potential energy changes. Thus the energy balance for a direct-contact heat exchanger is given by Eq. (2.14).

$$E_{in} - E_{out} = \frac{dE_{sys}}{dt} \tag{2.14}$$

Since there is no mass exchange between Fluid A and Fluid B, Eq. (2.15) also holds true.

$$\dot{m}_{A1} = \dot{m}_{A2} = \dot{m}_A, \;\; \dot{m}_{B1} = \dot{m}_{B2} = \dot{m}_B \tag{2.15}$$

For steady state, the right term on Eq. (2.14) is zero and from there we obtain Eq. (2.16)

$$\dot{m}_A(h_{A1} - h_{A2}) = \dot{m}_B(h_{B2} - h_{B1}) \tag{2.16}$$

The total heat transfer $\dot{Q}_A$ to Fluid A is given by Eq. (2.17)

$$\dot{Q}_A = \dot{m}_A(h_{A1} - h_{A2}) \tag{2.17}$$

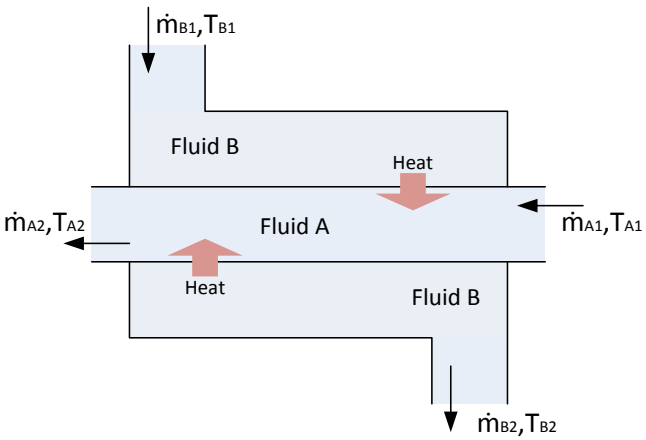

Figure 2.6. Schematic of a counter-flow direct-contact heat exchanger.

Direct-contact HEX can be further divided into counter flow and parallel flow. The schematic from Fig. 2.6 shows a counter-flow HEX, which is identified by the inlets of Fluid A and Fluid B being in opposite locations. In parallel flow HEX, inlet ports are close to each other and the fluids are subject to a large temperature gradient at the beginning of the heat transfer process. This case is useful when fast heat transfer is desired, which takes place at larger temperature gradients. Also, the outlet temperature of the cold stream in parallel flow HEX is always lower than the outlet temperature of the hot stream, which facilitates HEX design when the outlet temperature of the cold fluid needs to be preserved under a certain value.

For applications regarding hot water production, counter flow HEX are more commonly utilized because overall heat transfer is maximized. With counter flow, the outlet temperature of the cold fluid may reach higher temperatures than the outlet temperature of the hot fluid. The efficiency E_{HEX} of a counter flow HEX is given by Eq. (2.18), where C_{min} is the smaller of $\dot{m}_A C_{p,A}$ and $\dot{m}_B C_{p,B}$.

$$E_{HEX} = \frac{\dot{m}_A C_{p,A}(T_{A2} - T_{A1})}{C_{min}(T_{B1} - T_{A1})} \quad (2.18)$$

2.4.2 Heat driven absorption refrigerators

Absorption refrigeration has been receiving attention as an efficient method for exhaust heat recovery. Traditional refrigerators utilized for air conditioning utilize electricity driven compressors to increase the temperature of a refrigerant solution, to reach the conditions of saturated vapor. At these conditions, the solution temperature is higher than the ambient temperature thus allowing the rejection of heat that was absorbed from the refrigerated space. Electric heat pumps utilized for space heating utilize the same working principle in reverse, by cooling the outside air and rejecting heat into the desired space. These devices transform high quality electric energy into low quality thermal energy, which represents large energy losses in the form of irreversibilities. Although the development of the current energy infrastructure has favored the use of these electric devices, DER systems allow the introduction of more efficient technologies. In this case, absorption refrigerators that utilize low quality thermal energy as the driving force. Absorption refrigerators that can function for space heating as well, known as Absorption Chiller-Heaters (ACH), are also commercially available.

Figure 2.7 shows a schematic explaining the operation principle of ACH. Operation is divided into cooling and heating cycles through a changeover valve. The cooling process (Fig. 2.7 (a)) begins with the heating of a dilute solution of refrigerant (water) and an absorber, usually Lithium Bromide, contained in the generator. As the solution boils, a semi-concentrated vapor solution flows upwards to the first separator, where the refrigerant vapor is partly separated from the solution and the remaining semi-concentrated solution flows into the second separator. In this stage, part of the heat content of the previously obtained refrigerant vapor is used to finalize the separation of the semi-concentrated solution into a concentrated solution of the absorber. The water vapor is consequently cooled down in a condenser and the liquid refrigerant flows down into the evaporator. A low pressure in the evaporator is achieved due to the absorption process of water into Lithium Bromide. This low pressure decreases the boiling point of the refrigerant which boils on contact with the chilled water input. As the refrigerant boils, heat from the water input is consumed in the phase change of the refrigerant, lowering the temperature of the chilled water, which in turn cools down the ambient air. Finally, the refrigerant and the absorber recombine as cooling water removes the extra heat of the solution, and the diluted solution is pumped back into the generator.

a) Cooling cycle

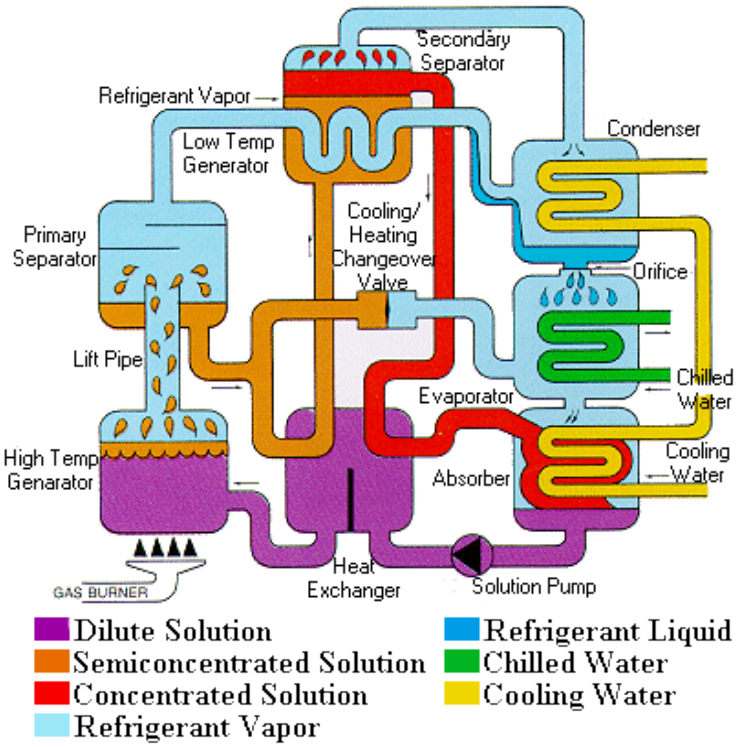

b) Heating cycle

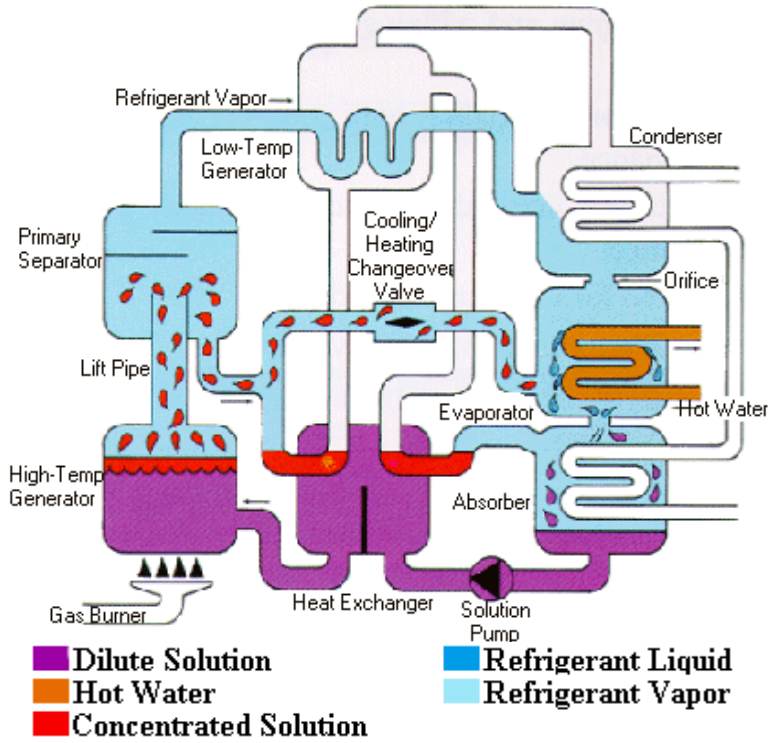

Figure 2.7. Schematic diagram of an Absorption Chiller-Heater during cooling (a) and heating (b) operation [6].

During the heating process (Fig. 2.7 (b)), the changeover valve opens, preventing the flow of the solution into the second separator. The dilute solution is heated in the generator, producing refrigerant vapor and droplets of concentrated solution, which flow directly into the evaporator. Here, pressure in the evaporator and condenser is similar, and thus the refrigerant's boiling point remains high. As the refrigerant comes in contact with the pipe surface of the input water, it condenses releasing its heat into the input water to increase its temperature. The condensed refrigerant recombines with the absorber once more and the diluted solution is pumped back into the generator.

The heat source for ACH may be as low as 55-70 °C, but temperatures of 110 °C are recommended in order to avoid crystallization inside the ACH. Higher input temperatures may also be used in double and triple effect ACH, which include multiple generators to generate more refrigerant vapor and thus extract/produce more heat. The work needed by the pump W_{pump} has been shown to be negligible compared to the heat input into the generator Q_{gen} and the heat extracted in the evaporator Q_{evap} [7]. The effective *COP* of an ACH can be then calculated with Eq. (2.19)

$$COP = \frac{Q_{evap}}{Q_{gen}} \tag{2.19}$$

The maximum output ratio COP_{rev} that can be obtained from the ACH without irreversibilities can be calculated with Eq. (2.20), where T_{Gen} is the temperature of the heat source at the generator, T_{CF} is the temperature of the chilled water at the inlet port, and T_{Cond} is the inlet temperature of the cooling water used in the condenser.

$$COP_{rev} = \left(\frac{T_{Gen}-T_{Cond}}{T_{Gen}}\right)\left(\frac{T_{CF}}{T_{Cond}-T_{CF}}\right) \tag{2.19}$$

Finally, the exergy efficiency *ECOP* of the ACH is given by the ratio of the effective *COP* over the efficiency for a reversible process COP_{rev}, as shown in Eq. (2.20).

$$ECOP = \frac{COP}{COP_{rev}} \tag{2.20}$$

A detailed energy and exergy analysis for absorption refrigerators can be found in [8]. In this study we can observe the change in *COP* and COP_{rev} at different operating conditions. For ACHs that operate using heat from fuel cell exhaust gases, the input energy to the ACH will vary depending on the current output of the fuel cell. Therefore it is important to notice the change in efficiency as the temperature in the generator (desorber) varies. From Fig. 2.8 (a) we see that as long as the temperature remains above a certain limit, dependent on the conditions of the refrigerant vapor and the diluted solution, the *COP* shows little to no variation. On the other hand, fewer irreversibilities are expected at higher temperatures and thus COP_{rev} is seen to increase linearly suggesting increasing exergy losses. In the same way, it is important to analyze the *COP* as the target cooling temperature (*i.e.*, the evaporator exit temperature) decreases. For air conditioning applications in occupied rooms, the target

temperature is expected to vary from 20-30 °C. Temperatures for computer server rooms can go as low as 10 °C, while refrigerated storage temperatures of 4 °C are suggested. An operation range from 0-30 °C (Fig. 2.8 (b)) of the absorption refrigerator shows very low variations in the *COP*, although the COP_{rev} does increase with higher temperatures as expected. The steadiness of the *COP* at the different operating conditions mentioned suggests that it is possible to consider a constant *COP* during further analysis. The absorption refrigerator seen in [8] corresponded to a *COP* close to 0.75, but current commercial ACH with *COP* values of 1.45 are available as well [9]. Furthermore, integration of absorption refrigeration systems with low quality heat sources such as fuel cells can be found in the literature [10].

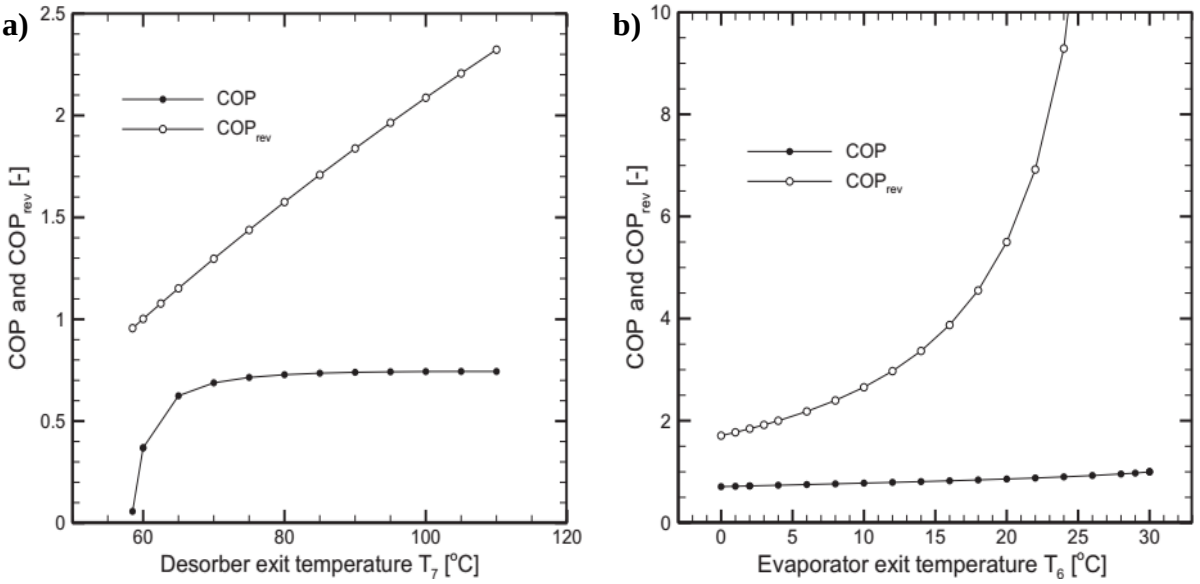

Figure 2.8. Efficiency analysis of an absorption refrigerator at varying temperatures of the exit fluid in the desorber (a) and the evaporator (b) [8].

2.5 Energy storage

For DER, efficient energy storage is of utmost importance since the introduction of intermittent renewable energies results in a power output that may not necessarily match the demand at all times. Various studies have discussed the available energy storage technologies [11-14]. Figure 2.5 shows the most commonly used types of energy storage technologies to this day: Pumped Hydro Storage (PHS), Compressed Air Energy Storage (CAES), capacitors, and rechargeable batteries (lead-acid, Nickel-Cadmium, Sodium-Sulfur, and Lithium-Ion). Other technologies such as flywheel mechanical storage and supercapacitors have been developed but are not yet being used extensively. Each of these technologies has advantages and disadvantages, as well as limitations for their use. PHS and CAES present the largest capacity for energy storage. In PHS, water is pumped to an upper reservoir when

electricity is available. The stored water presents a high potential energy based on the difference in height of the lower and higher reservoirs. When this energy is needed again, water returns to the lower reservoir after passing through a turbine that rotates an electric generator. A larger size of the reservoir gives a higher capacity for energy storage. In a similar manner, CAES utilizes underground caverns or empty water and gas reservoirs to store compressed air. Air is compressed when electricity is available, and the energy is extracted through a turbine powered by this compressed air. Although both of these systems have high efficiencies and large storage capacity, construction of energy storage plants depends on the geography of the area. CAES systems may only be built if a suitable reservoir is available, and PHS will need an adequate difference in the height of the terrain. Conservation of the local environment is also an important factor because construction of a PHS reservoir is generally expected to cover a large land area. When these systems are utilized with renewable energies, their power generation patterns are also considered. Solar PV in particular is subject to sudden fluctuations in power output, which can create a discontinuous signal. Although batteries and capacitors may still be recharged with a discontinuous power source, PHS and CAES require a stable power input to operate efficiently, and thus it may not be recommended to combine these technologies with solar PV.

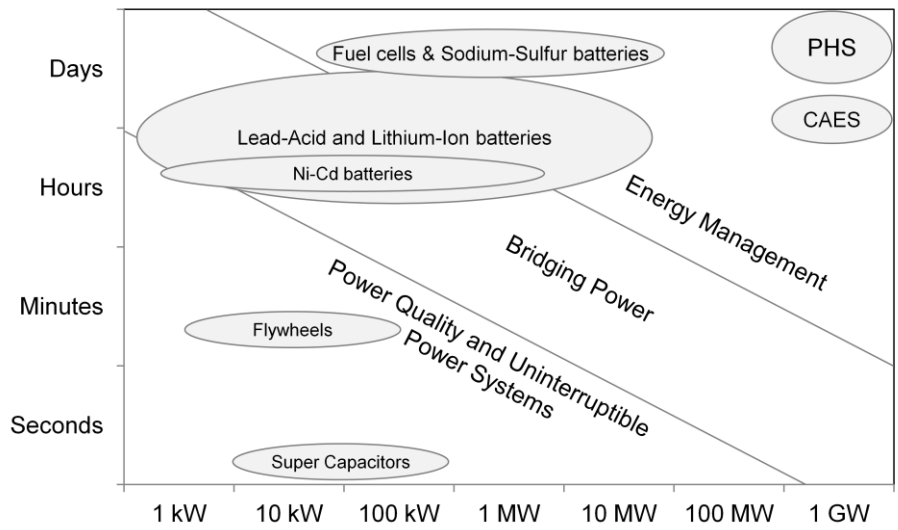

Figure 2.4. Scale and application of various energy storage technologies. Adapted from [12].

Rechargeable batteries present a more versatile option for energy storage thanks to their fast response, high efficiency and easy installation. They are non-intrusive and can be added to any system without significant reconfiguration. Batteries are however limited by their storage capacity and charge/discharge cycles. Furthermore, the lifetime of rechargeable batteries is around five years for lead-acid and Li-ion batteries, and 10 to 15 years for Ni-Cd batteries. In the long term, waste management of depleted batteries may also become a problem, in particular for Ni-Cd batteries since cadmium is a toxic material. Sodium-Sulfur batteries have a longer lifetime and their materials are

inexpensive and recyclable; however, they operate at high temperature (270 °C) and thus require additional thermal management and safety regulations.

With the increased development of fuel cell technologies during recent years, hydrogen generation has also been considered an attractive alternative for energy storage. Hydrogen can be used as fuel to generate energy, although hydrogen in its pure form is not commonly found in nature. Nevertheless, hydrogen can be generated through water electrolysis, using electricity to separate water into H_2 and O_2 molecules. Energy may be stored in this way and recovered through fuel cells to produce electricity and heat. Hydrogen storage is already being considered as a solution for energy independence in isolated micro-grids using renewable energies, such as solar PV [15] or wind power [16]. In PV systems, configuring the array so that the voltage output matches the electrolyzer's input can further improve efficiency [17]. Hydrogen storage in micro-grids using solar energy can serve as support for rechargeable batteries to increase the entire micro-grid's performance. Since power output from solar PV depends highly on weather, energy available during the year will vary between seasons. Therefore, relying on batteries during months with high solar output and using stored hydrogen to generate energy when solar output is low may reduce the micro-grid's total energy consumption [18]. As hydrogen storage is usually implemented together with fuel cells, these micro-grids can also benefit from cogeneration of heat and power. Shabani *et al.* [19] studied a hydrogen fueled micro-grid for a remote area in Australia, where solar energy is abundant. The results suggest that these systems could be sufficiently competitive to replace diesel generators within 30 years. A study by Brinkhaus *et al.* [20] analyzes the possibility of off-grid solar PV micro-grids for a typical household area in Europe. Energy storage using batteries and hydrogen is compared, and the hydrogen storage system appears to show higher reliability throughout the year in terms of stable power supply. They conclude that these off-grid systems are technologically viable and are expected to be more financially competitive as costs approach those offered by the main power network.

As many countries continue to expand their energy infrastructure, areas that are now isolated may be able to be connected to the main power network in the future. Therefore it is also worth considering whether the main power network will be compatible with the energy storage and generation systems used in the isolated micro-grid. In this regard, various studies [21-23] have suggested that electrolytic hydrogen can be helpful for load balancing when connecting micro-grids to the main power network. Load in the main power network may be stabilized by shifting energy variations into the electrolyzer and using fuel cells at peak times to generate electricity on-site for local consumption, improving the power quality of the network. With these considerations, countries where the main power network is still under development could rely on hydrogen fueled micro-grids to supply energy to isolated areas, and benefit from them for load balancing when the main network is expanded.

2.6 Conclusions

In this chapter, the operating principle of various DER technologies has been explained. Four major types of DER are addressed: Renewable energies, Fuel Cells, Exhaust heat recovery technologies, and Energy storage technologies. In renewable energies, wind and solar energy are the favored DER technologies due to the availability of resources that do not restrict installation. In fuel cells, high temperature Solid Oxide Fuel Cells and low temperature Polymer Electrolyte Fuel Cells are found to be the most common types of fuel cells used. Although high temperature theoretically leads to lower power output from the cell stack, the advantages of high temperature fuel cells are explained. Next, two major exhaust heat recovery technologies are addressed: heat exchangers and absorption refrigerators. The principle for operating absorption refrigerators for heating purposes are described as well. Finally, the major energy storage technologies are explained, and the viability for future systems utilizing hydrogen energy storage is discussed.

2.7 References

[1] Kumaravel, S. and Ashok, S. (2012). An Optimal Stand-Alone Biomass/Solar-PV/Pico-Hydel Hybrid Energy System for Remote Rural Area Electrification of Isolated Village in Western-Ghats Region of India. *International Journal of Green Energy,* 9, 398-408.

[2] JSA. (2012). Estimation method of generating electric energy by PV power system. *Japanese Standards Association*, Standard No. JIS C 8907:2005. (In Japanese).

[3] Larminie, J. and Dicks, A. (2003). *Fuel Cell Systems Explained*. England: Wiley.

[4] Singhal, S. and Kendall, K. (2003). *High-temperature Solid Oxide Fuel Cells: Fundamentals, Design and Applications*. Oxford: Elsevier Science Ltd.

[5] Çengel, Y.A. and Boles, M.A. (2004). *Thermodynamics: An Engineering Approach*. New York: McGraw-Hill.

[6] Yazaki Energy. (2016). Gas Fired Double Effect Chiller-Heaters: How they work. Retrieved May 1, 2016 from http://www.yazakienergy.com/gasfired.htm

[7] Gong S. and Boulama, K.G. (2014). Parametric study of an absorption refrigeration machine using advanced exergy analysis. *Energy,* 76, 453-67.

[8] Wonchala, J., Hazledine, M. and Boulama, K. G. (2014). Solution procedure and performance evaluation for a water–LiBr absorption refrigeration machine. *Energy,* 65, 272-84.

[9] Thermax. (2016). Hot water driven chillers, High temperature hot water (2G series). Retrieved May 1, 2016 from http://www.thermaxglobal.com/thermax-absorption-cooling-systems/vapour-absorption-machines/hot-water-driven-chillers/

[10] Margalef, P. and Samuelsen, S. (2010). Integration of a molten carbonate fuel cell with a direct exhaust absorption chiller. *Journal of Power Sources,* 195, 5674-85.

[11] Ritchie, A.G. (2001). Recent developments and future prospects for lithium rechargeable batteries. *Journal of Power Sources,* 96, 1-4.

[12] Kaldellis, J.K. and D. Zafirakis. (2007). Optimum energy storage techniques for the improvement of renewable energy sources-based electricity generation economic efficiency. *Energy,* 32, 2295-305.

[13] Beaudin, M., Zareipour, H., Schellenberglabe, A. and Rosehart, W. (2010). Energy storage for mitigating the variability of renewable electricity sources. *Energy for Sustainable Development,* 14, 302-14.

[14] Connolly, D. (2010). A review of Energy Storage Technologies: For the integration of fluctuating renewable energy (Master's thesis). Aalborg University.

[15] Paul, B. and Andrews, J. (2008). Optimal coupling of PV arrays to PEM electrolysers in solar-hydrogen systems for remote area power supply. *International Journal of Hydrogen Energy,* 33, 490-98.

[16] Yu, S., Mays, T.J. and Dunn, R.W. (2009). A new methodology for designing hydrogen energy storage in wind power systems to balance generation and demand. *In Proceedings of the 1st International Conference on Sustainable Power Generation and Supply (SUPERGEN), Nanjing, 2009*, 1-6.

[17] Gibson, T.L. and Kelly, N.A. (2010). Predicting efficiency of solar powered hydrogen generation using photovoltaic-electrolysis devices. *International Journal of Hydrogen Energy,* 35, 900-11.

[18] Avril, S., Arnaud, G., Florentin, A. and Vinard, M. (2010). Multi-objective optimization of batteries and hydrogen storage technologies for remote photovoltaic systems. *Energy,* 35, 5300-08.

[19] Shabani, B., Andrews, J. and Watkins, S. (2010). Energy and cost analysis of a solar-hydrogen combined heat and power system for remote power supply using a computer simulation. *Solar Energy,* 84, 144-55.

[20] Brinkhaus, M., Jarosch, D. and Kapischke, J. (2011). All year power supply with off-grid photovoltaic system and clean seasonal power storage. *Solar Energy,* 85, 2488-96.

[21] Li, X., Song, Y.J. and Han, S.B. (2008). Frequency control in micro-grid power system combined with electrolyzer system and fuzzy PI controller. *Journal of Power Sources,* 180, 468-75.

[22] Korpås, M. and Greiner, C.J. (2008). Opportunities for hydrogen production in connection with wind power in weak grids. *Renewable Energy,* 33, 1199-208.

[23] Gutiérrez-Martín, F., García-De María, J.M., Bairi, A. and Laraqi, N. (2009). Management strategies for surplus electricity loads using electrolytic hydrogen. *International Journal of Hydrogen Energy,* 34, 8646-475.

Chapter 3. Cogeneration systems

3.1. Introduction

This chapter gives an outline of cogeneration systems utilizing DER, in particular fuel cells and solar energy systems. The viability of utilizing hydrogen as a method for energy storage is analyzed for a Japanese household, with a novel approach to hydrogen utilization in methane-fed commercial fuel cell systems. The fuel cell cogeneration system is compared against its common competitor in Japan, PV systems with electric batteries for energy storage, and their capability to approach grid independence is evaluated, as well as their performance regarding primary energy consumption and energy cost. After this analysis, the system scale is raised from the residential to the micro-grid scale and an original micro-grid structure is described, using hydrogen fuel and cogeneration systems for energy supply in communities without access to the main power grid.

This chapter begins with an overview on cogeneration systems in Section 3.2, focused mainly on systems utilizing fuel cells. In Section 3.3, the effects that hydrogen addition in commercial methane-fueled SOFC cogeneration systems has on its heat to power ratio is described. Section 3.4 presents an analysis for residential fuel cell cogeneration system for Japanese households using solar PV and hydrogen energy storage, evaluating its capability for reaching grid independence. In Section 3.5, the implementation of cogeneration systems for communities without access to the power grid is discussed. The problem presented in this Section requires an optimization study, which is to be described in detail during following chapters. A realistic approach to implementation of the proposed micro-grid structure is given in detail in Section 3.5 as well.

3.2 Cogeneration overview

Cogeneration systems are a common addition to micro-grids and smart-grids. Fuel based systems such as microturbines, reciprocating engines, Stirling engines and fuel cells are often used in cogeneration systems because they generate large amounts of waste heat during operation. This generated heat can be utilized as the driving energy input for refrigeration equipment, air conditioning, and hot water production. In this way, efficiency can be increased from 30-45% of pure electric generation to over 80% for cogeneration systems. A study by Maidment and Prosser [1] compares the performance of cogeneration systems for cold storage facilities with and without absorption chiller technology. The hourly load considered for the facility was between 320 and 400 kW. Utilizing cogeneration to provide electricity, hot water and ambient heating for a cold storage facility using only conventional vapor compression refrigeration would present a payback period between 7.9 and 10.6 years. In contrast, using waste heat from the cogeneration system in an absorption chiller instead of ambient heating, the system’s payback period was expected to decrease to 4.6 years.

From the technologies available for cogeneration systems, fuel cells appear to offer the highest electric efficiency [2]. Compared to turbines and engines, fuel cells operate on an electrochemical process that does not produce NOx and soot emissions that result from combustion [3]. On the other hand, fuel cell systems require complex fuel flow, pressure and temperature management systems to control the power output.

Table 3.1. Summary of the cogeneration characteristics of available fuel cell technologies [2].

	Polymer Electrolyte Membrane Fuel Cell	**Phosphoric Acid Fuel Cell**	**Solid Oxide Fuel Cell**	**Molten Carbonate Fuel Cell**
Type of Electrolyte	H^+ ions	H^+ ions	O^{2-} ions	CO_3^{2-} ions
Operating temperature	65-85° C	190-210° C	750-1000° C	650-700° C
Electrical efficiency (HHV)	35%	36%	45%	46%
Cogeneration efficiency (HHV)	72%	75%	70%	70%
Power/heat ratio	0.95	0.92	1.79	1.92

The characteristics of the available fuel cell generation technologies are presented in Table 3.1. The two main types of fuel cells utilized for residential energy generation are Polymer Electrolyte Membrane Fuel Cells (PEFC) and Solid Oxide Fuel Cells (SOFC). The electrolyte in PEFCs is activated at low temperature (65 °C), which allows for fast startups and effective load following operation. However, the material of the electrolyte is very sensitive to impurities and moisture levels in the fuel; therefore auxiliary systems are used to maintain this delicate balance. In SOFCs, the electrolyte is very resilient to impurities and can utilize carbon monoxide as fuel along with hydrogen. This electrolyte however, is activated at high temperature (750 °C) and thus requires preheating stages for the cell stack and the fuel input which consume additional energy, and in addition elongate its startup time. For both types of fuel cells, hydrogen (and CO in the case of SOFCs) is usually obtained by reformation of natural gas. Therefore, both systems also need a gas reforming unit if pure hydrogen cannot be supplied. Through reutilization of exhaust heat, researchers have been able to reduce the energy needed for auxiliary elements in fuel cells, increasing the overall efficiency of the system [4]. In the same way, fuel cells have shown promising results as part of efficient residential cogeneration systems with decreased emissions of CO_2 [5, 6].

For fuel cell systems, the main setback has been that the industry is relatively new and development and production costs remain high. Current studies indicate that the viability of residential fuel cell systems are often limited by the equipment costs. One study in Malaysia reports that if replacement and maintenance costs for the fuel cell systems can be lowered to one third, fuel cell cogeneration systems would be able to replace the conventional system of electricity supply through power networks [7]. Fortunately, as it happens with most technologies, fuel cell production costs are expected to fall dramatically as production volume increases in the following years. An

increase in production from 5 to 500 MW per year is expected to reduce costs by a factor of four to eight times [8].

3.3 Effect of hydrogen addition on heat to power ratio in SOFC systems

Residential fuel cell systems with cogeneration of power and hot water have been successfully implemented in Japan during recent years. These fuel cell systems are fueled mainly by methane, which is obtained from the existing city gas infrastructure in a convenient matter. After removing the sulfur content, the city gas composed mainly of methane undergoes reformation in order to generate hydrogen. Internal reformation units can be commonly found on commercial fuel cell systems, which eliminate the need to build an infrastructure for pure hydrogen. Furthermore, city gas is a commodity used for cooking and hot water in most households, thus it can be considered as reliable and robust.

Methane reformation in fuel cells systems is carried out through Steam Methane Reformation (SMR). Figure 3.1 shows a common configuration for fuel cell systems with internal SMR units. In this process, methane and steam react over a catalyst at temperatures above 500 °C. The reactions taking place in the SMR unit are endothermic methane reforming (3.1) and exothermic water gas shift reaction (3.2) [9]. The fraction of gas species over the catalyst's length is shown in Fig. 3.2, for a given nickel catalyst of 380 g at a temperature of 750 °C, where the initial gas flow inputs are 7500 mol/hr of H_2O, 5000 mol/hr of CH_4 and 50 mol/hr of H_2. Part of the exhaust gases resulting from the reactions in the fuel cell stack can be utilized to supply the needed steam for these reactions. The overall SMR reaction is endothermic, meaning that a fraction of the exhaust heat from fuel cells needs to be reserved for hydrogen generation. As heat is consumed in the SMR reactions, the amount of heat available for hot water generation that can be recovered from the cell stack exhaust gases decreases. It is worth mentioning that in PEFC systems, CO and CO_2 must be removed before entering the cell stack since its platinum electrodes can be easily poisoned by any contaminants, reducing the active area of the electrode and degrading performance. In contrast, SOFC electrodes are nickel based and not only offer much higher resistance to poisoning, but the cell stack in SOFCs can utilize CO as a reactant as well. Cogeneration systems based on PEFC and SOFC are both commercially available. While PEFC systems are often favored for their rapid response to load changes, SOFC systems offer a much higher electric efficiency, which is expected to help reach the goal of grid independence. Furthermore, SOFC offer higher flexibility for fuel inputs giving them an advantage on the choice of fuels, thus they are here considered as the cogeneration plant for residential energy systems.

$$CH_4 + H_2O \rightarrow CO + 3H_2 \qquad \Delta H = +206.16 \text{ kJ/mol} \qquad (3.1)$$

$$CO + H_2O \rightarrow CO_2 + H_2 \qquad \Delta H = -41.17 \text{ kJ/mol} \qquad (3.2)$$

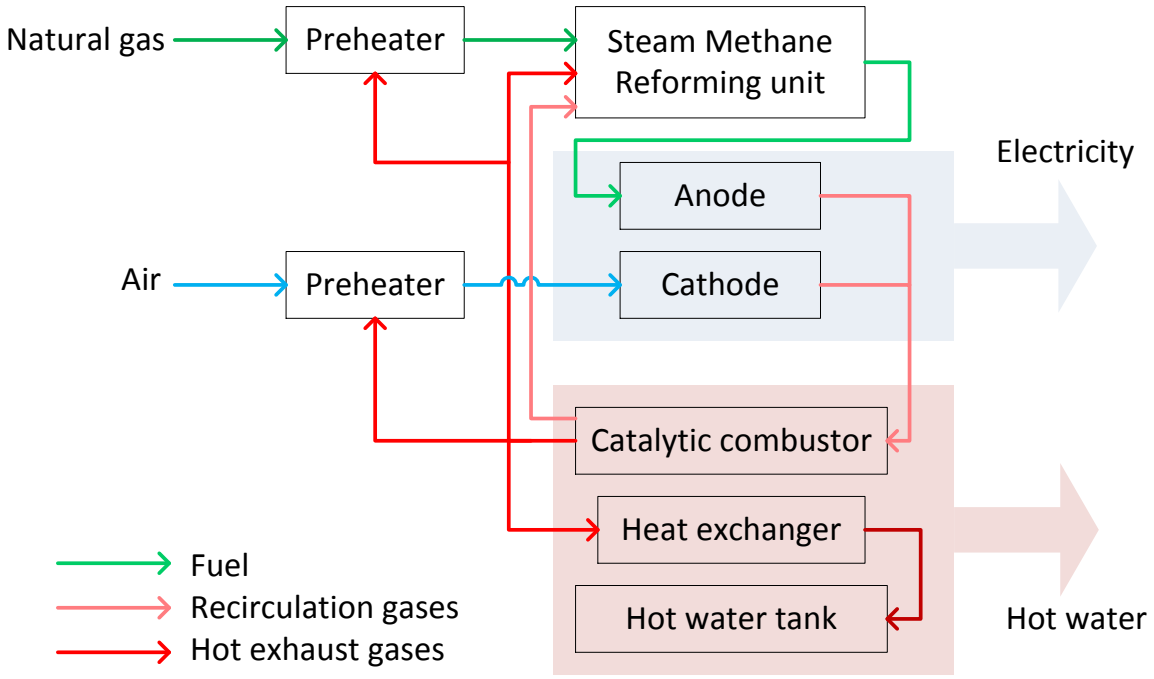

Figure 3.1. Internal diagram of a residential fuel cell system with exhaust heat recovery.

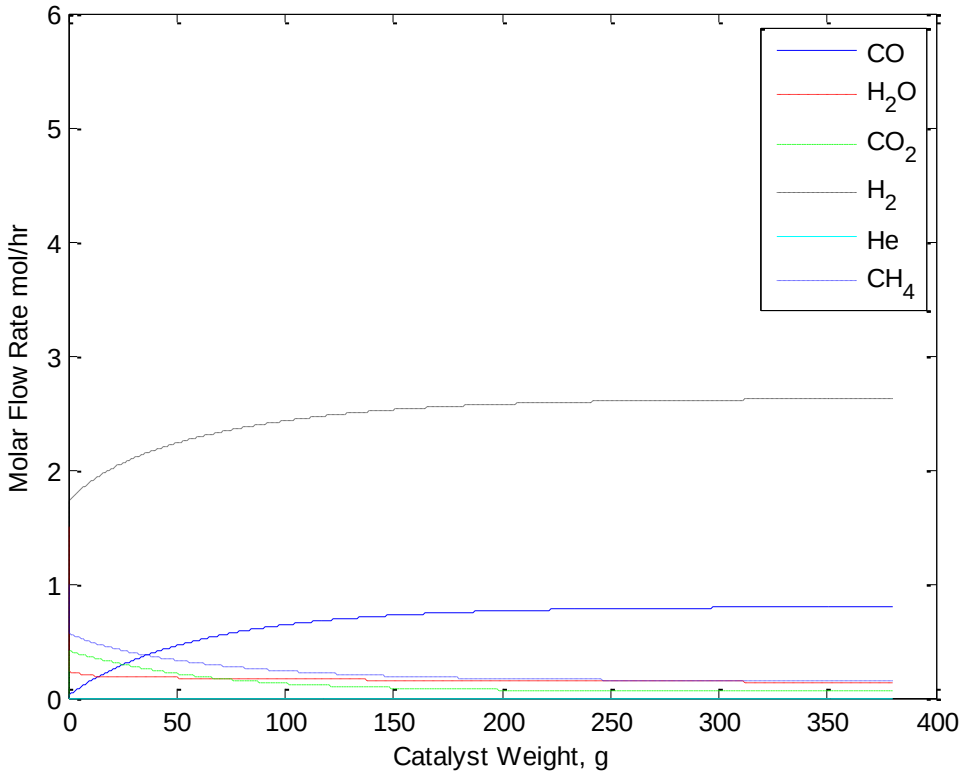

Figure 3.2. SMR kinetics along a 380g nickel catalyst at 750 °C.

The products of reformation go then into the fuel cell anode, while preheated air goes into the fuel cell cathode. In an SOFC, oxygen anions flow through the electrolyte and combine with H_2 and CO molecules in the anode, while the flow of free electrons between the cathodes produces electricity. The fuel cell stack in the SOFC remains at temperature of 750 °C, and the reactions (3.3) and (3.4) that take place are slightly exothermic.

$$H_2 + O^{2-} \rightarrow H_2O + 2e^- \qquad T\Delta S = 56.52 \text{ kJ/mol} \qquad (3.3)$$

$$CO + O^{2-} \rightarrow CO_2 + 2e^- \qquad T\Delta S = 89.01 \text{ kJ/mol} \qquad (3.4)$$

Unreacted H_2 and CH_4 are burned in a catalytic burner to produce additional heat. This heat is used to maintain the SMR reaction, to preheat the input fuel and air flows, and to generate hot water for residential consumption. In the catalytic burner, oxidation of the remaining species of methane, hydrogen and carbon monoxide is carried out [10]. Reactions (3.5)-(3.7) take place in the catalytic burner. An auxiliary gas boiler provides additional heat for hot water production. All hot water is stored in an insulated tank.

$$CH_4 + 2\ O_2 \rightarrow CO_2 + 2\ H_2O \qquad \Delta H = -802.28 \text{ kJ/mol} \qquad (3.5)$$

$$CO + \tfrac{1}{2}\ O_2 \rightarrow CO_2 \qquad \Delta H = -282.98 \text{ kJ/mol} \qquad (3.6)$$

$$H_2 + \tfrac{1}{2}\ O_2 \rightarrow H_2O \qquad \Delta H = -241.82 \text{ kJ/mol} \qquad (3.7)$$

For a given electric current *I*, the flow of hydrogen moles $\dot{n}_{H2}$ that are needed in a cell stack to produce such current can be calculated with Eq. (3.8), where *F* is the faraday constant.

$$I = \dot{n}_{H2} \cdot F \qquad (3.8)$$

If a fuel cell system with an external input of hydrogen in addition to methane is considered, then the same electric current can be maintained with a smaller fraction of hydrogen produced from SMR, and thus methane input can be reduced. As the flow of methane decreases, the endothermic process of reactions (3.1) and (3.2) will decrease as well, resulting in a larger amount of heat available for recovery. For an SOFC system however, decreasing the flow of methane will also decrease the number of CO moles that will react in the cell stack. The electric efficiency η_{Ele} and heat recovery efficiency η_{HR} of a fuel cell system can be calculated with Eq. (3.9) and (3.10), respectively, where Q_{LHV} is the lower heating value of the fuel input, W is the electric power output of the system and Q_{HR} is the heat recovered from the system.

$$\eta_{Ele} = \frac{Q_{LHV}}{W} \qquad (3.9)$$

$$\eta_{HR} = \frac{Q_{LHV}}{Q_{HR}} \qquad (3.10)$$

When a mixture of methane and hydrogen is used as fuel input, the total LHV of the mixed fuel can be maintained constant in order to observe the effects of hydrogen addition ratio, defined here as λ_{H2}, on the system's efficiency. Figure 3.3 shows the effect of hydrogen addition ratio λ_{H2} on the electric and heat recovery efficiencies of a 700 W SOFC system at different loads. The percentage of hydrogen addition is given in terms of the LHV of the fuel mixture. At full load (*i.e.* 700 W), the LHV of the fuel input flow is 5.6 MJ/h. The LHV of H_2 is 10.78 MJ/Nm^3 and that of methane is 40.6 MJ/Nm^3. In terms of volumetric ratio, a hydrogen addition ratio of 20% for example would correspond to 48.5% of the gas flow. Since methane provides more calorific value per volumetric unit, the hydrogen addition ratio in terms of volume increases faster than λ_{H2}. The decrease in electric efficiency seen in Fig. 3.3 (a) is due to a lower amount of CO moles that go into the cell stack, resulting from the decreasing input of methane at higher values of λ_{H2}. In contrast, the increase in heat recovery efficiency is due to the exhaust heat that becomes available when the rate of SMR reactions decreases with lower methane input. Therefore at values of λ_{H2} larger than 60%, the ratio of heat to power in an SOFC system is expected to rapidly increase.

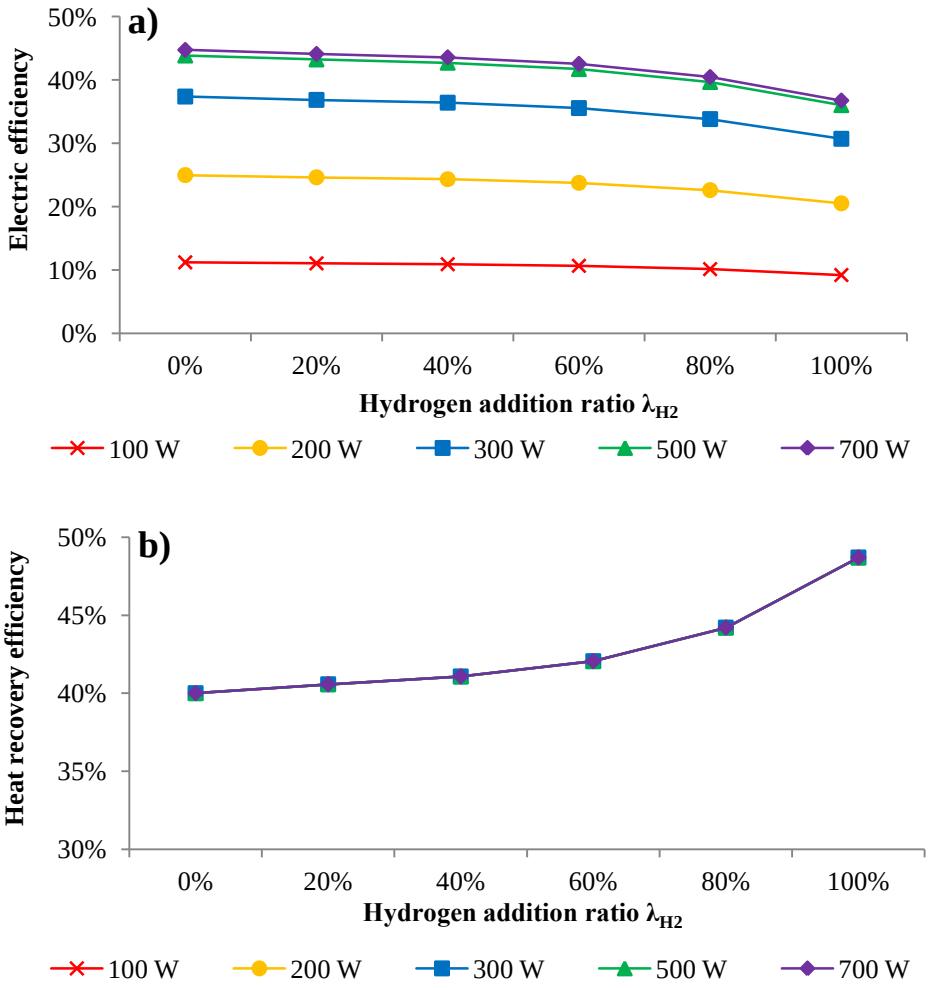

Figure 3.3. Electric (a) and heat recovery (b) efficiencies of a fuel cell system at varying loads using a mixed fuel of methane and hydrogen.

3.4 Grid independence study of residential SOFC cogeneration systems

Considering the effects of hydrogen addition to SOFC systems, a residential cogeneration system utilizing a mixture of hydrogen/methane fuel is analyzed for a Japanese household. As discussed in Chapter 2, Section 2.2.3.1, hydrogen has been considered an alternative method for energy storage. In Japan, penetration of solar PV into the residential sector has been following an increasing trend [11]. To provide additional power when the PV systems are inactive, fuel cells can be used to generate power on-site without being restricted to the main power grid. Furthermore, surplus electricity of PV during daytime can be stored in the form of hydrogen through water electrolysis which can then be utilized as fuel for the SOFC.

The system analyzed in this study is designed for a four person household in the central area of Kansai, Japan. The household area is 120 m^2. Energy demands are obtained from [12]. Figure 3.4 shows the average of the electric and hot water demands divided in three seasons: winter, from December to March; summer, from June to September; and the shoulder season, composed of April, May, October, and November. In this study, air conditioning is obtained from an electric heat pump, thus the energy demands for this purpose are included in the electric demand. The heat pumps are considered to operate with an Annual Performance Factor (AFP) of 5.9. Compared to the Coefficient of Performance (COP) for heat pumps, the AFP takes into account load conditions, outside air temperature and power consumption at rated time, giving a more accurate estimate of energy consumption against utilization [13].

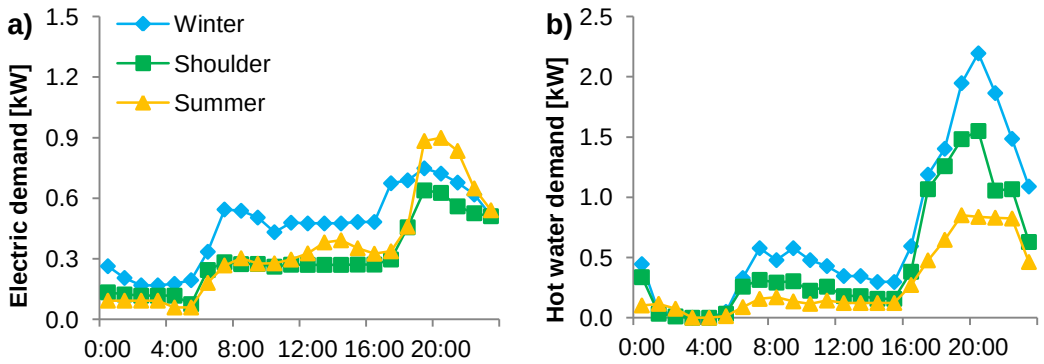

Figure 3.4. Seasonal electric (a) and hot water (b) energy demands for a four person household.

The diagram of the proposed system is presented in Fig. 3.5. Electric demand is met with power generated from the PV array and SOFC. A PV array facing south at a 30° angle is considered, using solar irradiation data for Kyotanabe, Kyoto, Japan (34.8167° N, 135.7667° E) during 2012. Power output data was obtained from a 3 kW PV array in this area. Figure 3.6 shows the average power output grouped into three seasons. Winter is composed of months December through March; Summer, from June through September; and the Shoulder season contains the remaining months. When only solar irradiation data is available, W_{PV} for the PV system can be estimated using Eq. (3.11). P_{cap} is the

array's total rated capacity, I_{sun} is solar irradiance, K_{pa} is the correction factor for electric losses (0.97), K_{pm} is the load matching correction factor (0.94), η_{inv} is the inverter's efficiency (0.95), α_{Pmax} is the temperature coefficient (0.4%/K), T_{av} is the monthly average of the solar cell's surface temperature in °C, and G_s is the solar irradiation intensity in standard conditions (1000 W/m^2).

$$W_{PV(h,m)} = P_{cap} \cdot I_{sun(h,m)} \cdot K_{pa} \cdot K_{pm} \cdot \eta_{inv} \cdot \left[1 - \alpha_{Pmax}\left(T_{av(m)} - 25\right)/100\right] \cdot G_s^{-1} \qquad (3.11)$$

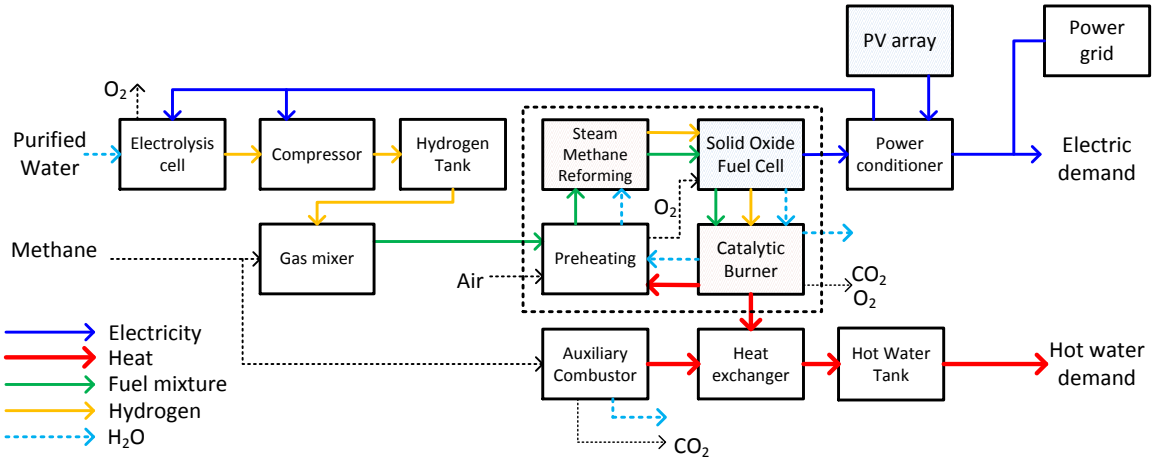

Figure 3.5. Diagram of the proposed PV-SOFC cogeneration system.

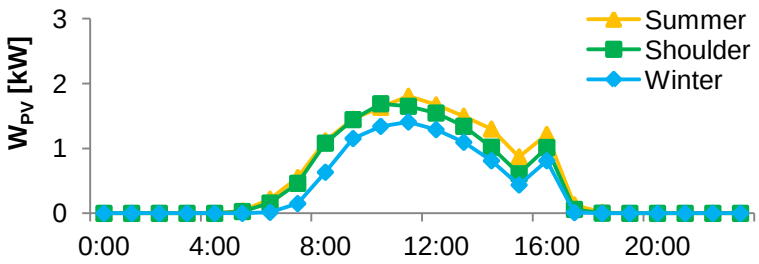

Figure 3.6. Seasonal power output for a 3kW PV array in Kyotanabe city, Kyoto.

In the proposed system, grid connection is still considered, although power is only imported when electric demands surpass the capacity of the system. In order to maintain the lowest possible interaction with the grid, Feed-in Tariff (FIT) for selling surplus power is not considered in this case. Instead, surplus electricity is used to power a water electrolyzer to generate hydrogen fuel, which is stored in a pressurized tank using a compressor.

The objective of the SOFC in the proposed system is to provide energy when the solar PV is inactive to avoid interaction with the power grid. Currently, the common alternative for solar PV systems is with electric storage using rechargeable batteries. The performance of the proposed cogeneration system is compared against two other systems, illustrated in Fig. 3.7. PV-SOFC system is the proposed system. PV-Battery uses a solar PV array, a rechargeable Lithium-ion battery, and a gas boiler for hot water supply. This system also consumes power from the grid when needed. The

conventional system is supplied with electricity exclusively from the grid, and hot water from a gas boiler.

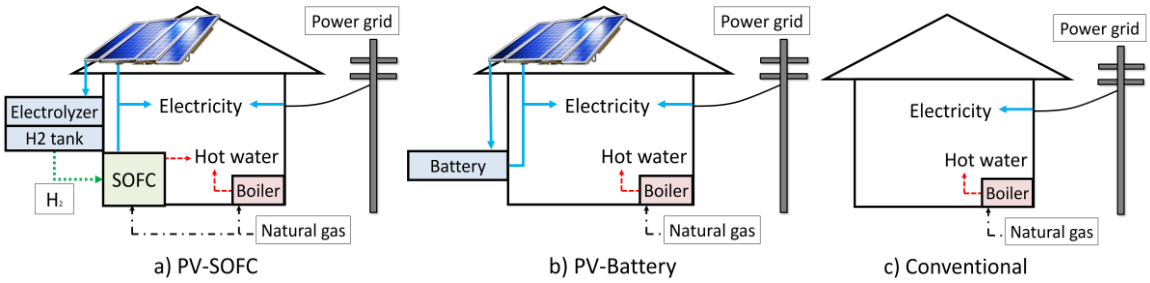

Figure 3.7. Diagrams of systems selected for comparison.

The capacities of the components were selected to fit the selected energy demands, as summarized in Table 3.2. The capacity and pressure of the hydrogen tank will be calculated after analyzing the surplus energy of the PV panels and the fuel demand of the SOFC.

Table 3.2. Capacity of selected components for each system.

PV-SOFC		
PV array	Rated output	3 kW
SOFC	Rated output	0.7 KW
	Electric efficiency	45%
	Heat recovery efficiency	40%
Electrolyzer	Efficiency	30%
	Output pressure	300 kPa
Gas boiler	Heating efficiency	80%
	Tank size	200 L
PV-Battery		
PV array	Rated output	3 kW
Lithium-Ion battery	Rated capacity	5.5 kWh
	Max. current permitted	1.4 kWh
	Min. state of charge	15%
	Recharging efficiency	90%
Gas boiler	Heating efficiency	80%
	Tank size	400 L
Conventional		
Gas boiler	Heating efficiency	80%
	Tank size	400 L

3.4.1 SOFC parameterization

To estimate fuel consumption for the proposed system, operation parameters for the SOFC were first obtained. A commercial 700 W SOFC system was utilized for analysis. The SOFC was operated from 100 W to 700 W at intervals of 100 W, measuring input fuel flow, output power, and heat recovery rate at a frequency of 2 Hz. The fuel input consisted of a mixture of 70.5% volume of natural gas and 29.5% volume of hydrogen, controlled by a mixed gas generator. This ratio corresponds to a

hydrogen addition of 10% of the mixed fuel's Lower Heating Value (LHV). Due to the SOFC's operation limits, the manufacturer specified a hydrogen addition limit of 20% of the input fuel's LHV. The strategy discussed in Section 3.3 shows that a hydrogen rich input flow could improve heat recovery rate in an SOFC system by reducing heat consumption in the SMR unit. An analysis based on this strategy is given in detail in a previous study [14]. Unfortunately, for the manufacturer specified hydrogen addition limit of 20%, the impact on electric and heat recovery efficiency is not expected to be evident.

With the measurements taken, polynomial curves were obtained to calculate the LHV of the fuel input $\dot{Q}_{LHV,fuel}$ (Eq. 3.12) and heat recovery efficiency η_{HR} (Eq. 3.13) at a given load x. For Eq. (3.12), residual sum of squares analysis showed no improved accuracy above a degree of four. Heat recovery efficiency presented followed a linear trend; therefore a linear approximation was utilized.

$$\dot{Q}_{LHV,fuel}(x) = 50.4x^4 - 84.3x^3 + 50.6x^2 - 7.1x + 2.5 \quad (3.12)$$

$$\eta_{HR}(x) = 0.0041x + 0.3675 \quad (3.13)$$

3.4.2 Operation profile of the SOFC

To avoid operating the SOFC at low efficiencies, limits were set on its operation profile. During daytime when the solar PV's output is able to meet the electric demand, the SOFC is turned off. During startup fuel is consumed to gradually increase the fuel cell stack's temperature to 1023 K. The shutdown stage also consumes fuel to avoid rapid cooling of the stack which could cause thermal fatigue. Fuel consumption during both stages is shown in Fig. 3.8. These stages were identified through the status signal that the control system of the SOFC provides. After the status signal changes, power output of the SOFC is stabilized within one minute. The startup stage lasted between 110 and 120 minutes, with an average fuel consumption of 299 L. In the shutdown stage there was more variation, lasting between 70 and 130 minutes, with an average fuel consumption of 64 L. After shutdown, the SOFC enters a cool down stage in which it is not recommended to start the SOFC again. The safe time span to start the SOFC after the shutdown stage begins is four hours. The present analysis assumes that weather forecast is able to predict if enough solar irradiation will be available for a minimum of four hours. If this is not the case, the SOFC is not shut down. Although intermittent operation for SOFCs is not recommended, some techniques have been introduced to reduce energy consumption during these stages [15].

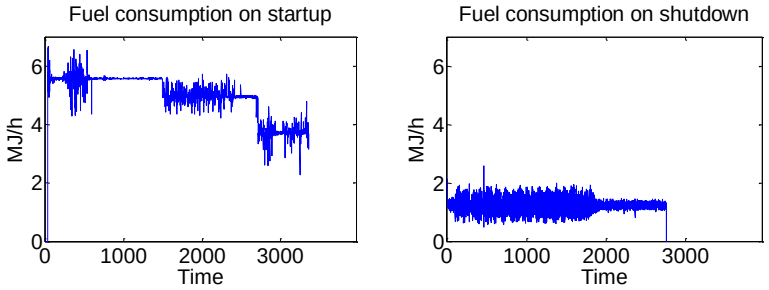

Figure 3.8. Fuel consumption at startup and shutdown stages of the SOFC.

Since the SOFC's electric efficiency decreases rapidly at lower loads, operation of the SOFC below 20% of its rated load is not recommended [16]. Therefore, the SOFC is limited to operate between the range of 140 W and 700 W. Using this lower load limit, Eq. (3.12) was used to estimate hourly fuel consumption by the SOFC. Figure 3.9 shows a comparison between the actual SOFC operation and the polynomial approximation, for an average daily electric demand pattern in each season. Adding the average fuel consumption for startup and shutdown, the model predicted fuel consumption for any season within ±5% error. The intense rapid oscillations in the experimental data are attributed to the gas mixer attempting to stabilize the fuel flow rate and methane/hydrogen ratio.

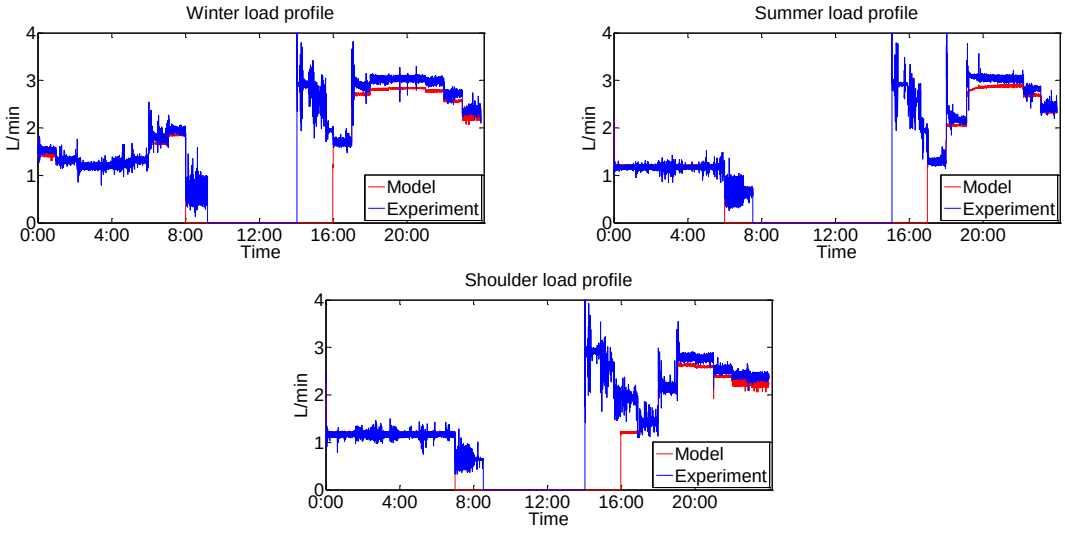

Figure 3.9. Modeled and experimental data for average daily SOFC fuel consumption in each season.

3.4.3 Hydrogen generation rate

Using the solar PV output calculated with Eq. (3.11) and the criteria for SOFC operation, the total power output of the system is compared against the electric demand presented in Fig. 3.4. When the system's power output W_{sys} is higher than the demand W_{dem}, surplus electricity is used to generate hydrogen through the water electrolyzer. The volume of generated hydrogen is calculated using Eq.

3.14, where η_{elz} is the electrolyzer efficiency, η_{tank} is the pressurized tank's round trip efficiency (91% [17]), and $Q_{LHV,H2}$ is hydrogen's LHV.

$$V_{H2} = (W_{sys} - W_{dem}) \cdot \eta_{elz} \cdot \eta_{tank} / Q_{LHV,H2} \quad (3.14)$$

After calculating the daily hydrogen production, a hydrogen addition ratio λ_{H2} is specified for each month, depending on the availability of hydrogen. Currently, modifying the hydrogen addition ratio requires technical support and thus it cannot be modified on a daily basis. Equation (3.15) is used to calculate λ_{H2}, using the daily sum of consumed fuel, obtained from Eq. (3.12). The resulting hydrogen addition for each month is given in Fig. 3.10. From November to March, the combination of low solar PV output and high electric demand result in a lower value for λ_{H2}. However, from April to August the generated hydrogen is enough to reach the specified limit of 20%, with September and October close to this value as well.

$$\lambda_{H2} = V_{H2} \cdot Q_{LHV,H2} / \left(\sum_{day} \dot{Q}_{LHV,fuel}\right) \quad (3.15)$$

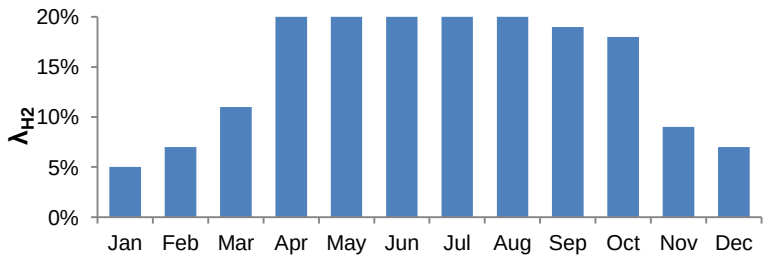

Figure 3.10. Monthly hydrogen addition ratio possible.

Consequently, the capacity of the hydrogen tank is specified using Eq. (3.16). The highest amount of generated hydrogen was obtained in May, corresponding to 1740 L at 0.3 MPa. Since the volume V_{tank} and pressure P_{tank} of the tank are inversely proportional, one must propose one of the values to calculate the other. Commercial low pressure hydrogen tanks are available at pressures of 3 MPa, and metal tanks at pressures of 20 MPa, which would correspond to a volume of 180 L and 27 L, respectively. Although lower pressure tanks would reduce load on the compressor and provide better safety, a tank with a larger volume would be subject to space availability limitations and higher cost.

$$P_{tank} = V_{H2,max} \cdot P_{elz} / V_{tank} \quad (3.16)$$

3.4.4 Heat recovery from exhaust gases

Heat recovery from the SOFC is calculated after obtaining the daily fuel consumption and hydrogen addition ratio for each month. Considering the internal processes of the SOFC discussed on

Section 3.2, heat consumed and generated in each process is calculated. Table 3.3 gives a list of the constants used in Eqs. (3.17) through (3.26).

Table 3.3. Constants used for heat recovery analysis.

Constants			
LHV of methane	$Q_{LHV,CH4}$	910.04	kJ/mol
LHV of hydrogen	$Q_{LHV,H2}$	242	kJ/mol
HHV of methane	$Q_{HHV,CH4}$	286	kJ/mol
HHV of hydrogen	$Q_{HHV,H2}$	889	kJ/mol
Anode heat release: H_2	$T_{an}\Delta S_{H2}$	56.52	kJ/mol
Anode heat release: CO	$T_{an}\Delta S_{CO}$	89.01	kJ/mol
SMR heat consumption	Q_{SMR}	206	kJ/mol
SMR heat consumption	Q_{WGS}	-41	kJ/mol
Ambient temperature	T_{amb}	278	K
Preheated fuel temperature	T_{fuel}	1097	K
Preheated air temperature	T_{air}	1024	K
Specific heat: Air	Cp_{air}	31.31	J/mol·K
Specific heat: H_2	Cp_{H2}	29.64	J/mol·K
Specific heat: CH_4	Cp_{CH4}	57.84	J/mol·K
Specific heat: CO_2	Cp_{CO2}	57.11	J/mol·K
Specific heat: H_2O	Cp_{H2O}	75.31	J/mol·K
Specific heat: O_2	Cp_{O2}	35.84	J/mol·K
Specific heat: N_2	Cp_{N2}	33.96	J/mol·K
Air to fuel ratio	λ_{air}	2	
O2 concentration in air	x_{O2}	20.8%	
Heat losses	x_{loss}	3%	
SMR: H2 output	x_{H2}	280%	
SMR: CO output	x_{WGS}	80%	
SMR: CO2 output	x_{CO2}	6%	
SMR: CH4 output	x_{SMR}	15%	
Fuel utilization factor	U_f	85%	
HEX input temperature	T_{hot}	1073	K
HEX output temperature	T_{cold}	355	K
Methane combustion	$Q_{com,CH4}$	-802.275	kJ/mol
CO oxidation	$Q_{com,CO}$	-282.984	kJ/mol
H2 oxidation	$Q_{com,H2}$	-241.82	kJ/mol

Firstly, the reactions in the SMR unit are analyzed. Reaction kinetics analysis of CH_4 on a nickel catalyst gives that output molar flow from a SMR unit is composed of 15% unreacted CH_4, 80% of CO, 6% of CO_2, and 280% of H_2. The net heat consumption $\dot{Q}_{SMR,net}$ from reactions (3.1) and (3.2) is calculated with Eq. (3.17), where $\dot{m}_{CH4}$the input flow of methane, x_{SMR} is the ratio that reacts in Eq. (3.1) and x_{CO2} is the flow ratio of CO_2 (6% of CH_4 input flow) that resulted from the water gas shift reaction (3.2).

$$\dot{Q}_{SMR,net} = \dot{m}_{CH4} \cdot Q_{SMR} \cdot (1 - x_{SMR}) + \dot{m}_{CH4} \cdot Q_{WGS} \cdot x_{CO2} \quad (3.17)$$

Hydrogen flow into the anode is the sum of hydrogen resulting from SMR and hydrogen from electrolysis. Hydrogen flow input is calculated with Eq. (3.18), which incorporates Eq. (3.15). Heat

generation in the anode Q_{an} is calculated next, using Eq. (3.19). The resulting gases from the SMR reactions are those shown in Fig. 3.2. Hydrogen molar flow is the sum of SMR output (282% of CH_4 input flow) plus the amount specified by the hydrogen addition ratio λ_{H2}. Molar flow of CO is the SMR output that did not undergo reaction (3.2) (80% of CH_4 input flow). T_{an} is the anode temperature. The fuel utilization factor U_f represents the share of the flow that reacts on the anode. Nernst voltage of the cell stack decreases rapidly at utilization factor >90%. At utilization factor of 100%, local gas concentration at the anode would become zero, resulting in a voltage of zero and thus no current would exist. The typical value for U_f is 85% [18].

$$\dot{m}_{H2} = \dot{m}_{elz} + \dot{m}_{CH4} \cdot x_{H2} = \frac{\lambda_{H2}}{Q_{LHV,H2}} \dot{Q}_{LHV,fuel} + \dot{m}_{CH4} \cdot x_{H2} \tag{3.18}$$

$$\dot{Q}_{an} = (\dot{m}_{H2} \cdot T_{an} \Delta S_{H2} + \dot{m}_{CH4} \cdot x_{WGS} \cdot T_{an} \Delta S_{CO}) \cdot U_f \tag{3.19}$$

Next, heat release Q_{CB} at the catalytic burner is calculated with Eq. (3.20). Unreacted methane from the SMR unit is burned, along the remaining flow of CO and H_2 coming out of the anode. Q_{com} is the heat of combustion of each component.

$$\dot{Q}_{CB} = \dot{m}_{CH4} \cdot x_{SMR} \cdot Q_{com,CH4} + \left(\dot{m}_{CH4} \cdot x_{WGS} \cdot Q_{com,CO} + \dot{m}_{H2} \cdot Q_{com,H2}\right) \cdot (1 - U_f) \tag{3.20}$$

Subsequently, air input into the preheater is calculated with Eq. (3.21). The amount of O_2 moles that need to react are 0.5 per reacting mole of each H_2 and CO, thus U_f is included. Excess air input λ_{air} is used to improve the Nernst voltage at the cell stack. Standard excess air input value is taken as λ_{air}=2. The heat needed to preheat air and fuel is then calculated with Eqs. (3.22) and (3.23), respectively, where C_p is the specific heat, T_{amb} is the ambient temperature (298 K), T_{air} and T_{fuel} are the temperatures to which air and fuel are heated, respectively.

$$\dot{m}_{air} = \frac{(\dot{m}_{H2} + \dot{m}_{CH4} \cdot x_{WGS}) \cdot U_f \cdot \lambda_{air}}{2 x_{O2}} \tag{3.21}$$

$$\dot{Q}_{air} = \dot{m}_{air} \cdot Cp_{air} \cdot (T_{air} - T_{amb}) \tag{3.22}$$

$$\dot{Q}_{fuel} = (\dot{m}_{elz} \cdot Cp_{H2} + \dot{m}_{CH4} \cdot Cp_{CH4}) \cdot \left(T_{fuel} - T_{amb}\right) \tag{3.23}$$

Heat recovered in the heat exchanger Q_{HEX} is calculated with Eq. (3.24). Specific heat C_p for each species is multiplied by their respective concentration in the exhaust flow $\dot{m}_{exh}$ times the temperature difference of the exhaust temperature T_{exh} and the heat exchanger outlet T_{out}.

$$\dot{Q}_{HEX} = \dot{m}_{exh}(Cp_{CO2} \cdot x_{CO2} + Cp_{H2O} \cdot x_{H2O} + Cp_{O2} \cdot x_{O2} + Cp_{N2} \cdot x_{N2}) \cdot (T_{exh} - T_{out}) \tag{3.24}$$

Heat losses of the system are taken as 3% of the higher heating value (HHV) of the fuel input [19], and are calculated with Eq. (3.25).

$$\dot{Q}_{loss} = \dot{Q}_{HHV,fuel} \cdot x_{loss} = \left(\dot{Q}_{HHV,CH4} + \dot{Q}_{HHV,H2}\right) \cdot x_{loss} \quad (3.25)$$

The net heat available for recovery $\dot{Q}_{total}$ in the system is the sum of heat flows as given in Eq. (3.26). Preheating of the gases, the SMR reaction and the heat losses are exothermic processes. Equations (3.17) through (3.26) were evaluated for the daily operation of the system. To validate the thermal model, actual heat recovery from the SOFC taken from Eq. (3.13) is used. Figure 3.11 shows the comparison between the model and the experimental data. The model goes in accordance with the results, although July and August show the highest disparity. This is attributed to the difference of data points used for analysis, as solar irradiation data for these months was only available from July 10th to July 31st, and August 1st to August 25th, resulting in an underestimation of fuel consumption. The same behavior had been present before when data points from September were low, and the model results were 11% below the experimental data. Increasing the data points for analysis improved the model results by 5%. Although the impact of hydrogen addition in heat recovery efficiency, discussed in Section 3.3, is not evident at the specified λ_{H2} of 20%, the amount of hydrogen generated by electrolysis presented in Section 3.4.3 suggests that for this system it would be difficult to generate higher volumes of hydrogen fuel unless a PV system of higher capacity is installed. Nevertheless, the utilization of hydrogen calculated in this analysis still present a reduction in primary energy consumption corresponding to a lower methane demand.

$$\dot{Q}_{total} = \dot{Q}_{an} + \dot{Q}_{CB} + \dot{Q}_{HEX} - \dot{Q}_{SMR,net} - \dot{Q}_{air} - \dot{Q}_{fuel} - \dot{Q}_{loss} \quad (3.26)$$

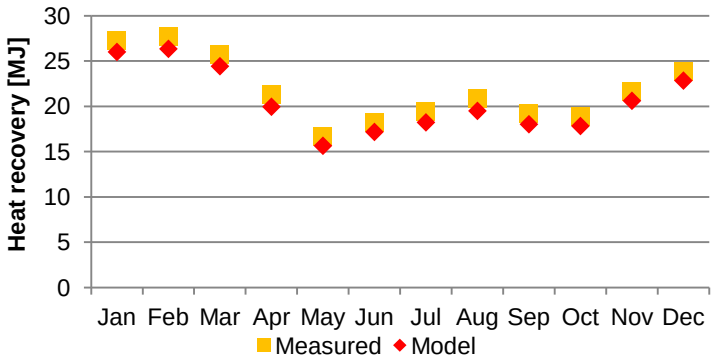

Figure 3.11. SOFC total heat recovery for hot water production.

3.4.5 PV-Battery system operation

The operation profile of the PV-Battery system for comparison was evaluated next. The power output data from a 3 kW array shown in Fig. 3.6 is also used for this system. A 5.5 kWh Lithium ion rechargeable battery stores surplus electricity when the PV array's output is higher than the demand.

Figure 3.12 shows a decision flowchart for battery charging and discharging, with respect to the maximum current permissible I_{max} and the state-of-charge (SOC) of the battery.

When demand W_{dem} is higher than the PV output W_{PV}, the battery is discharged to meet the demand. On the contrary case, the battery is recharged. Electricity going in and out of the battery is here defined as W_{batt}. When the minimum discharge limit P_{min} is set at 15% of the maximum capacity P_{max}, to avoid reducing the lifetime of the battery [20]. The maximum current I_{max} going in and out of the battery is limited to 1.4 kWh. The recharging efficiency is taken as 90%. If the net demand is higher than the energy stored in the battery, electricity from the grid W_{grid} is imported. When the current for recharging is above I_{max}, or when the battery has been charged to maximum capacity, additional power is not utilized. The excess energy W_{feed} may utilized for any other purpose (not discussed here), or be fed back into the grid, although feed-in tariffs are not considered into this study as the purpose is to minimize interaction with the grid. Using these criteria, operation of the system was modeled and total energy consumption was estimated. In this system, all hot water demand is supplied by a gas boiler using natural gas.

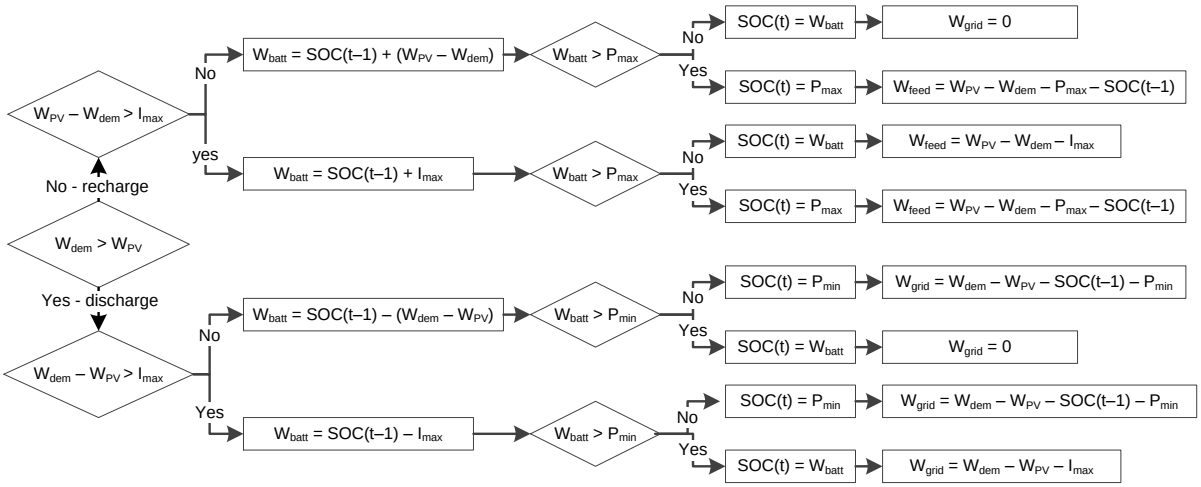

Figure 3.12. Decision flowchart for battery recharge/discharge operation.

3.4.6 Results and discussion

To compare the systems, primary energy consumption for each system was calculated. Primary energy consumption includes electricity from the power grid and natural gas consumed by each system. In the PV-SOFC system, electricity is imported when the demand surpasses the system's capacity, while natural gas is consumed at the SOFC and auxiliary boiler. In the PV-Battery system, electricity is imported from the grid when the demand is higher than the output current of the battery or when the SOC of the battery cannot meet the demand; natural gas consumption in this system

comes only from the gas boiler. In the conventional system, all electricity comes from the grid and all hot water is supplied by the gas boiler. The grid's efficiency was taken as 35% [21]. Figure 3.13 shows the primary energy consumption for each system. Both the PV-SOFC and PV-Battery systems are able to reduce consumption significantly. From June to September, the PV-SOFC benefits less from cogeneration as the hot water demand decreases, while the PV-Battery system benefits from the high solar PV output and lower natural gas demand. On the other hand, the PV-SOFC achieves higher savings on primary energy consumption during winter and shoulder seasons. Furthermore, the PV-Battery system remains highly dependent on the grid throughout the year. Grid dependency ratio of the PV-Battery system resulted in 36.4%, compared to a dependency ratio of 3.3% for the PV-SOFC system. Grid power consumption in the PV-SOFC system is due to high electric demand for air conditioning on the evening, which surpasses the SOFC's capacity of 0.7 kW. Electric demand in the shoulder seasons is always less than 0.7 kW and thus we see no grid consumption on these months for the PV-SOFC system. In the same way, grid power consumption in the PV-Battery system is due to the battery's limitations. Even when the PV array's output is high, the battery cannot store all the surplus electricity and thus this energy is not available for when the electric demand surpasses the PV power output. Figure 3.13 also shows the amount of excess electricity in the PV-Battery system that could be fed back into the grid (discussed in Section 3.4). Even if FIT were to be considered, the PV-Battery system would only benefit from them during summer, as excess energy is lower than grid consumption in winter and shoulder seasons.

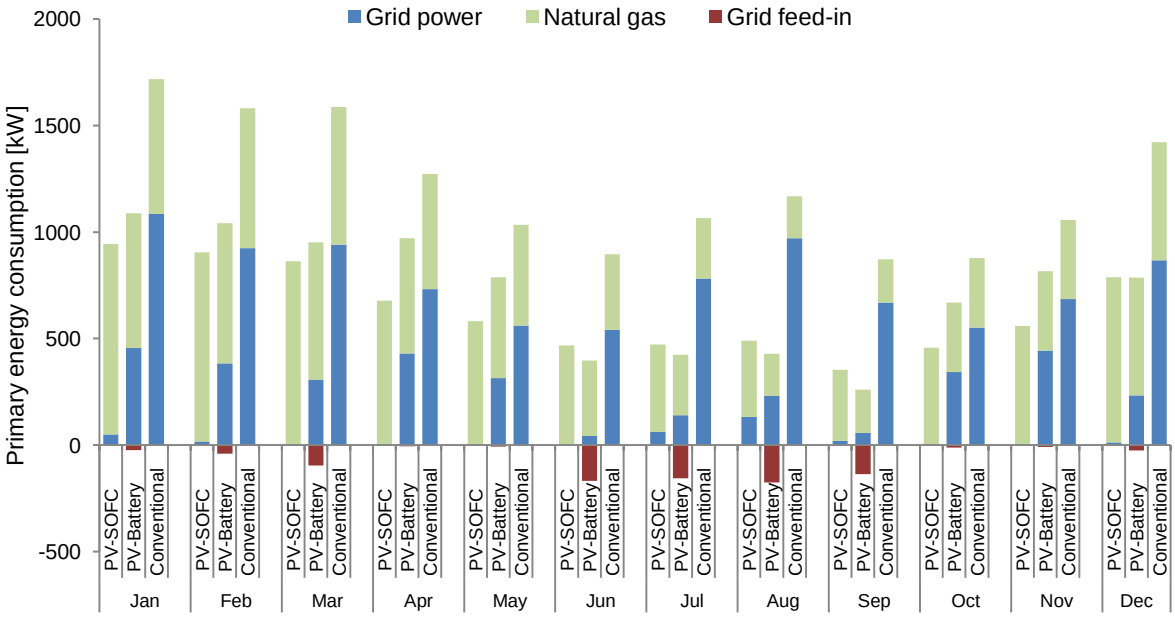

Figure 3.13. Primary energy consumption for each system.

3.4.7 Lifetime cost analysis

The impact of investment cost over energy savings ability was analyzed next. Table 3.4 shows the cost of the devices considered in systems PV-SOFC and PV-Battery, as well as their rated lifetime. Taking the SOFC's lifetime as base, both systems are compared on a 10 year period. In this case, the gas boiler in both systems and the battery would have to be replaced once. The subsidies available were also taken into account.

Table 3.4. Investment cost and subsidies for selected components [22-25].

Component costs [in Japanese Yen]			
	Cost	Lifetime	Subsidies
PV-SOFC			
PV array	¥1,650,000	20 years	¥ 90,000
SOFC	¥3,000,000	10 years	¥700,000
Electrolyzer	¥ 300,000	10 years	
Compressor	¥ 200,000	20 years	
Hydrogen tank	¥ 140,000	10 years	
Gas boiler	¥ 395,000	5 years	
PV-Battery			
PV array	¥1,650,000	20 years	¥ 90,000
Li-Ion battery	¥1,670,000	5 years	¥500,000
Gas boiler	¥ 395,000	5 years	

The operation costs during this period were consequently calculated. Current prices for electricity from the grid and natural gas for the selected region were utilized. Available economic plans for natural gas consumption in residential fuel cell systems were also considered [26]. Energy costs for the conventional system during the same period were calculated to estimate the savings related to energy consumption in PV-SOFC and PV-Battery systems. Figure 3.14 shows the accumulated costs for both of these systems. Operation costs for the conventional system during the 10 year period resulted in 1.56 million JPY. A Savings/Investment ratio was calculated with respect to the conventional system's operation costs, where the Savings is the difference between operation costs of each system against the conventional system, and the Investment is the sum of Initial investment and replacement costs during the 10 year period. As seen from Fig. 3.14, although the investment costs for the PV-SOFC system are higher, the achieved energy savings and the long lifetime of the components, place the PV-SOFC system slightly above the PV-Battery system regarding their Savings/Investment ratio. Furthermore, the high grid dependency of the PV-Battery system (explained in Section 3.4.6) demands a stable power grid infrastructure for which the costs are complicated to evaluate. In contrast, the PV-SOFC system has low dependency on the grid, and thus it may be possible to replace the grid connection with energy management measures in order to reduce the power peaks below the SOFC's output capacity.

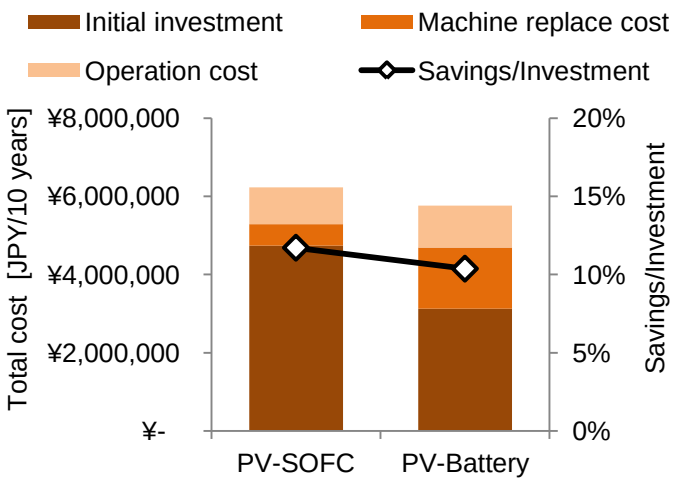

Figure 3.14. Initial investment and 10 year operation costs for PV-SOFC and PV-Battery systems.

3.5 Cogeneration systems for isolated micro-grids

Although the proposed residential cogeneration system presented high costs compared to systems with high grid dependence, access to the power grid is not available everywhere and several communities rely on expensive fossil fuel imports to meet their energy demands. In the southern region of Japan for example, close to 300,000 people live in remote islands without a land route to the main island, and over 99% of the power demand in these islands is supplied through internal combustion generators using fuel oil. Transporting fuel oil into each of these islands results in highly elevated electricity costs, and the oil imports into Japan that come from the Middle East represent a large carbon footprint for their current power generation system. Because of the high oil dependency of island communities, the availability of oil and its variable price puts serious pressure in the energy security of these areas. Therefore, it is important to consider a different approach to electrification of remote islands.

Several energy supply systems for residential sectors in isolated areas using DER have been previously studied, with systems that include wind turbine/diesel generator [27], wind turbine/fuel cells [28], wind turbine/solar PV/diesel generator [29], solar PV/fuel cell/hydrogen storage [30-32], solar PV/fuel cell/electric battery [33], wind turbine/solar PV/fuel cell/hydrogen storage/electric battery [34], biomass/solar PV/pico-hydro [35]. Although these studies agree on the viability of DER to supply energy in the residential sector, there is still a lack of studies that include basic infrastructure from the public sector, such as administrative offices, hospitals, schools, and buildings in the commercial sector. Energy demands in these sectors have different magnitudes and patterns than the residential sector, and may also have abrupt changes in their demand loads. Nayar's study on DER for remote islands in the Republic of Maldives [29] covers energy demands from all sectors in the

community, but in this case we see that diesel fuel still remains a major contributor for meeting those demands.

Hydrogen fuel offers an alternative to minimize oil dependency for remote islands, while providing a reliable infrastructure that can quickly respond to changes in energy demands. Although natural gas is currently the main source for generating hydrogen, it can also be generated through water electrolysis using surplus energy from renewable energies or nighttime electricity from base load power plants, as well as from reforming biogas and industrial waste products [36-38]. Although hydrogen generation capacity using this method may not be enough to meet the demands of large cities, it may be sufficient for island communities. Hydrogen may be generated on-site at each island, or generated at the main islands and transported if the demand is high, allowing the system in this way to provide energy on-demand.

In this regard, a hydrogen fueled micro-grid is proposed for power generation in islands. Since these areas have no access to power generated at large scale power plants, their grid independence is considered initially to be 100%, and the purpose of this micro-grid is to shift the dependence on imported oil-products into locally generated hydrogen-fuel. The goal of this micro-grid is then to operate with minimal hydrogen consumption while meeting all energy demands, corresponding to the size of the micro-grid. To achieve this, the required capacity of the micro-grid components and their operating schedule present a problem of mathematical optimization.

3.5.1 Structure of the hydrogen fueled micro-grid

The structure of the proposed micro-grid is illustrated in Fig. 3.15, and it is as follows. The main electric generation system is installed on a central facility, which is taken as any building from the commercial or public sector. This central facility is connected to a number of residences through a power grid, in which electricity is shared. For the main electric generation system, a fuel cell system composed of a Solid Oxide Fuel Cell (SOFC) and a Polymer Electrolyte Fuel Cell (PEFC) is used. The part-load generation efficiency of SOFCs decreases rapidly as part-load operation decreases. Meanwhile, the PEFC's generation efficiency is less affected by the operating load. Therefore, in the considered micro-grid a SOFC is used as the base load generator and the PEFC as the variable load generator. Although using two fuel cell systems may represent increased installation and maintenance costs, smaller capacity systems and the potential savings in energy consumption are expected to offset these costs. Such configuration has been proposed in previous researches [16]. Furthermore, prolonged operation of PEFCs at minimum loads has been reported to cause degradation in the anode, thus maintenance costs may be reduced as well by using the two-fuel cell configuration [39]. Both fuel cells produce exhaust heat at high temperatures from which thermal energy may be extracted.

This exhaust heat is utilized to meet the thermal energy demands of the facility. Part of the exhaust gas flow is used in a Heat Exchanger (HEX) to produce hot water for the facility. The rest of the exhaust gas is used in an Absorption Chiller-Heater (ACH) for air conditioning purposes in the facility. Integration of ACH systems with fuel cells can be found elsewhere [40]. Should the ACH not be able to meet the required demands, the model considers the use of electric Heat Pumps (HP) to cover the rest of the demand.

For each of the residences, an area of 25 m^2 is considered as the average installation area in Japan for residential solar energy systems: Solar Photovoltaics (PV) and Solar Heat Collectors (HC). Solar irradiation generally resembles more the daily power load for commercial buildings than that for residences. On the other hand, the spatial distribution of residences can usually offer a much larger area than what commercial buildings can. Roof rental [41] is a strategy currently in use by non-residential sectors to take advantage of the area that households offer for solar energy systems. Although larger scale solar energy systems could be installed in the island to lower primary energy consumption, they are not included as part of the optimization problem. The area ratio of PV to HC that is to be installed on the residences is decided by the model. Electricity produced by PV is fed into the micro-grid and hot water obtained from the HC is stored in residential hot water tanks. Heat Pump Water Heaters (HPWH) in each residence supply hot water to the residential hot water tanks in addition to the HC. Residential air conditioning demands are met only through electric HP. If the amount of electricity generated in the micro-grid is higher than the total demand, surplus electricity is used to generate hydrogen gas in a water electrolyzer, which is used as the fuel for the fuel cell system. The amount of hydrogen net imports into the micro-grid is then calculated as the total hydrogen fuel consumption needed by the fuel cell system to meet the demands, minus the amount of hydrogen generated through electrolysis.

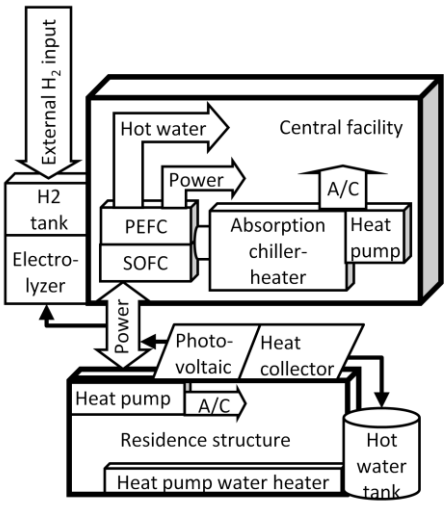

Figure 3.15. Basic structure of the proposed micro-grid for areas without access to the main power grid.

3.5.2 Implementation scheme

The structure of the micro-grid is designed for a single facility in the commercial or public sector. In order to supply the entire community through the proposed system, several of these micro-grids will need to be installed. This strategy is believed to present the following benefits:

- The proposed micro-grid can be installed gradually, without the need to commit to large scale infrastructural changes. Such changes require large investments that are difficult to justify given the scale of the community in isolated areas. During actual implementation and trial phases, the reliability of the power grid needs to be ensured to customers. The proposed micro-grid structure is able to function while connected to the main power grid before it can transition into stand-alone operation. Once the micro-grid exhibits successful results, implementation of the proposed structure into other areas can follow.
- Single micro-grids are expected to show relatively low hydrogen fuel demands, which gives time for the hydrogen supply infrastructure to develop and grow. Expecting to fully provide a large community with hydrogen fuel without reliable supply channels would most likely result in failure and a waste of resources. Since the proposed micro-grid can operate independently, small amounts of hydrogen can be supplied during the implementation and trial phases without the need for large investments beforehand.
- The gradual growth of installed micro-grids allows for the transition of hydrogen tanks into hydrogen pipelines. Although hydrogen pipelines have been successfully implemented in some areas such as California, they have done so as a result of extensive research and economic analyses that justify their high costs. For the proposed micro-grid, hydrogen tanks seem to be the rational choice for hydrogen supply during the initial implementation phases. However, as the number of micro-grids increases, the amount of resources required to maintain the hydrogen tanks increases as well. At this point, the number of customers that require a hydrogen supply could justify the transition into hydrogen pipelines. In contrast to complex city structures like in California, isolated areas generally present straightforward circuits or coastlines that can simplify the costs for the installation of hydrogen pipelines.
- The proposed micro-grid structure decreases hydrogen distribution points compared to residential fuel cell systems. When the objective of isolated communities is to minimize their dependence on fossil fuels, residences are expected to be left out without a supply of natural gas as well. A hydrogen supply infrastructure that includes every single residence would inevitably result in high investment costs. Thus it may not be possible to install the fuel cell system for residences with access to the grid presented in Section 3.4. On the other hand, retaining the current energy supply system based on centralized generation does not allow the implementation of cogeneration systems, as distribution of heat resources has a low efficiency in areas without high population density. With the proposed micro-grid structure, hydrogen

fuel needs only be supplied to central facilities, where cogeneration can be applied to maximize the system's efficiency. Furthermore, residential energy demands can be met solely through an electric grid, which for islands does not imply high transmission losses.

In isolated areas such as islands, it is safe to assume that the number of commercial and public sector buildings is never higher than the number of households, therefore it is expected that in the proposed micro-grid structure, a number of households will be available for each central facility to balance the energy loads. Implementation of the proposed micro-grid is considered to occur in the following sequence:

1. Initial trial: a single facility is selected for implementation of the micro-grid. The fuel cell cogeneration system generates heat that is utilized in the facility, and power generated is fed into the existing grid.
2. Household integration: the proposed residential structure is implemented in the number of residences that the optimization model suggests, and their energy demands are measured to ensure they match the expected values.
3. Independent operation: the micro-grid is allowed to operate without connection to the grid to ensure that all energy demands are being met.
4. Additional trials: other micro-grids are fully implemented and tested for reliability.
5. Widespread implementation: once the micro-grids have proven to be reliable, further implementation is expected as long as the budget and hydrogen supply capacity allow.
6. Transition into hydrogen pipelines: in order to avoid the costs and space requirements of hydrogen tanks, hydrogen supply through pipelines should be considered. Ideally this would happen at the end of lifetime of the current hydrogen tanks to prevent additional investments.

3.6 Conclusions

This chapter begins with a proposal, modeling and analysis for a residential cogeneration system utilizing fuel cells and solar energy for Japanese households. The following conclusions have been drawn from this study:

(1) Hydrogen energy storage from surplus solar energy can be effectively implemented for use in cogeneration fuel cell systems in Japanese households to minimize dependence from the main power grid.

(2) Hydrogen addition into methane fueled SOFC systems has an effect on heat recovery and electric generation efficiencies. Increased hydrogen addition to the system results in a higher heat to power output ratio.

(3) Compared to solar PV systems utilizing electric batteries for energy storage, the proposed SOFC cogeneration system with solar PV and hydrogen storage achieves much higher independence from the power grid.

(4) An economic analysis for the proposed system shows that installation costs result higher than the solar PV and battery system. However, the benefits from grid independence are described in detail.

Finally, finalizes with the proposal for a micro-grid consisting on cogeneration fuel cell systems and solar PV, which can operate with full independence from the main power grid. The high costs from current DER technologies are expected to become more competitive in areas without access to the main power grid that rely on expensive and inefficient energy supply systems.

3.7 References

[1] Maidment, G.G. and Prosser, G. (2000). The use of CHP and absorption cooling in cold storage. *Applied Thermal Engineering*, 20, 1059-73.

[2] Onovwiona, H.I. and Ugursal, V.I. (2006). Residential cogeneration systems: review of the current technology. *Renewable and Sustainable Energy Reviews,* 10, 389-431.

[3] Larminie, J. and Dicks, A. (2003). *Fuel Cell Systems Explained*. England: Wiley.

[4] Moghaddam, A.A., Seifi, A., Niknam, T. and Alizadeh Pahlavani, M.R. (2011). Multi-objective operation management of a renewable MG (micro-grid) with back-up micro-turbine/fuel cell/battery hybrid power source. *Energy*, 36, 6490-507.

[5] Stambouli, A.B. and Traversa, E. (2002). Solid oxide fuel cells (SOFCs): a review of an environmentally clean and efficient source of energy. *Renewable and Sustainable Energy Reviews,* 6, 433-55.

[6] Tsay, D. (2003). Feasibility Study of Fuel Cell Residential Energy Stations. (Master's thesis). Massachusetts Institute of Technology.

[7] Mahlia, T.M.I. and Chan, P.L. (2011). Life cycle cost analysis of fuel cell based cogeneration system for residential application in Malaysia. *Renewable and Sustainable Energy Reviews,* 15, 416-26.

[8] Thijssen, J.H.J.S. (2007). The Impact of Scale-Up and Production Volume on SOFC Manufacturing Cost. *National Energy Technology Laboratory*.

[9] Liu J.A. (2006). Kinetics, catalysis and mechanism of Methane steam reforming. (PhD Thesis). Worcester Polytechnic Institute.

[10] Saarinen, J., Halinen, M., Ylijoki, J., Noponen, M., Simell, P. and Kiviaho, J. (2007). Dynamic Model of 5 kW SOFC CHP Test Station. *Journal of Fuel Cell Science and Technology*, 4 (4), 397-405.

[11] Japan Photovoltaic Energy Association. (2010). Shipment of Photovoltaic modules in Japan. Retrieved May 1, 2016 from http://www.jpea.gr.jp/pdf/qlg2010_eng.pdf

[12] Kashiwagi, T. (2002), Natural Gas Cogeneration Plan/ Design Manual 2002, *Japan Industrial Publishing Co., LTD*, 64-9.

[13] Horie, H. and Hihara, E. (2012). Study on Annual Performance of Room Air Conditioners under Partial Load Condition. *International Refrigeration and Air Conditioning Conference 2012*, Paper 1336.

[14] Lamas, J., Shimizu, H., Matsumura, E. and Senda, J. (2013). Fuel consumption analysis of a residential cogeneration system using a solid oxide fuel cell with regulation of heat to power ratio. *International Journal of Hydrogen Energy*, 38, 16338-43.

[15] Apfel, H., Rzepka, M., Tu, H. and Stimming, U. (2006). Thermal startup behavior and thermal management of SOFC's. *Journal of Power Sources*, 154, 370-78.

[16] El-Sayed, A.G. and Obara, S. (2010). Power Generation Efficiency of Photovoltaics and a SOFC-PEFC Combined Micro-grid with Time Shift Utilization of the SOFC Exhaust Heat. *International Power Electronics Conference 2010*, 2629-36.

[17] Jensen, J.O., Li, Q. and Bjerrum, N.J. (2010). The Energy Efficiency of Different Hydrogen Storage Techniques. *Energy Efficiency*, Jenny Palm (Ed).

[18] Singhal, S. and Kendall, K. (2003). *High-temperature Solid Oxide Fuel Cells: Fundamentals, Design and Applications*. Oxford: Elsevier Science Ltd.

[19] Braun, R.J., Klein, S.A. and Reindll, D.T. (2006). Evaluation of system configurations for solid oxide fuel cell-based micro-combined heat and power generators in residential applications. *Journal of Power Sources*, 158, 1290–305.

[20] Jossen, A., Garche, J. and Sauer, D.U. (2004). Operation conditions of batteries in PV applications. *Solar Energy*, 76, 759-69.

[21] Masahiro, O. (2004). *Technology of on-site energy supply*. Japan: Kaibundo publishing; 3-16. (In Japanese).

[22] Amos, W.A. (2014). Costs of Storing and Transporting Hydrogen. *National Renewable Energy Laboratory NREL/TP-570-25106*.

[23] Kyocera Corporation. (2014). Development completion of Residential Fuel Cell (SOFC) and beginning of sales of "Ene-Farm type S". (In Japanese). Retrieved May 1, 2016 from http://www.kyocera.co.jp/news/2012/0305_yuki.html

[24] NEC Corporation. (2014). Lithium Ion Rechargeable Battery Equipment for Residential Storage Systems. (In Japanese).

[25] Daikin Corporation. (2014). Daikin Eco-Cute. (In Japanese). Retrieved May 1, 2016 from http://www.daikinaircon.com/sumai/alldenka/ecocute/

[26] Osaka Gas. (2014). My home generation fees: Contracts for residential cogeneration systems. (In Japanese). Retrieved May 1, 2016 from http://home.osakagas.co.jp/price/menu/profitable/p_01.html

[27] Abbey, C. and Joos, G. (2009). A stochastic optimization approach to rating of energy storage systems in wind-diesel isolated grids. *IEEE Transactions on power systems*, 24, 418-26.

[28] Ntziachristos, L., Kouridis, C., Samaras, Z. and Pattas, K. (2005). A wind-power fuel-cell hybrid system study on the non-interconnected Aegean islands grid. *Renewable Energy*, 30, 1471-87.

[29] Nayar, C., Tang, M. and Suponthana, W. (2008). Wind/PV/Diesel Micro Grid System implemented in Remote Islands in the Republic of Maldives. *IEEE International Conference on Sustainable Energy Technologies 2008*.

[30] Paul, B. and Andrews, J. (2008). Optimal coupling of PV arrays to PEM electrolysers in solar-hydrogen systems for remote area power supply. *International Journal of Hydrogen Energy*, 33, 490-98.

[31] Brinkhaus, M., Jarosch, D. and Kapischke, J. (2011). All year power supply with off-grid photovoltaic system and clean seasonal power storage. *Solar Energy,* 85, 2488-96.

[32] Elamari, M.M. (2011). Optimisation of Photovoltaic-Powered Electrolysis for Hydrogen production for a remote area in Libya. (PhD thesis). University of Manchester.

[33] Morais, H., Kadar, P., Faria, P., Vale, Z.A. and Khodr, H.M. (2010). Optimal scheduling of a renewable micro-grid in an isolated load area using mixed-integer linear programming. *Renewable Energy*, 35, 151-6.

[34] Kyriakarakos, G., Dounis, A.I., Rozakis, S., Arvanitis, K.G. and Papadakis, G. (2011). Polygeneration microgrids: A viable solution in remote areas for supplying power, potable water and hydrogen as transportation fuel. *Applied Energy*, 88, 4517-26.

[35] Kumaravel, S. and Ashok, S. (2012). An Optimal Stand-Alone Biomass/Solar-PV/Pico-Hydel Hybrid Energy System for Remote Rural Area Electrification of Isolated Village in Western-Ghats Region of India. *International Journal of Green Energy*, 9, 398-408.

[36] Dincer, I. (2012). Green methods for hydrogen production. *International Journal of Hydrogen Energy*, 37, 1954-71.

[37] Onozaki, M., Watanabe, K., Hashimoto, T., Saegusa, H. and Katayama, Y., Hydrogen production by the partial oxidation and steam reforming of tar from hot coke oven gas. *Fuel*, 85, 143-9.

[38] Gutiérrez-Martín, F., García-De María, J.M., Bairi, A. and Laraqi, N. (2009). Management strategies for surplus electricity loads using electrolytic hydrogen. *International Journal of Hydrogen Energy*, 34, 8646-475.

[39] Yamazaki, O., Oomori, Y., Shintaku, H. and Tabata T. (2007). Study on Degradation of the Pt-Ru Anode of PEFC for Residential Application (2): Analyses of the MEAs Degraded in the Anode Performance. *ECS Transactions*, 11, 287-95.

[40] Margalef, P. and Samuelsen, S. (2010). Integration of a molten carbonate fuel cell with a direct exhaust absorption chiller. *Journal of Power Sources*, 195, 5674-85.

[41] Shanmugavalli, K. R. and Vedamuthu, R. (2015). Viability of solar rooftop photovoltaic systems in group housing schemes. *Current Science*, 108, 1080-5.

Chapter 4. Mathematical optimization

4.1 Introduction

In this chapter, an introduction to mathematical optimization is presented, followed by a description of the optimization model designed for isolated micro-grids. Section 4.2 gives a description of mathematical optimization, followed by an introduction to the General Algebraic Modeling System and the Branch-and-Reduce optimization navigator for solution of problems with global optima. A model based on this optimization methodology is described in Section 4.3, with the intent to solve the energy supply problem for isolated areas described in Chapter 3.

4.2 Mathematical Optimization

4.2.1 Optimization overview

Mathematical optimization is a methodology used for the solution of complex decision and allocation problems. Optimization involves the decision of several interrelated variables for which the value of a single objective variable can be maximized or minimized, depending on the nature of the problem. More advanced problems may involve functions of equality and/or inequality constraints, as well as variable bounds. As the complexity of the problem increases, it becomes nearly impossible for optimization methods alone to provide a single absolute solution to the problem. Instead, optimization provides a good approximation to the sought value, as long as suitable parameters are utilized. Optimization is regarded a valuable tool for conceptualization and analysis of a problem that involves the understanding of the problem and critical analysis and interpretation of results.

Mathematical optimization can be mainly divided into two types of problems: linear and nonlinear. In linear programming, the objective and related variable have a linear relation, and the equality or inequality constraint are linear as well. Linearity in the problems is generally easier to solve than nonlinearities in regards of processing power. Linearization of apparently nonlinear problems is thus a major stage in this methodology. However, complete linearization is not always possible and thus optimization for nonlinear problems has also been an area of extensive study. In nonlinear problems, the geometric nature of optimization problems becomes evident, in particular, the convexity of the data sets that are analyzed. Convexity is defined in [1] as: “A point $\mathbf{x}$ in a convex set C is said to be an *extreme point* of C if there are no two distinct points $\mathbf{x}_1$ and $\mathbf{x}_2$ in C such that $\mathbf{x} = \alpha\mathbf{x}_1 + (1 - \alpha)\mathbf{x}_2$ for some α, $0 < \alpha < 1$.” Convex points thus represent the maxima and minima of problems, and the number of feasible solutions that the program for optimization can find depends on the specified range for analysis. In practice, many nonlinear problems will be composed of discrete decisions and nonlinear system dynamics. Solutions to such problems can be found utilizing Mixed Integer Nonlinear Programming (MINLP). A mixed integer nonlinear problem can be given by an n

dimensional vector **P** of design parameters, an objective function *f*(**P**), where *f*: $\mathbb{R}^n \rightarrow \mathbb{R}$, and a vector function **G**: $\mathbb{R}^n \rightarrow \mathbb{R}^m$ returns an *m* length vector containing the equality and inequality constraints evaluated at **P**. The problem is given in the following form, considering parameter bounds $\mathbf{P}_l$ and $\mathbf{P}_u$.

$$\text{minimize/maximize } f(\boldsymbol{P}) \in \mathbb{R}$$

$$\text{subject to}$$

$$G_i(\boldsymbol{P}) = 0, \qquad i = 1, \dots, m_e$$

$$G_i(\boldsymbol{P}) \leq 0, \qquad i = m_e + 1, \dots, m$$

$$\boldsymbol{P}_l \leq \boldsymbol{P} \leq \boldsymbol{P}_u$$

It is worth noting that not all problems can be guaranteed to have convexity. Software for the solution of nonlinear problems in MINLP can be found for both convex and non-convex problems. All MINLP solvers generally involve some sort of tree search, such as the one presented in Fig. 4.1 [2]. Many of these solvers have been made for implementation in the General Algebraic Modeling System (GAMS) framework.

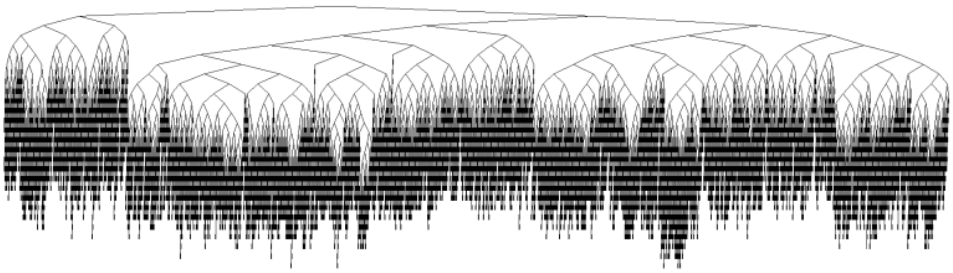

Figure 4.1. Branch-and-bound tree without presolve after 360 s CPU time has more than 10,000 nodes [2].

4.2.2 GAMS framework

The General Algebraic Modeling System (GAMS) was a framework funded by the World Bank and developed around the decade of the 1970's by mathematical economists as a way to standardize the method in which problems of development were addressed over different sectors. The GAMS language structure consists of series of simple algebraic statements and the utilization of sparse data structures that can translate complex mathematical problems into easy to interpret sequential programs that can be easily modified or upgraded to fit different scenarios. GAMS was the first algebraic modeling system, and it is designed to solve large scale linear, nonlinear and mixed integer optimization problems. Although the commercially available GAMS releases have the capacity to solve most optimization problems, it is also compatible for use with other solvers that are able to handle problems with different natures. An extensive list of these solvers and their descriptions are presented in Table 4.1.

Table 4.1. Currently available solvers compatible with GAMS (non-exhaustive list).

Solver	Description
ALPHAECP	MINLP solver based on the extended cutting plane (ECP) method
AMPL	A link to solve GAMS models using solvers within the AMPL modeling system
ANTIGONE 1.1	Deterministic global optimization for MINLP
BARON 16.3	Branch-And-Reduce Optimization Navigator for proven global solutions
BDMLP	LP and MIP solver that comes with any GAMS system
BENCH	A utility to facilitate benchmarking of GAMS solvers and solution verification
CBC 2.9	High-performance LP/MIP solver
CONOPT 3	Large scale NLP solver
CONVERT	Framework for translating models into scalar models of other languages
COUENNE 0.5	Deterministic global optimization for (MI)NLP
CPLEX 12.6	High-performance LP/MIP solver
DECIS	Large scale stochastic programming solver
DICOPT	Framework for solving MINLP models
EXAMINER	A tool for examining solution points and assessing their merit
GLOMIQO 2.3	Branch-and-bound global optimization for mixed-integer quadratic models
GUROBI 6.5	High performance LP/MIP solver
IPOPT 3.12	Interior Point Optimizer for large scale nonlinear programming
JAMS	Solver to reformulate extended mathematical programs (incl. LogMIP)
KESTREL	Framework for using remote NEOS solvers with a local GAMS system
KNITRO 10.0	Large scale NLP solver
LGO	A global-local nonlinear optimization solver suite
LINDOGLOBAL 9.0	MINLP solver for proven global solutions
LINGO	A link to solve GAMS models using solvers within the LINGO modeling system
LOCALSOLVER 6.0	Hybrid neighborhood local search solver
LS	A Linear Regression Solver for GAMS
MILES	MCP solver
MINOS	NLP solver
MOSEK 7	Large scale LP/MIP plus conic and convex non-linear programming system
MSNLP	Multi-start method for global optimization
NLPEC	MPEC to NLP translator that uses other GAMS NLP solvers
OQNLP	Multi-start method for global optimization
OsiCplex	Bare-Bone link to CPLEX
OsiGurobi	Bare-Bone link to Gurobi
OsiMosek	Bare-Bone link to Mosek
OsiSoplex	High-performance LP solver
OsiXpress	Bare-Bone link to Xpress
PATHNLP	Large scale NLP solver for convex problems
PATH	Large scale MCP solver
PYOMO	A link to solve GAMS models using solvers within the PYOMO modeling system
SBB	Branch-and-Bound algorithm for solving MINLP models
SCIP 3.2	High-performance Constraint Integer Programming solver
SNOPT	Large scale SQP based NLP solver
SULUM 4.3	Large scale LP/MIP solver
XA	Large scale LP/MIP solver
XPRESS 28.01	High performance LP/MIP solver

4.2.3 Branch and Reduce Optimization Navigator

Problems in mathematical optimization often involve the selection of initial values that can find the local minima or maxima under specific bounds. However, some problems exhibit a large number of global optima that may not be easily found with common local search methods for constrained optimization. Load balancing and energy optimization, such as the energy allocation among components in the micro-grid structure described in Chapter 3, Section 3.5.1 of this thesis, have been regarded as problems that require global optimization. On one hand, constrained optimization can change the operating load of the energy components in the micro-grid over their capacity ranges. But on the other hand, global optimization recognizes that components may be shut down, such as the water electrolyzer having no surplus energy to operate or the PEFC being shut down because the SOFC can cover alone the base-load. Global optimization is also able to decide when is the best time to operate residential HPWH to charge the tank beforehand, as well as deciding which ratio of SOFC to PEFC capacity and PV to HC area is best. Therefore, a global optimization solver is regarded as the appropriate solver method for the current problem.

In Table 4.1 we can see that there are a few global optimization solvers available that are compatible with GAMS. From these solvers, the Branch and Reduce Optimization Navigator (BARON) has been regarded as being the fastest and most robust one. BARON is fast solver with high accuracy in correctly identifying feasible solutions [3]. GAMS models using BARON for micro-grid optimization has been previously utilized in other studies as well [4-6]. The solving algorithm for BARON is illustrated in Fig. 4.2. We can see here that the algorithm includes only two decision steps before branching, to check if the node is between the specified bounds. Infeasibility of the solution is identified during preprocessing and discarded if no solution is found. To solve the discrete and continuous parts of the problem, BARON makes use of other commercial solvers included in Table 4.1, which the users can select themselves.

Another advantage from the BARON solver is that initial values are not needed in order to find a feasible solution, unlike many other nonlinear programming algorithms. BARON initializes variables automatically and may even override user specified boundaries if the specified starting point cannot be evaluated. BARON is also able to operate without certain variable bounds, in which case BARON will try to search for possible bounds by itself unless told otherwise. Although in this case, the feasible solutions found cannot be guaranteed to represent global optima. Preprocessing in BARON eliminates an extensive amount of variable ranges, decreasing total computation time and increasing the likelihood of finding high quality local optima, from which the branching navigation can begin after preprocessing.

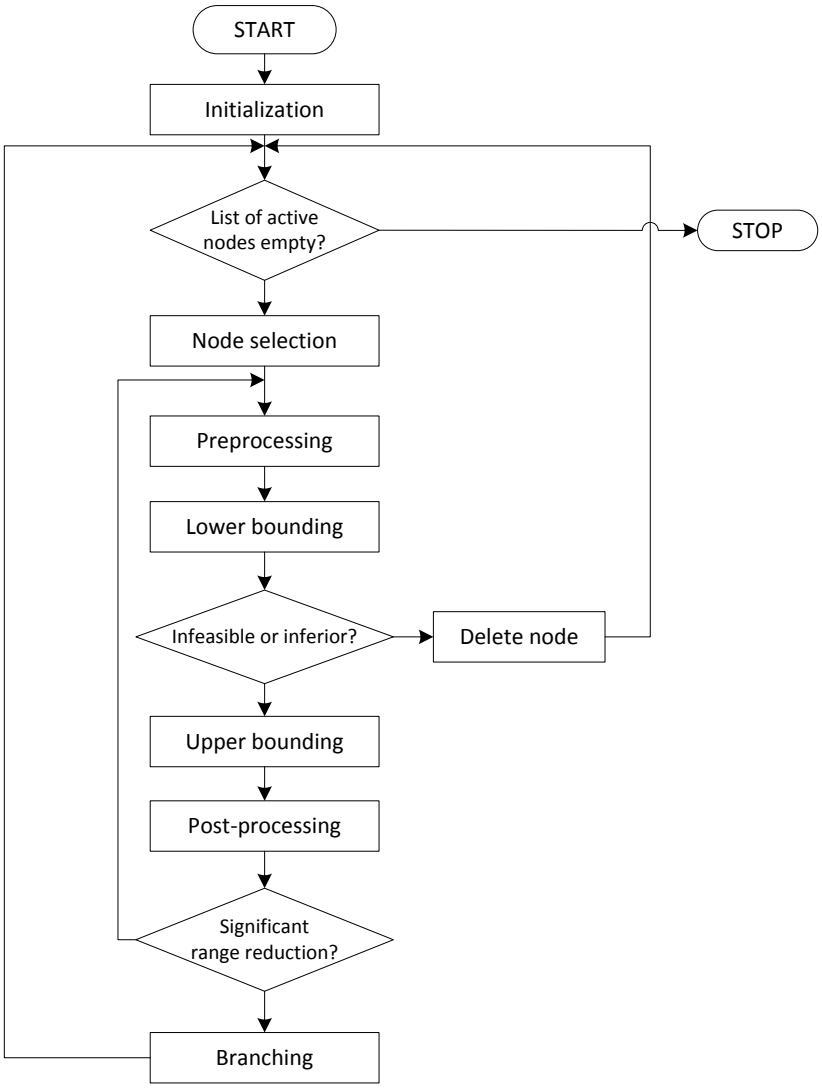

Figure 4.2. Main steps in the BARON solver algorithm.

4.3 Model for the proposed micro-grid

A model is built to find the optimum size and operation schedule of each component in the proposed micro-grid described in Chapter 3, Section 3.5.2. The objective of the optimization program is to minimized hydrogen consumption per household, through the selection of the component capacities and their optimum operation profiles. The model is written in GAMS, using BARON as the solver for this problem. The solver requires that all variables and expressions be bounded on both ends. The final model used in this thesis in the GAMS programming language is presented in Appendix A. The optimization model utilizes three sets of data input: central facility energy demands, residential energy demands, and solar irradiation in the selected region. The model is divided into four main blocks.

1. Electric load balance: the electric loads in the grid are first balanced to calculate total electric energy demands. Only in this step is there interaction between the facility and the residences. The added output of the fuel cells and the residential solar PV systems are balanced against the input energy demands plus the added electric demands for the residential and facility heat pumps.
2. Residential hot water balance: hot water in the residence is supplied by the solar HC and the HPWH. As the charge of the hot water tank is calculated, the needed electricity for the HPWH is adjusted on the first block.
3. Facility hot water and air conditioning balance: once that the operating loads of the SOFC and PEFC are established, the corresponding output of exhaust heat for both fuel cells is calculated. The heat output is balanced against the facility demands and the needed electricity for the facility HP is adjusted on the first block as well.
4. Hydrogen consumption: the available surplus electricity is calculated here, and with it the possible output from the electrolyzer. Hydrogen consumption is calculated from the fuel cell's demand minus the available hydrogen generated from surplus power.

It is worth noting that this block structure is purely for interpretation purposes if the reader wishes to implement it in other programming languages. GAMS/BARON coding does not take into account the order in which the algebraic expressions are defined, as it creates its own interpretation of the program before execution.

4.3.1 Optimization model

First, the solar energy output from PV and HC is calculated from the solar irradiation available on the selected region, using Eq. (4.1) and (4.2) [7]. For Eq. (4.1), W_{PV} [kWh] denotes solar PV electric output, KC_{PV} is the monthly temperature correction factor, KD_{PV} is the power density of the panels (0.140 kW/m^2), A_{PV} [m^2] is the total area covered by solar PV, Irr [kWh/m^2] is the hourly solar irradiation, and G_S is the solar irradiation intensity at standard test conditions (1 kWh/m^2). For Eq. (4.2), Q_{HC} [kWh] is the thermal power output of solar HC, KC_{HC} is the correction factor taken as 0.44, and A_{HC} [m^2] is the total area covered by solar HC. For consistency, all further units of energy, including electricity, thermal demands and fuel heat content, will be expressed in terms of kWh.

$$W_{PV(h,m)} = KC_{PV(m)} \cdot KD_{PV} \cdot A_{PV} \cdot Irr_{(h,m)} / G_S \tag{4.1}$$

$$Q_{HC(h,m)} = KC_{HC} \cdot A_{HC} \cdot Irr_{(h,m)} \tag{4.2}$$

(1) Electric load balance.

The total electric energy demand of the micro-grid W_{Tdem} is calculated with Eq. (4.3), where W_{RdemE} is the electric demand of a single residence, W_{HPWH} is the additional electricity consumed by residential HPWHs, W_{FdemE} is the total electric demand of the facility, and W_{FHP} is the additional electricity consumed when HP are needed in the facility. The indexes *h* and *m* are hour and month respectively. Consecutive days in each month are represented as cumulative hours from previous days.

$$W_{TdemE(h,m)} = (W_{RdemE(h,m)} + W_{HPWH(h,m)}) \cdot N_R + W_{FdemE(h,m)} + W_{FHP(h,m)} \quad (4.3)$$

Considering the case when solar PV output is zero, the combined size of the fuel cells is required to cover the value of the highest peak of electric demand. Their added capacity is defined to be greater than the maximum value of W_{TdemE}, as Eq. (4.4) shows. $W_{SOFCsize}$ and $W_{PEFCsize}$ are the SOFC and PEFC rated capacities, respectively.

$$W_{SOFCsize} + W_{PEFCsize} \geq W_{TdemE(h,m)} \quad (4.4)$$

Since the SOFC is used to cover the base load demand, its electric and thermal energy outputs are always constant. PEFC operation is then scheduled to cover the rest of the electric demand as given in Eq. (4.5). Here, the SOFC electric output and the respective hourly solar PV output of the micro-grid are subtracted from the electric demand to calculate the required output of the PEFC, W_{PEFC}. The PEFC output is upper bound by the previously determined capacity $W_{PEFCsize}$, as given in Eq. (4.6).

$$W_{PEFC(h,m)} \geq W_{TdemE(h,m)} - W_{PV(h,m)} \cdot N_R - W_{SOFCsize} \quad (4.5)$$

$$W_{PEFC(h,m)} \leq W_{PEFCsize} \quad (4.6)$$

An auxiliary variable W_{Grid} is used to keep track of the total electricity available in the micro-grid. W_{Grid} is calculated with Eq. (4.7) as the sum of the PEFC and SOFC's electric output and the solar PV's output multiplied by the number of residences in the micro-grid.

$$W_{Grid(h,m)} = W_{PEFC(h,m)} + W_{SOFCSize} + W_{PV(h,m)} \cdot N_R \quad (4.7)$$

(2) Residential hot water balance.

Residential hot water supply is met through Eqs. (4.8) to (4.17), where Q_{prov} is the amount of heat that can be provided at time *(h,m)*, Q_{HPWH} is the heat output of the HPWH, Q_{FromTK} is the hot water that is supplied from the hot water tank. $Q_{Rdem,HW}$ is the residential hot water demand, Q_{in} is hot water that came into the tank, Q_{out} is hot water that goes out of the tank, and Q_{loss} are heat losses from the water stored in the tank. The amount of hot water consumed Q_{HPWH} in Eq. (4.10) is that of the residential

demand, plus hot water that is sent to the tank Q_{ForTK}. Hot water production and consumption are balanced with Eq. (4.11). Energy losses from extracting hot water from the tank are taken from the tank's supply efficiency η_{outTK}. In the same way, heat losses that would arise from sending hot water to the tank are taken from the tank's charging efficiency η_{inTK}, while η_{decay} is the tank's insulation efficiency. Hot water amount that goes out of the tank and amount that is used for consumption, and water that is reserved for storage and sent to the tank are related through the tank's maximum and minimum flow capacities, η_{MaxIn} and η_{MaxOut}, respectively, which depend on the tank's volumetric capacity V_{Tank}. To calculate the corresponding electrical input for the HPWH, the coefficient of performance for the HPWH is defined as COP_{HPWH}. Electricity needed to supply the residential HPWH is calculated with Eq. (4.17).

$$Q_{prov(h,m)} = Q_{HC(h,m)} + Q_{HPWH(h,m)} + Q_{FromTK(h,m)} \tag{4.8}$$

$$Q_{RHWTank(h,m)} \leq Q_{RHWTank(h-1,m)} + Q_{in(h,m)} - Q_{out(h,m)} - Q_{loss(h,m)} \tag{4.9}$$

$$Q_{cons(h,m)} = Q_{Rdem,HW(h,m)} + Q_{ForTK(h,m)} \tag{4.10}$$

$$Q_{cons(h,m)} = Q_{prov(h,m)} \tag{4.11}$$

$$Q_{FromTK(h,m)} = Q_{out(h,m)} \cdot \eta_{outTK} \tag{4.12}$$

$$Q_{in(h,m)} = Q_{ForTK(h,m)} \cdot \eta_{inTK} \tag{4.13}$$

$$Q_{loss(h,m)} = Q_{Rdem,HW(h-1,m)} \cdot \eta_{decay} \tag{4.14}$$

$$Q_{Rdem,HW(h,m)} \leq Q_{Rdem,HW(h-1,m)} + V_{Tank} \cdot \eta_{MaxIn} \tag{4.15}$$

$$Q_{out(h,m)} \leq V_{Tank} \cdot \eta_{MaxOut} \tag{4.16}$$

$$W_{HPWH(h,m)} = Q_{HPWH(h,m)} / COP_{HPWH} \tag{4.17}$$

(3) Facility hot water and air conditioning balance.

For the facility case, hot water demand is considered to be low enough to be constantly supplied by fuel cell exhaust heat recovery, thus no storage is considered in the model. The constraint for facility hot water supply is given in Eq. (4.18), where Q_{FHW} is the hot water output at the facility, and Q_{FdemHW} is the hot water demand. The remaining energy in the exhaust heat is used in an ACH for air conditioning. The amount of heat that may be used for this purpose is constrained in Eq. (4.19), where Q_{ACH} is the heat input to the ACH and Q_{recFC} is the amount of heat that can be recovered from the fuel cells. In this equation, the variable *Exh* represents the unused exhaust heat from the fuel cells that is

released into the environment. Without this variable, the model would force the ACH to utilize all recovered heat despite the lack of demand, resulting in a large calculated ACH capacity and thus increased installation costs. The constraint in Eq. (4.20) ensures that the facility air conditioning demands are met. Here, COP_{ACH} is the ACH's coefficient of performance. Q_{HP} is the heat output from HP in the facility, and Q_{demFAC} is the facility's air conditioning demands. The annual performance factor (APF) of the facility HP is defined in the variable *APF*. Electricity needed to supply the facility HP is calculated with Eq. (4.21).

$$Q_{FHW(h,m)} \geq Q_{FdemHW(h,m)} \tag{4.18}$$

$$Q_{recFC(h,m)} = Q_{FHW(h,m)} + Q_{ACH(h,m)} + Exh_{(h,m)} \tag{4.19}$$

$$Q_{ACH(h,m)} \cdot COP_{ACH} + Q_{HP(h,m)} \geq Q_{FdemAC(h,m)} \tag{4.20}$$

$$W_{FHP(h,m)} = Q_{HP(h,m)} / APF \tag{4.21}$$

The total heat recovery from the fuel cells is calculated with Eq. (4.22), where $\eta_{SOFC,Th}$ is the heat recovery rate of the SOFC, $\eta_{PEFC,Th}$ is the heat recovery rate of the PEFC, and η_{HEX} is the HEX's heat recovery efficiency. Dividing the electric output by its electric efficiency gives the energy input, which multiplied by the thermal efficiency gives the total heat output.

$$Q_{recFC(h,m)} = \left(\frac{W_{SOFCSize}}{\eta_{SOFC}} \cdot \eta_{SOFC,Th} + \frac{W_{PEFC(h,m)}}{\eta_{PEFC}} \cdot \eta_{PEFC,Th} \right) \cdot \eta_{HEX} \tag{4.22}$$

(4) Hydrogen consumption.

During daytime when solar PVs are active, surplus electricity may be generated if the total output is higher than the total electric demand. In this case, a water electrolyzer is used to generate hydrogen gas which will be used as fuel for the fuel cells. The maximum amount of surplus electricity W_{Surp} is given from Eq. (4.23)

$$W_{Surp(h,m)} = W_{Grid(h,m)} - W_{TdemE(h,m)} \tag{4.23}$$

From the surplus electricity, fuel heat content of the hydrogen generated by the electrolyzer $Q_{H2,elz}$ is calculated using Eq. (4.24), where η_{elz} and η_{HTank} are the electrolyzer and the hydrogen storage tank's efficiencies, respectively.

$$Q_{H_2,elz(h,m)} = W_{Surp(h,m)} \cdot \eta_{elz} \cdot \eta_{HTank} \tag{4.24}$$

The total hydrogen consumption by the fuel cells is calculated subsequently. Since the fuel cell's output is dictated by the electric demand, the fuel input is calculated through their energy conversion efficiency. The SOFC is operated with a constant output, considering an electric efficiency η_{SOFC}. The PEFC's electric efficiency varies with respect to its partial load operation, from 26% at low loads, 30% at half load, to 32% at maximum output [8, 9]. Recent PEFC units report full-load efficiencies as high as 49% [10]. This efficiency curve may be approximated with a 3rd grade polynomial equation with the load as the independent variable. However, implementing such function in the BARON solver results in much larger computation times and requires additional variable bounds. In this study, PEFC efficiency η_{PEFC} was considered to be constant. Total hydrogen consumption by the grid $Q_{H2,bought}$ is then calculated with Eq. (4.25).

$$Q_{H_2,bough(h,m)} \geq \frac{W_{SOFCSize}}{\eta_{SOFC}} + \frac{W_{PEFC(h,m)}}{\eta_{PEFC}} - Q_{H_2,elz(h,m)} \tag{4.25}$$

4.3.2 Constraints

The model equations given in Section 4.3.2 are complemented with other constraints, in addition to the already presented inequalities related to the thermal energy demands (*i.e.*, hot water supply and air conditioning). As previously mentioned, this program considers exclusively the residential roof area A_{Roof} for installation of solar HC and PV. This forces the model to consider the tradeoffs from increasing PV output by increasing the number of residences, versus the added energy demands from doing so. Also, it allows the model to decide whether it is better to lose PV capacity by adding solar HC for hot water production, or maximize PV output despite the increased loads on residential HPWH. The area utilized for PV and HC panels is then constrained by Eq. (4.26).

$$A_{PV} + A_{HC} \leq A_{Roof} \tag{4.26}$$

Power input into the electrolyzer W_{Surp} also needs to be constrained by the electrolyzer's capacity Elz_{Cap}, as the inequality in Eq. (4.27) shows.

$$W_{Surp} \leq Elz_{Cap} \tag{4.27}$$

Additional constrains involve the upper and lower bounds from the currently unbounded variables. These variables are N_R, V_{Tank}, W_{HPWH}, $SOFC_{Size}$ and $PEFC_{Size}$. Their lower bounds can be set to zero by defining the variables as positive, but the upper bound must be selected by the user.

4.3.3 Objective function

Finally, the objective function of the problem is defined as Eq. (4.28). Minimization of $Q_{H2,bought}$ alone would imply a minimum number of N_R, since lower base energy demands directly result in reduced primary energy consumption. With this function, the model is expected to balance the addition of residences to increase in energy consumption they entail. The final size of the micro-grid will be the result of by the calculated number of residences and the size of the central facility. Although many studies focus on the minimization of costs in the objective function [11-13], the variability in costs of DER technologies and hydrogen fuel are regarded as parameters that are better studied in a separate analysis. With the minimization of hydrogen consumption of the micro-grid, fuel generation, storage and transport costs are expected to substantially reduce the total system's costs.

$$\text{Minimize: } Q_{H2,RES} = \frac{Q_{H_2,bought}}{N_R} \tag{4.28}$$

4.4 Conclusions

In this chapter, an optimization model for the semi-independent micro-grid proposed in Chapter 3 is presented. First, the basics of mathematical optimization have been explained, and the utilization of the GAMS framework for developing the model is justified. The robustness and speed of the BARON solver for finding global optimality make this the favored algorithm for implementing in the model. The structure, constraints and input parameters for the model are described in detail. The objective function for the optimization model minimizes the amount of external hydrogen input that is needed to operate the proposed micro-grid with absolute zero shortages of energy supply. The capacity of the energy supply in the system is expected to fully meet energy demands even when solar energy is unavailable. The minimal input parameters of the system allow the model to be easily implemented for any kind of energy demands without the need to modify the model equations.

4.5 References

[1] Luenberger, D.G. and Ye, Y. (2008). *Linear and Nonlinear Programming*. Hillier F.S. (Ed.). New York: Springer.

[2] Belotti, P., Kirches, C., Leyffer, S., Linderoth, J., Luedtke, J. and Mahajan, A. (2012). Mixed-Integer Nonlinear Optimization. *Argonne National Laboratory ANL/MCS-P3060-1112*.

[3] Neumaier, A., Schcherbina, O., Huyer, W. and Vinkó, T. (2005). A comparison of complete global optimization. *Mathematical programming*, 103 (2), 335-56.

[4] Bando, S., Watanabe, H., Asano, H., and Tsujita, S. (2009). Impact of various characteristics of electricity and heat demand on the optimal configuration of a microgrid. *Electrical Engineering in Japan,* 169 (2), 6-13.

[5] Bando, S. and Asano, H. (2013). Optimal capacity sizing of an energy supply system in a microgrid by considering the effect of backup contract and scale economy. *Intelligent Automation & Soft Computing*, 16 (2), 273-87.

[6] Higuchi, Y., Nakayama, S., Saito, A., Matsumura, E. and Senda, J. (2015). Environmental evaluation of a combined system composed of micro grid and district heating and cooling. *Transactions of the JSME,* 81, Paper 14-00448. (In Japanese).

[7] NEDO. (2015). New Energy and Industrial Technology Development Organization, Meteorological Test Data for Photovoltaic Systems (METPV-11). *Department of the New Energy and Industrial Technology Development Organization.*

[8] Koyanagi, H., Mori, N., Murakami, S., Saito, M., Ichihashi, T., Watanabe, K. and Fukao, H. (2005). Study on Planning Method of Polymer Electrolyte Membrane Fuel Cells (PEFC) - Evaluation of Economical Efficiency at Residential House-. *Report of Taisei Technology Center*, 38, 1-8. (in Japanese).

[9] Goto, R., Hamada, Y., Kubota, H., Nakamura, M., Kuwabara, K., Ochifuji, K. and Murase, M. (2006). Study on residential cogeneration systems in cold regions. *The Society of Heating, Air-Conditioning Sanitary Engineers of Japan,* 3, 1793-6. (in Japanese).

[10] Yang, C., Moon, S. and Kim, Y. (2015). A self-operated polymer electrolyte fuel cell system operating at dead-end conditions using pure hydrogen and oxygen gases. *Journal of Mechanical Science and Technology,* 29 (8), 3541-7.

[11] Kyriakarakos, G., Dounis, A.I., Rozakis, S., Arvanitis, K.G. and Papadakis, G. (2011). Polygeneration microgrids: A viable solution in remote areas for supplying power, potable water and hydrogen as transportation fuel. *Applied Energy,* 88, 4517-26.

[12] Abbey, C. and Joos, G. (2009). A stochastic optimization approach to rating of energy storage systems in wind-diesel isolated grids. *IEEE Transactions on power systems,* 24, 418-26.

[13] Moghaddam, A.A., Seifi, A., Niknam, T. and Alizadeh Pahlavani, M.R. (2011). Multi-objective operation management of a renewable MG (micro-grid) with back-up micro-turbine/fuel cell/battery hybrid power source. *Energy,* 36, 6490-507.

Chapter 5. Optimization of isolated micro-grids

5.1 Introduction

In this Chapter, the micro-grid optimization model described in Chapter 4 is simulated using two regions in Japan for analysis. Section 5.2 begins with an explanation the selected regions, followed by a description of the input parameters utilized in the model. The simulation results are presented in Section 5.3, including optimized size of micro-grid components, individual component operating schedule, and fuel savings compared to the conventional energy supply system. In Section 5.4, the results from implementing an alternative objective function that reduces computation time are presented. The same variables of interest from Section 5.3 are presented for this case, and their results are compared to evaluate their differences. Finally, an additional brief discussion of the simulation results is included in Section 5.4.

5.2 Model simulations

The micro-grid optimization model described in Chapter 4, Section 4.3 is now tested using actual input parameters from two regions in Japan. The southern region of Kyushu and the central region of Kansai were selected for analysis. In northern regions with colder climates, heat to power demand ratio becomes increasingly high compared to the two selected regions. Furthermore, snow in the winter prevents the solar systems to function properly, which corresponds to a large fraction of energy input in the proposed micro-grid structure. Also, the unavailability of roads during this season may not permit allow for a reliable fuel supply channel when it is needed most. For these reasons, northern Japanese regions are not considered during this study.

The electricity, air conditioning and hot water demands for a common residence and an office type facility are obtained from [1], for the regions of Kansai and Kyushu. These energy demands are given with respect to the total floor area of the building in the form of kilowatt per square meter. Therefore in this study, floor area is utilized as a primary variable to represent the size of the facility. Nevertheless, the input parameters for the developed optimization model are only energy demands and solar irradiation, thus if a particular facility needs to be analyzed, its actual energy demands may be utilized regardless of its total floor area. Regarding the residential energy demands, all residences are considered to be identical, representing a four person household with a total floor area of 120 m^2. Due to the large amount of households that needs to be considered, therefore it is impractical and resource consuming to specify their individual energy demands. However, this also allows the combined residential area to share their energy fluctuations enough for their average energy demands to be considered fairly stable. Figure 5.1 shows the energy demands for three months representative of the seasons (*i.e.*, January, May and August). During analysis, all months from January to December

are taken into account. In the proposed micro-grid structure, residential air conditioning demands are covered exclusively using electric HP. Thus energy demands for air conditioning have been included in the electric demand considering HP with an annual performance factor of 5.9 [2]. For this simulation, an office type building is selected for the central facility. The total floor space of the office is varied from 100 m^2 to 1000 m^2 during analysis. Electric, hot water, heating, and cooling demands for a 100 m^2 office building are presented in Fig. 5.2, for three January, May and August [1]. The same energy demands of the facility are used for both regions.

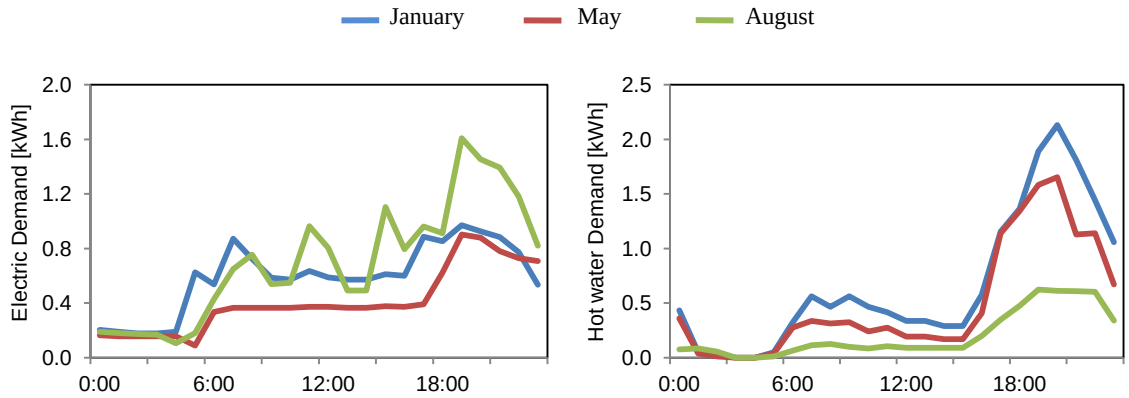

a) Kansai

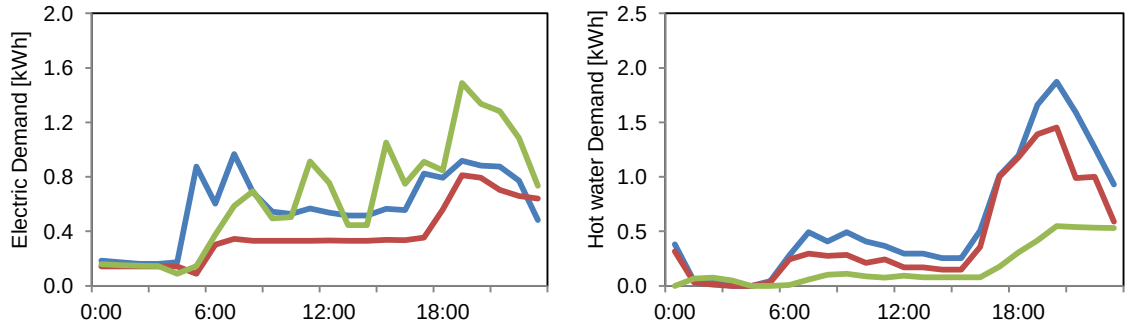

b) Kyushu

Figure 5.1 Residential daily electric and hot water demands for three representative months (January, May and August) in Kansai and Kyushu. These demands correspond to a 120 m^2 four person household.

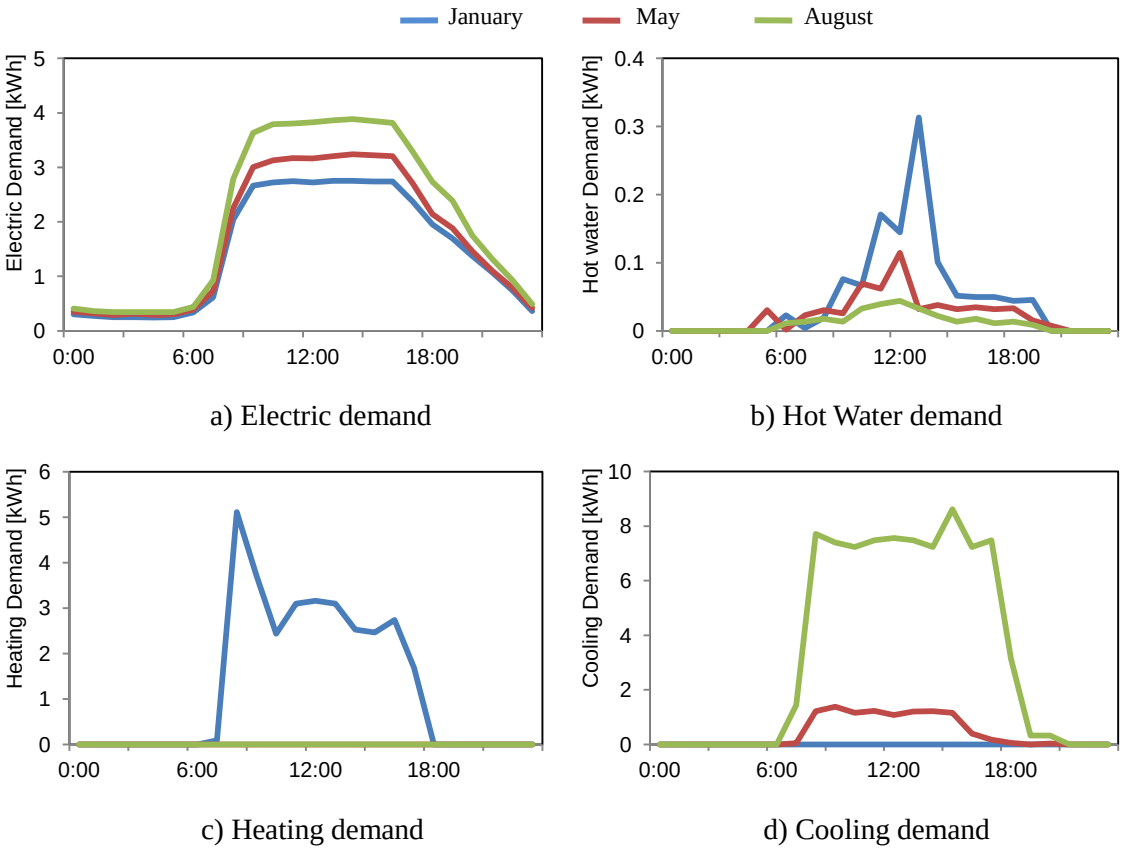

a) Electric demand

b) Hot Water demand

c) Heating demand

d) Cooling demand

Figure 5.2. Daily energy demands for a 100 m^2 office type building during three representative months (January, May and August). Energy demands scale linearly with the facility floor area.

The output from solar PV and HC is calculated using the solar irradiation data for Kansai and Kyushu regions [3]. Solar irradiation together with the energy demands are the only external inputs considered in this model. Figure 5.3 shows the average daily solar irradiation for three months in each region, representative of the different seasons. During analysis, all months from January to December are taken into account. Using this solar irradiation data, Solar PV and HC output is calculated with Eq. (5.1) and (5.2) [4]. For Eq. (5.1), W_{PV} [kWh] denotes solar PV electric output, KC_{PV} is the monthly temperature correction factor, shown in Table 5.1, KD_{PV} is the power density of the panels (0.140 kW/m^2), A_{PV} [m^2] is the total area covered by solar PV in one residence, Irr [kWh/m^2] is the hourly solar irradiation, and G_S is the solar irradiation intensity at standard test conditions (1 kWh/m^2). For Eq. (5.2), Q_{HC} [kWh] is the thermal power output of solar HC, KC_{HC} is the correction factor taken as 0.44, and A_{HC} [m^2] is the total area covered by solar HC in one residence. Total roof area of a single household is considered to be 25 m^2, corresponding to the typical area of a solar PV residential array in Japanese residences.

$$W_{PV} = KC_{PV} \cdot KD_{PV} \cdot A_{PV} \cdot Irr / G_S \tag{5.1}$$

$$Q_{HC} = KC_{HC} \cdot A_{HC} \cdot Irr \tag{5.2}$$

Table 5.1. Monthly temperature correction factor KC_{PV} for solar PV output calculation, for Kyushu and Kansai.

	Jan	Feb	Mar	Apr	May	Jun	Jul	Aug	Sep	Oct	Nov	Dec
Kansai	0.92	0.91	0.90	0.87	0.86	0.85	0.83	0.82	0.84	0.87	0.89	0.91
Kyushu	0.91	0.91	0.90	0.88	0.86	0.86	0.83	0.82	0.84	0.87	0.88	0.91

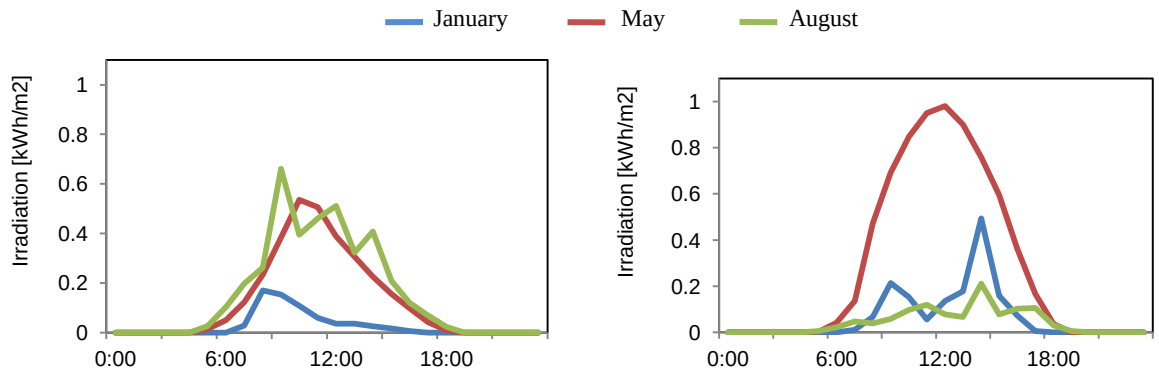

a) Kansai b) Kyushu

Figure 5.3. Daily solar irradiation for Kansai (a) and Kyushu (b) during three representative months (January, May and August). The low irradiation seen in Kyushu for August is attributed to unfavorable weather.

The capacity and efficiency of the DER devices specified in the micro-grid structure are specified next. These values are common for all simulations and represent those values of commercially available products or feasible targets for the near future. Table 5.1 shows the selected values for the ACH, HP, SOFC, PEFC, Electrolyzer (ELZ), and the hydrogen tank.

Table 5.2. Constant parameters used in the optimization model [5-10].

Electrolyzer maximum capacity [kW]	150
Electrolyzer efficiency	80%
Hydrogen tank efficiency	90%
Absorption chiller-heater maximum capacity [kW]	175
Absorption chiller-heater APF [-]	1.45
Electric heat pump APF [-]	5.9
Heat pump water heater maximum capacity [kW]	1.5
Residential hot water tank capacity [L]	300
Heat pump water heater COP [-]	2.2
SOFC efficiency	45% (electric), 40% (heat recovery)
PEFC efficiency	35% (electric), 55% (heat recovery)

The simulation results are to be compared against the conventional energy supply system, in order to evaluate the capability of the proposed micro-grid to reduce primary energy consumption. In the conventional energy supply system, all electricity is obtained through the main power grid. The electric efficiency of the grid, considering generation, transmission and distribution losses, is estimated to be 35% [11]. Hot water supply in the conventional system is entirely obtained through gas water boilers with a generation efficiency of 80%. Air conditioning is supplied through electric heat pumps with an APF of 5.9, identical to that considered for the proposed micro-grid.

5.3 Simulation results

5.3.1 Minimize hydrogen consumption

The model was run using the energy demands and the solar irradiation data for Kansai and Kyushu discussed in Section 5.2. In this section, the results utilizing the objective function to minimize hydrogen consumption are presented. In order to reduce computation time, only five days per month were used to account for the daily variability in solar irradiation. The size of the micro-grid is determined with the resulting values of the scalar variables N_R, A_{PV}, A_{HC}, $SOFC_{Size}$ and $PEFC_{Size}$. Vector variables were those used to obtain the operating schedule of the components. All variables were defined as positive, setting their lower bound to zero. The initial values and bounds defined are given in Table 5.3. The linear solver used was CPLEX, and the nonlinear solver was MINOS. Computation time was limited to 72 hours, although all simulations were solved within one to ten hours.

Table 5.3. Initial values and limits utilized in the optimization model.

Variable	Initial value	Lower limit	Upper limit
N_R [-]	2	1	100
A_{PV} [m^2]	15	1	24
A_{HC} [m^2]	10	1	24
$Q_{RHWTank}$ [kWh]	1	0	30
Q_{HPWH} [kWh]	N/A	1	3

First, the model's results regarding hydrogen consumption and the optimized capacity for each component are presented. Figure 5.4 shows the model results of annual hydrogen consumption per household, for a constant size facility of 1000 m^2 and varying number of residences. The trend shows that hydrogen consumption per household decreases as the number of residences increases, although the decrease ratio is lower at higher number of residences. This occurs as the burden of hydrogen consumption by the facility is distributed among an increasing number of residences of the grid. As en economic strategy, this would allow the facility to do away with energy expenses and in exchange provide management and maintenance of the system. The figure also shows that a small SOFC size is enough to manage the base load. The increasing size of the PEFC with the number of residences is

expected, as the total electric demand increases. The ratio of SOFC size to PEFC size is maintained relatively constant at 10%. Regarding the PV to HC area ratio, the model results show no apparent trend with respect to the number of residences. However, it does seem to maintain constant over a value of 75%, with an average of 86% in Kansai and 89% in Kyushu, suggesting that dedicating a portion of the roof area for installing HC does help in decreasing hydrogen consumption by decreasing the electric load on the residential HPWH.

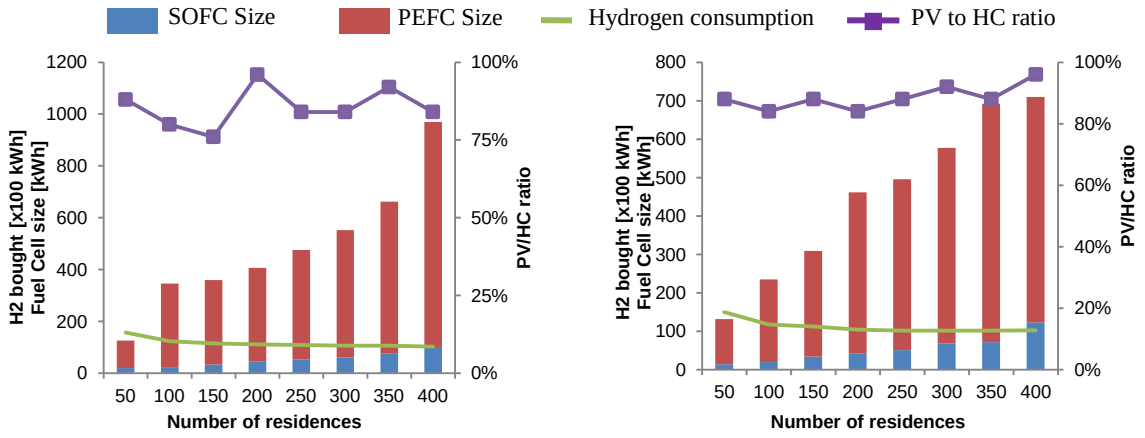

a) Kansai b) Kyushu

Figure 5.4. Variation of annual H_2 consumption per household, fuel cell size, and PV/HC ratio for a 1000 m^2 facility.

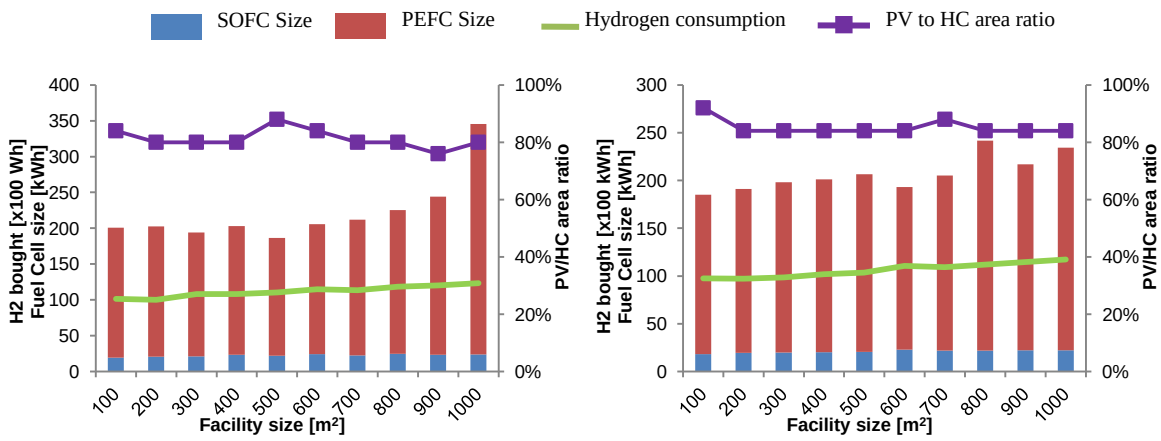

a) Kansai b) Kyushu

Figure 5.5. Variation of annual H_2 consumption per household, fuel cell size, and PV/HC ratio for a 100 residence grid in Kansai (a) and Kyushu (b).

Figure 5.5 shows the annual hydrogen consumption per household in the case of a 100 residence grid with increasing facility size the Kansai (a) and Kyushu (b) regions. In both cases, hydrogen consumption seems to increase with higher facility size, which is expected as well as the electricity demands increases. The increase in facility size also shows no apparent effect on the SOFC to PEFC

size, and PV to HC area ratios. Since these ratios were independent of the micro-grid size, they may be used as a benchmark to estimate the capacity needed for any micro-grid size while using the model to evaluate the operating profile of the additional grid components.

Furthermore, because the total hydrogen consumption per household is minimized at the highest number of residences and lowest facility floor area, the model will only give the results at these conditions. To obtain the hydrogen consumption at different cases, the respective limits were varied for each case. During actual implementation of the proposed micro-grid, the amount of residences and commercial sector buildings, as well as their spatial distribution, should then be taken into account to apply the appropriate boundaries for the model.

Next, the simulation results regarding the operation schedule for each component in the micro-grid are presented. Operation scheduling has been considered a valuable tool for management and control of micro-grids, and it has been included in other models as well [12]. To illustrate the seasonal differences, only the first day of the months of January, May and August were selected for comparison. Figure 5.6 shows the obtained operating profile of the electric components (*i.e.*, PEFC, SOFC, PV and Electrolyzer). These graphs correspond to a 50 residence grid and a 1000 m^2 area facility, in both the Kansai (a) and Kyushu (b) regions.

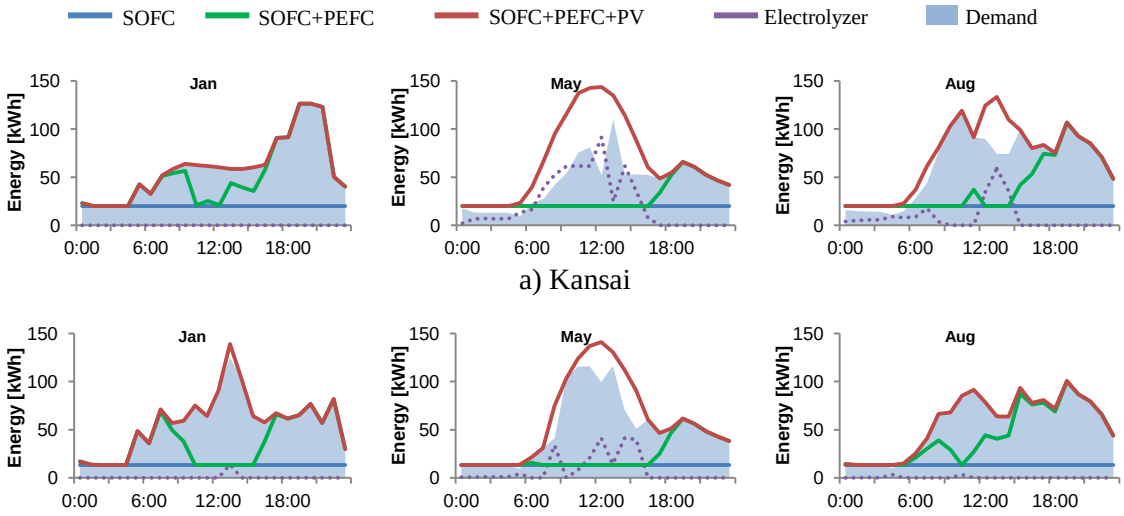

a) Kansai

b) Kyushu

Figure 5.6. Operation schedule for the micro-grid's electric components, for one day in each representative month in the Kansai (a) and Kyushu (b) regions.

From these results we can observe the capacity factor achieved by each component. The capacity factor is the ratio between the actual capacity utilized and the maximum available capacity. A low capacity factor in a specific component would suggest that its impact is minimal on the total operation of the micro-grid and thus should be avoided, so as to not induce additional costs. For the 50 residence and 1000 m^2 facility micro-grid in the Kansai region, the calculated annual capacity factors corresponding to the PEFC, PV and Electrolyzer are, respectively, 17%, 14% and 6%. For the same

micro-grid in the Kyushu region, the calculated annual capacity factors are 18% for the PEFC, 14% for PV and 5% for the electrolyzer. Since SOFC operates as the base-load at full capacity, capacity factor is always 100%. However, the power output from the SOFC is still higher than the demand in certain seasons, in which case the surplus energy is sent into the electrolyzer, as we can see in the graph for August in Fig. 5.6 (a). In both regions, the capacity factors for PEFC, PV and the electrolyzer were very similar. Although these capacity factors may be regarded as low, we can see that the model favors immediate energy consumption as opposed to energy storage, which helps reduce energy losses. Furthermore, since the difference between the minimum and maximum energy demand is high, a low capacity factor is expected. What is more important is to observe whether the electrolyzer is being utilized at all, and compared to the PEFC and PV capacity factors, we can see that the electrolyzer does in fact contribute to the optimum use of energy. In fact, the calculated capacity factor of the electrolyzer reaches a maximum of 18% in May in the Kansai region, while the PEFC capacity factor in the same month decreases to 9%. In the Kyushu region, electrolyzer capacity factor reaches its maximum of 12% in October, while the PEFC capacity factor for this month decreases to 10%.

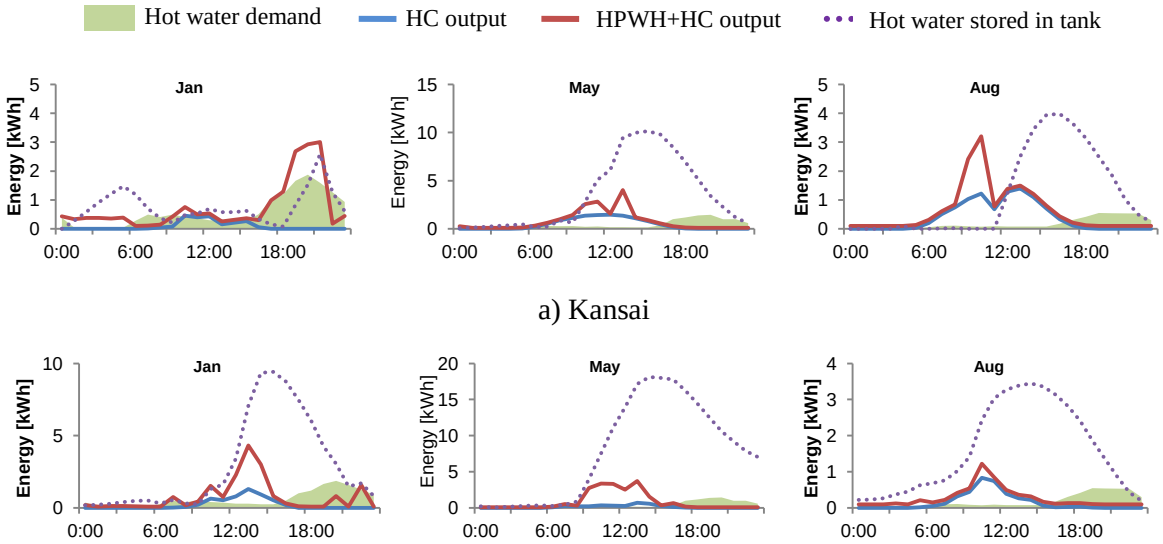

a) Kansai

b) Kyushu

Figure 5.7. Scheduled operation for the residences' thermal components, for one day in each representative month in the Kansai (a) and Kyushu (b) regions.

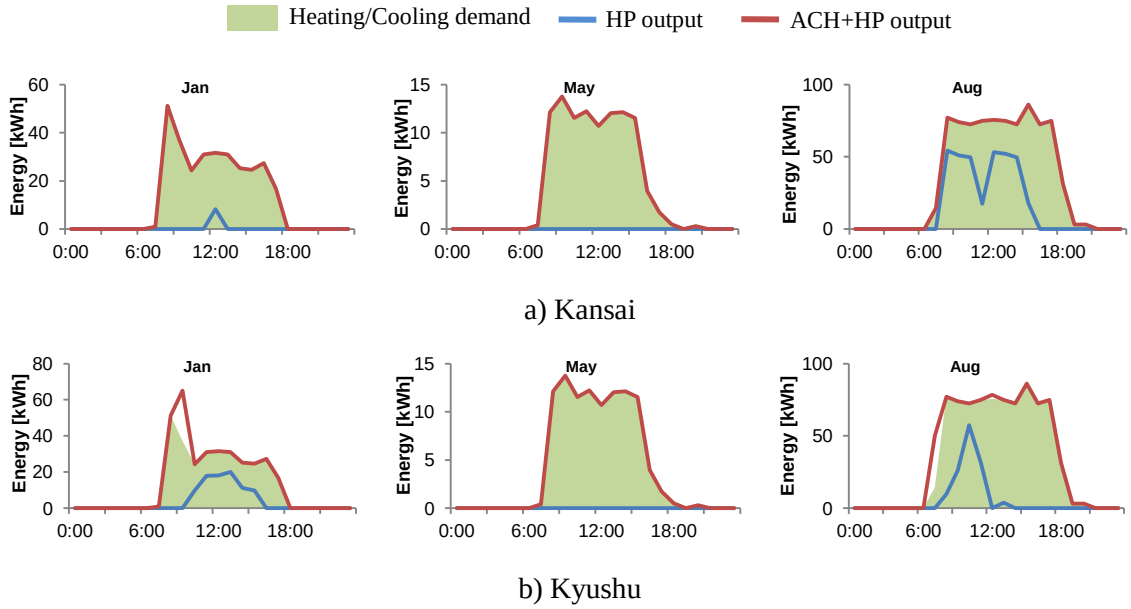

a) Kansai

b) Kyushu

Figure 5.8. Operation schedule for the facility's air conditioning, during one day in each representative month for the Kansai (a) and Kyushu (b) regions.

The operation profiles for the thermal energy demands are obtained from the model as well. Figure 5.7 shows the cases for the residences and Fig. 5.8 for the facility, for a 50 residence and 1000 m^2 area facility as well. In Fig. 5.7 it can be seen how the model controls the output of the HPWH during the day in order to accumulate enough hot water in the tank to be discharged at night if needed. For the results of May in Kyushu (Fig. 5.7(b)), the charge in the tank is not fully utilized during the day shown. This remaining charge however, remains available during the following day. In the case of the facility in Fig. 5.8, it can be seen that the ACH can meet most of the demands except on August, when cooling demand is at its highest (refer to Fig. 5.2 (d)). Furthermore, the high HP demand for the case of Kyushu in January is due to the PEFC not being operated during daytime, from 10:00 to 15:00, which lowers the heat output available for the ACH.

With the model results, energy savings with respect to the conventional diesel generator system were calculated. The Fuel Savings Ratio (FSR) of the proposed micro-grid for each month is obtained using Eq. (5.3), where Q_{conv} is the monthly primary energy consumption if the conventional system is utilized, and Q_{MG} is the monthly primary energy consumption of the proposed micro-grid. For this equation, an identical facility and number of residences are considered in the conventional system than those obtained from the micro-grid optimization model.

$$FSR = \frac{Q_{conv} - Q_{MG}}{Q_{conv}} \tag{5.3}$$

Figure 5.9 shows the monthly primary energy consumption and calculated FSR for the proposed micro-grid and the conventional system in both regions, for a 1000 m^2 facility and 50 residences.

Under the model conditions, high energy savings were observed in all months for both the Kansai and Kyushu areas. The calculated FSR shows that monthly savings go up to 58%. For the total annual primary energy consumption, Kansai presented an FSR of 59.5% and Kyushu an FSR of 55%.

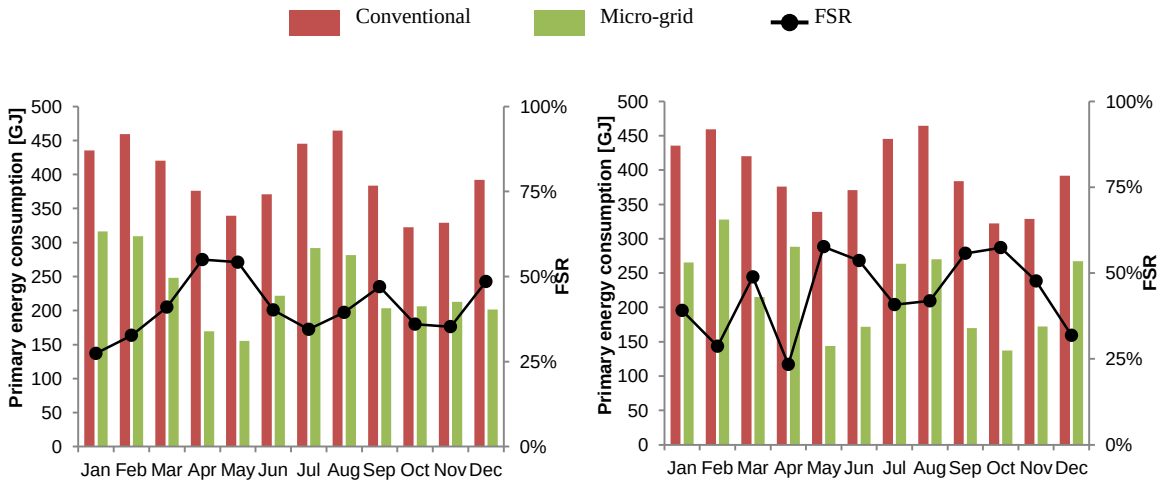

a) Kansai b) Kyushu

Figure 5.9. Monthly hydrogen consumption and FSR for a grid size of 50 residences and facility size of 1000m^2 for the Kansai (a) and Kyushu (b) regions.

5.3.2 Maximize Fuel Savings Ratio

The previous results were able to successfully show the advantages of the proposed micro-grid in terms of smart resource allocation and the capacity to reduce primary energy consumption. However, the simulation process revealed to have opportunities for improvement, particularly in the time needed to reach a feasible solution. As it is evident from the hydrogen fuel consumption shown in Fig. 5.4, the current objective function is not able to actually find the optima within the specified parameters and variable bounds. Since hydrogen consumption per household decreases with increasing number of residences, the model continues to iterate in this direction unless an upper bound is defined. The previous results were obtained by specifying these bounds in order for the model to stop and return the feasible solution that best fits the objective function. Even so, calculation times were in the range of hours, when performed on a PC with 2.40 GHz of processor speed and 4.00 GB of memory capacity. Additionally, the model did not necessarily find the best balance between facility and residential energy demands.

Therefore, an alternative objective function to introduce higher convexity into the problem is proposed. Maximizing the FSR previously shown in Eq. (5.3) is expected to offer solution to this. Since the primary energy consumption of the conventional system Q_{conv} is constant for a given number of residences, maximizing Eq. (5.3) inherently minimizes primary energy consumption of the micro-

grid Q_{MG}. Furthermore, since FSR does not necessarily follow the same trend as those seen in Fig. 5.4 and 5.5, the BARON solver is expected to follow a different path that does not constantly lead to ever dividing branches. Instead, maximizing FSR is predicted to find the optimum balance between residential and facility energy demands that can provide a more stable demand that lowers the gaps between minimum and maximum load.

Simulations utilizing Eq. (5.3) as the objective function were carried out, considering the same input parameters and values specified in Section 5.2. Furthermore, it was seen in the previous results that PEFC operated constantly at very low loads. In the results corresponding to a 1000 m^2 and 50 residence facility, PEFC operated below 20% of its rated load during 30% of the total time that the PEFC was active in the Kansai region. In Kyushu, PEFC operated below this value during 32% of the time. PEFC operation below 10% of the rated load in Kansai was during 15% of the time, and 18% of the time in Kyushu. Although the PEFC presents little variation in generation efficiency within a wide range of part-load operation, operation at low loads for long periods of time can degrade the cell stack. Therefore, further simulations include a binary variable to limit PEFC operation over a certain load, defined as $PEFC_{MinL}$. Since a lower bound for the PEFC output is introduced, the model would not be able to virtually shut down the PEFC. With this new variable, defined as $PEFC_{SW}$, PEFC output W_{PEFC} can be controlled from zero at the false state, to $PEFC_{Size}$* $PEFC_{MinL}$ at the true state. Thus, an additional constraint for PEFC output is added (Eq. (5.11)), and Eq. (4.5) described in Chapter 4, Section 4.3.1 is then modified to the form of Eq. (5.2).

$$W_{PEFC(h,m)} \geq PEFC_{Size} \cdot PEFC_{MinL} \tag{5.1}$$

$$W_{PEFC(h,m)} \cdot PEFC_{MinL(h,m)} \geq W_{TdemE(h,m)} - SOFC_{Size} - W_{PV(h,m)} \cdot N_R \tag{5.2}$$

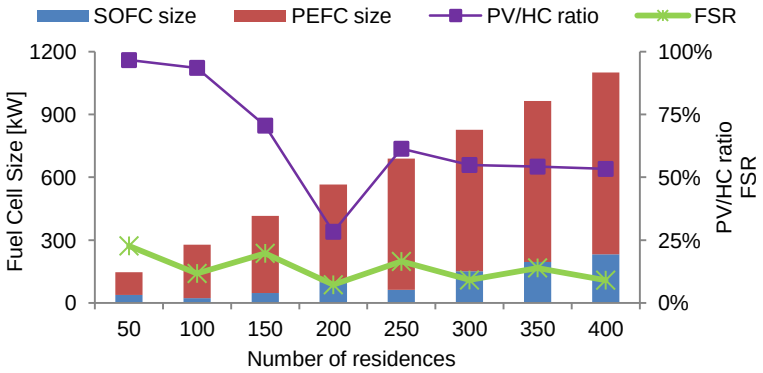

Figure 5.10. Variation of FSR, fuel cell size, and PV/HC ratio for a 1000 m^2 facility with respect to number of residences for the Kansai region.

Results from these simulations are presented in Fig. 5.10. As we can see, the FSR does not appear to show a trend corresponding to number of residences. Indeed, the expected behavior of this

objective function was to find the highest FSR value within the specified boundaries. Since this unique maximum is taken from the total possible FSR values corresponding to different numbers of residences, the new objective function is expected to perform best if the number of residences is not fixed. That is, the number of residences will now become an output variable that will help define the size of the micro-grid. The trends in FSR are thus analyzed for increasing facility sizes, for different facility types.

Two facility types are analyzed next: an office type facility and a hotel type facility. In contrast to the office type building, hotel type buildings show a much higher heat to power demand ratio. Also, energy demands in the hotel are high even during the night. Total floor area for the office is now considered to be 1000, 1500, 2000, 2500 and 3000 m^2. For the hotel type facility, total floor area is 1000, 2000, 3000, 4000 and 5000 m^2. Hotel energy demands for a building with total floor area of 1000 m^2 are presented in Fig. 5.11. For simplicity reasons, only simulations using data from the Kansai region will be addressed during the following analyses.

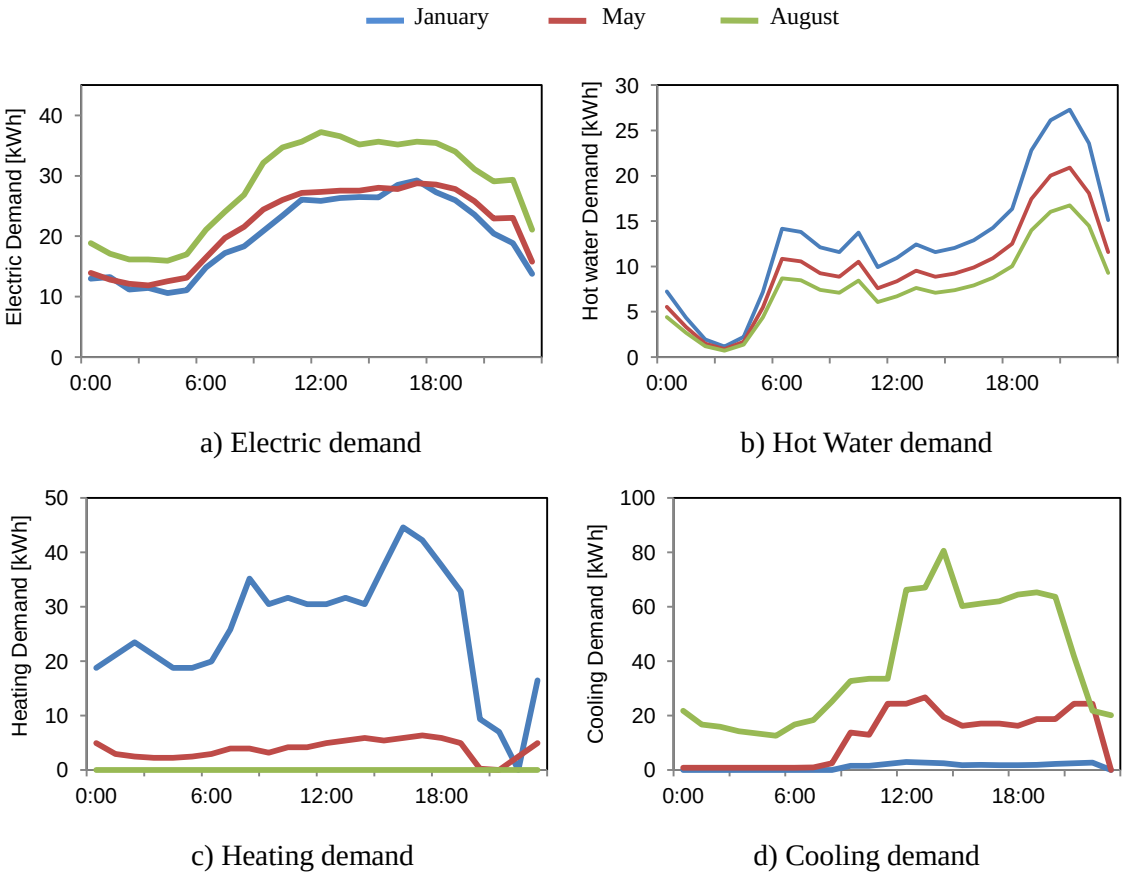

a) Electric demand

b) Hot Water demand

c) Heating demand

d) Cooling demand

Figure 5.11. Daily energy demands for a 1000 m^2 hotel type building during three representative months (January, May and August) in the Kansai region. Energy demands scale linearly with the facility floor area.

Figure 5.12 shows the trend of FSR values obtained by the model for these two facility sizes, as well as the optimal number of residences for each case. For the office type facility, FSR shows a slightly increasing trend as facility size increases, although little variation is seen on the number of residences. In contrast, the hotel type facility case shows an increase in both FSR and number of residences with a larger facility size. Compared to the office type facility, however, the hotel type facility case shows a lower number of residences overall. In the 4000 m^2 hotel case, we see a decrease in FSR, followed by an increased FSR in the 5000 m^2 case, but this time with lower number of residences. In Fig. 5.13, we see a change in behavior during this case as well. This figure shows the optimized SOFC and PEFC size and the PV to HC ratio for residential rooftops for the micro-grid. For the office type facility, we see little variation in the PEFC size with increasing facility size, and the SOFC size is increased to keep up with the energy demands at larger facility sizes, while PV to HC ratio appears to slightly decrease. Finally, the PV to HC ratio on residential rooftops appears to be selected case by case. The first point on the hotel PV/HC ratio might have been a result of high PV output compensating for the smaller capacity of the SOFC and PEFC compared to larger facilities, and therefore one may decide to treat it as an outlier. In this case, the PV to HC ratio appears then to follow a similar trend to the FSR for both office and hotel type facility cases.

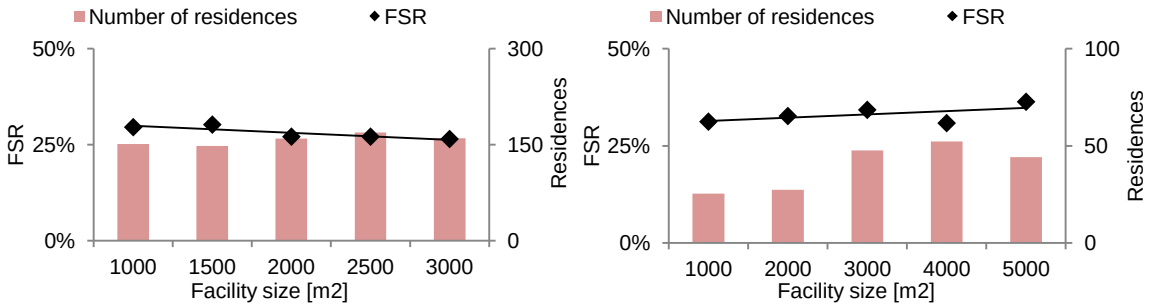

a) Office b) Hotel

Figure 5.12. Optimized FSR and number of residences for different sizes of an Office (a) and Hotel (b) type facilities in the Kansai region.

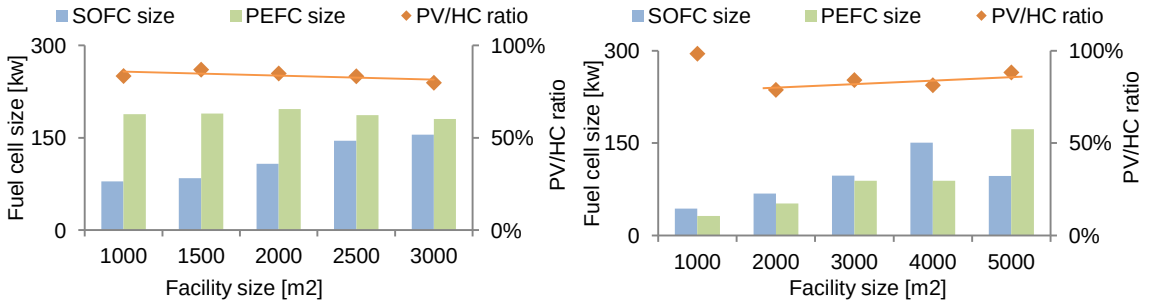

a) Office b) Hotel

Figure 5.13. Optimized SOFC size, PEFC size, and PV/HC ratio for different sizes of an Office (a) and Hotel (b) type facilities in the Kansai region.

However, for the hotel type facility case we see that both SOFC and PEFC size increase with larger facility size, with the SOFC being of higher capacity until the 4000 m^2 hotel case. For the 5000 m^2 case, SOFC size decreases now considerably and in turn the capacity of the PEFC is increased. This behavior is attributed to the large energy demand for heating and cooling in the hotel, which appears to escalate much faster than the electric demand. When the hotel size is less than 4000 m^2, the electric HP in the hotel is utilized sparingly as the ACH can manage most of the load. When hotel size is 4000 m^2, the electric HP is active almost half of the time and the model tries to fit this demand as part of the base load, increasing SOFC size (Fig. 5.13). However, low electric demand during nighttime (23:00 to 10:00) results in surplus electricity, which represents energy losses and may explain the sudden decrease in FSR. As hotel size increases to 5000 m^2 and heating and cooling demands are higher, the electric HP introduces more variation to the electric demand, which can be better managed by the PEFC. The model thus reduces the SOFC size and allows the PEFC to manage the large variations in load, which were not present at lower facility sizes.

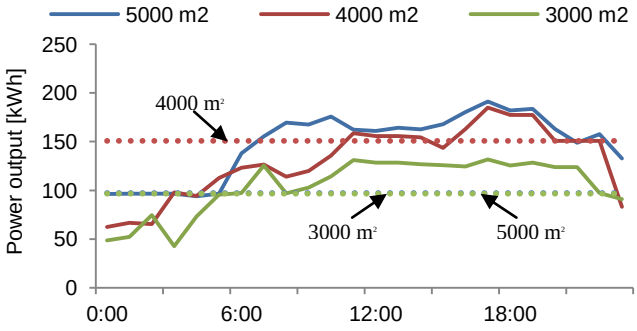

Figure 5.14. Total power generated in the micro-grid for one day in January for a Hotel type facility in the Kansai region. The dotted line shows the optimized SOFC (base load) capacity for the shown facility sizes.

Figure 5.15 shows the operating profile of the PEFC, SOFC, PV and Electrolyzer for this simulation. The results shown here correspond to the highest FSR case for each facility type: a 1500 m^2 office with 148 residences, and a 5000 m^2 hotel with 44 residences. From Fig. 5.15 we can see that surplus energy is much lower for the hotel type facility case than for the office type, and thus input to the electrolyzer is low as well. Although this low utilization points to a diminished capacity factor for the electrolyzer, especially compared to the office case, we can see that in months with high solar irradiation, the electrolyzer continues to be utilized. Furthermore, we can see in the operation schedule for August in the hotel type building how the PEFC needs to be turned on to cover a small portion of the electric demand during the morning. However, since the PEFC has been limited to a minimum operation of 30% of its rated load, the model here utilizes the electrolyzer as an extra load onto the grid, instead of deciding to opt for an SOFC with larger capacity that can increase the base-load.

In Fig. 5.15 we can also see how the difference between the minimum and maximum loads for the

hotel is much lower than the office type facility, which makes it easier for the system to generate energy on-demand without the need for large storage capacity.

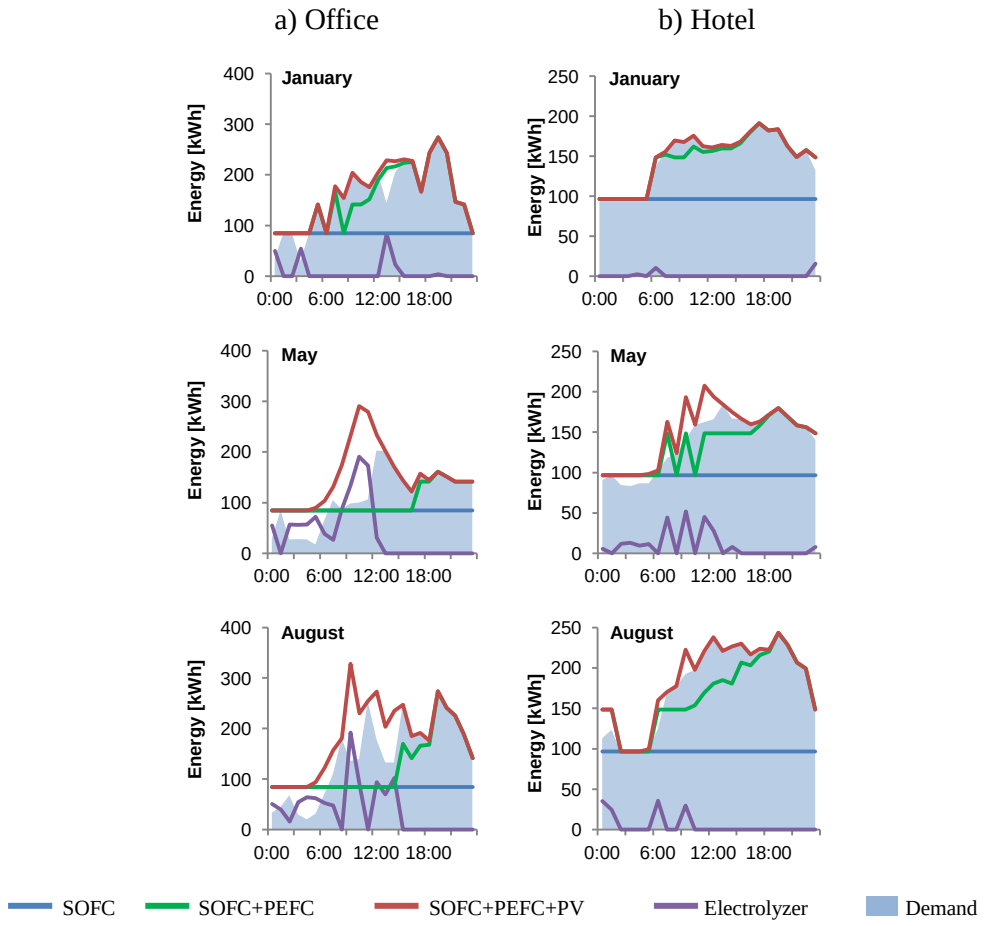

Figure 5.15 Optimized one-day operation scheduling for the SOFC, PEFC and Electrolyzer of a micro-grid composed of a 1500 m2 office with 148 residences (a), and a 5000 m2 hotel with 44 residences (b).

The operation profiles for the thermal energy demands corresponding to the residential hot water supply are presented in Fig. 5.16, and those for the heating and cooling demand for the facility are shown in Fig. 5.17. In Fig. 5.16 it can be seen how the model schedules the recharge of the residential hot water tank with anticipation. For this particular aspect, not much change is seen with respect to the previous objective function for minimizing hydrogen consumption per household. If anything can be pointed out, it may be that a smarter use of the HPWH is seen in this case, which is operated at intervals throughout the day not only to fill the hot water tank in advance, but to act as a stabilizing load for the micro-grid. The added power demand from these devices can have a significant impact on the PEFC operation, deciding even whether it is better to turn the PEFC on or off. As seen from the remaining hot water in the tank (dotted line), it is clear that the scheduled operation of the HPWH does not generate hot water in excess.

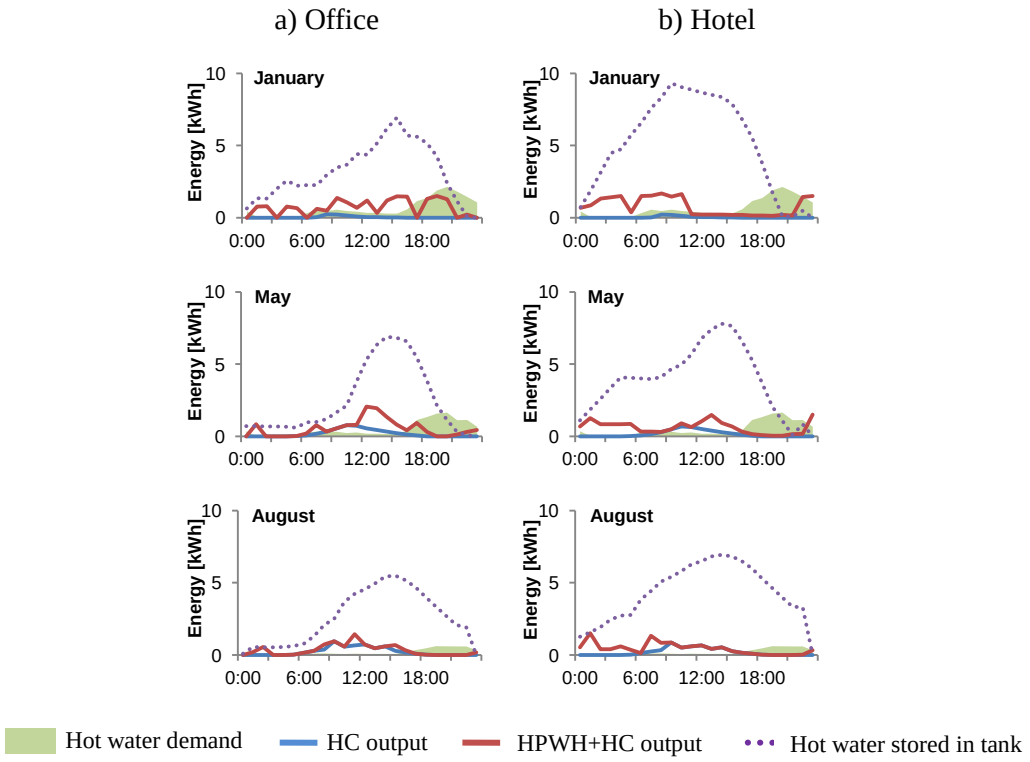

Figure 5.16. Optimized one-day operation scheduling for the residential HPWH and hot water tank of a micro-grid composed of a 1500 m^2 office with 148 residences (a), and a 5000 m^2 hotel with 44 residences (b).

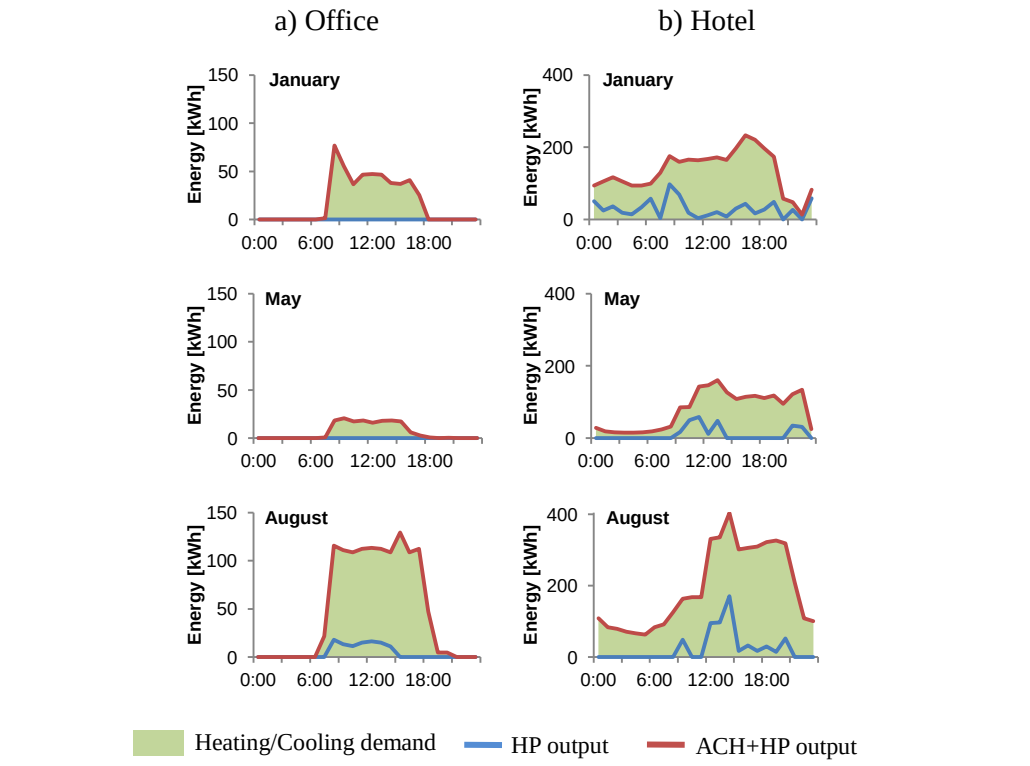

Figure 5.17. Optimized one-day operation scheduling for the facility's HP and ACH of a micro-grid composed of a 1500 m^2 office with 148 residences (a), and a 5000 m^2 hotel with 44 residences (b).

Regarding air conditioning for the facility (Fig. 5.17), we can see that the ACH appears be somewhat oversized for the office type building, since it is only utilized during daytime and receives very little use during mid-season months such as May. For this case it might be worth considering to use the fuel cell exhaust heat not for cogeneration, but to generate additional electricity using a small gas turbine. Such configurations can be found in the literature for reference [13]. For the hotel type facility case, the selected ACH seems to be appropriate. As discussed before (Fig. 5.14), the optimized PEFC capacity is able to handle the variation in power demand introduced by the facility HP, and like the residential HPWH, the HP output may also be utilized as an added load to stabilize the operation of the PEFC.

5.4 Effect of variable bounds

Regarding computation time, the objective function using FSR as the target was able to find an optimal solution within minutes, up to a few hours if more days are considered in the input data. If the solver found the problem to have no feasible solution using the specified parameters, computation ended immediately during preprocessing, saving additional time. In contrast, the objective function utilizing hydrogen energy consumption per household was never able to converge, and instead a computation time limit had to be defined. If the solver did not find a feasible solution for the problem within the specified time, this was not detected until the program reached its end. Thus it can be said that the objective function using FSR performed better in terms of calculation time.

However, the new objective function also increased the dependence on appropriate variable bounds in order to find optimal results. As discussed in Chapter 4, the BARON solver has the benefit of not needing initial values to solve a problem, but the variables do need to be bound for it to guarantee global optimality of the solution. The values presented in Section 5.3.2 were those that presented the best solution among several iterations of the same simulation run, each with different variable bounds. The variables that required bounds were three in total: PEFC size, SOFC size, and number of residences. The lower bound for number of residences was set constant at 10, and the PEFC and SOFC size were lower bound by zero. The specified upper bounds and their respective results are presented in Fig. 5.18 (office) and Fig. 5.19 (hotel).

It should be noted that all results shown here are feasible solutions to the problem. What this graphs show is that a simulation that returns a low FSR value may be improved if different variable bounds are used. Although computation time for each simulation was low, searching for the variable bounds that can generate the absolute highest FSR value will likely result time consuming. Currently, no methodology for selecting the appropriate variable bounds for the BARON solver has been found in literature, with which variable bound selection can be facilitated. However, feasible solutions do appear to exist within certain bound ranges on each variable.

Figure 5.18. Upper variable bounds for $SOFC_{size}$, $PEFC_{size}$ and number of residences N_R utilized in simulation iterations and the resulting FSR values in each case. Results correspond to different sizes of an office type building in the Kansai region. Iterations for the 3000 m^2 office case stopped when not much variation in FSR was observed.

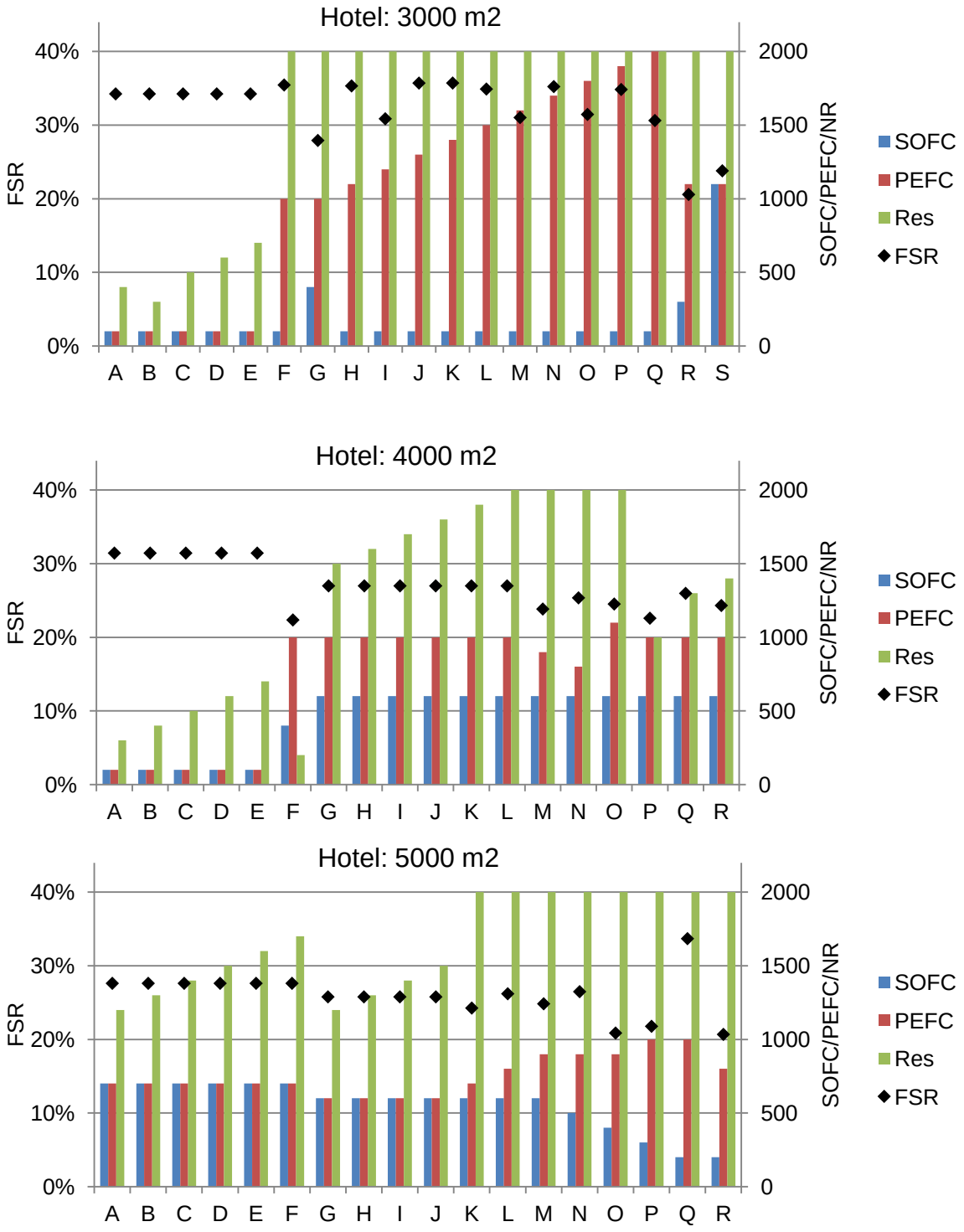

Figure 5.19. Upper variable bounds for $SOFC_{size}$, $PEFC_{size}$ and number of residences N_R utilized in simulation iterations and the resulting FSR values in each case. Results correspond to different sizes of a hotel type building in the Kansai region.

It is evident that there is no clear relation between the variable bounds and the global optimality of the solution. As energy demands grow larger however, it appears that the resulting FSR has less variation with different variable bounds. Such is the case with all facility sizes for the hotel type

facility, as well as the 3000 m^2 office type facility. Further research should be conducted in this regard, not only for the present thesis, but for general optimization problems utilizing branch and reduce algorithms such as BARON.

5.5 Discussion

The proposed micro-grid is believed to offer additional benefits in comparison to other alternatives for energy supply, that are not evident in the results obtained from the optimization model. These include flexibility in energy demands, easy interconnection of grids, capacity for growth, as well as contributing to the learning curve of hydrogen technologies and infrastructure.

1. Flexibility in energy demands: the operation schedule patterns obtained from the optimization model never operated at full capacity during a complete day. Fuel cell capacity remains available for cases where power demands are higher than usual. In communities that seek social development, seasons with intense energy demands may appear as the economic sector progresses. Stand-alone renewable energy systems using only rechargeable batteries for energy storage are limited by the battery capacity and may not be able to vary their demands easily, especially when accompanied by unfavorable weather. In such cases, additional energy supply systems such as diesel generators need to be available, which brings back the problem of oil dependence and the reliance on its infrastructure. In the proposed system, the fuel cells can adapt quickly to changes in energy demand patterns only by increasing or decreasing the amount of fuel consumed. Since hydrogen can be used to provide all forms of energy for human consumption, no additional installation of components is needed. This is believed to offer the very much needed flexibility in energy demands that renewable energies alone cannot achieve.
2. Interconnection of grids: in the proposed micro-grid structure, only electricity is exchanged between customers and every micro-grid component operates independently. If all components are to follow the proposed operating schedule, it can be assumed that all energy demands in the micro-grid are being covered. Therefore, interconnection of two micro-grids is believed to have no influence on the individual operating schedules. On the contrary, sudden fluctuations in individual component loads can be distributed among interconnected micro-grids, allowing the fuel cells to operate with improved stability. Furthermore, considering again the case where intense energy demands are expected, interconnection of micro-grids results in an overall higher capacity in which the loads can be distributed. Whether individual or interconnected operation is considered, the proposed micro-grid is expected to operate reliably.
3. Capacity of growth: as more micro-grids are implemented, the management of hydrogen supply channels is able to evolve from hydrogen storage in tanks, into a small network of hydrogen pipelines where hydrogen generation can be centralized, utilizing hydrogen generation methods that will be described in the next chapter. Compressed hydrogen storage still faces several

challenges, especially at higher volumetric capacities due to the extremely low density of hydrogen gas. For initial stages in the implementation of the proposed micro-grid, compressed hydrogen tank is regarded to be the best, if not only the choice. However, the nature of this micro-grid encourages its growth into several interconnected grids, which is expected to improve technical and economical feasibility.

4. Learning curve: as it is the case with most technologies, low prices can be expected once as the demand increases and products are manufactured in mass. To this day, hydrogen technologies for energy supply have not had a large demand and thus prices remain high. Recent advances in fuel cell technologies have shown an impact in prices, but their demand still needs to grow further in order to compete with mature energy supply technologies such as internal combustion engines and steam turbines. The proposed micro-grid offers an opportunity to increase the demand of hydrogen technologies through small energy supply systems that can be relatively easy to finance. Because the micro-grid encourages growth, successful implementation of one grid is likely to be followed by additional implementation trials. Even success is not achieved, the micro-grid has a structure that is compatible with the current infrastructure and allows it to integrate back without substantial modifications, ensuring that the investment is not wasted.

5.6 Conclusions

In this chapter, the optimization model for semi-independent micro-grids has been evaluated through simulations utilizing input data from different cities in Japan, corresponding to solar irradiation in each region, residential energy and hot water demands, and energy demands of different types and sizes of central facilities. The following conclusions have been drawn from this study:

(1) The objective function to minimize hydrogen consumption per household was found to not reach convergence in an acceptable time. An objective function with much faster results was obtained by maximizing savings fuel savings compared to the currently implemented energy supply system.

(2) PEFC operation at minimum loads was observed on the original optimization model. Since low load operation is known to degrade the cell's electrodes, the function that controls PEFC operation was modified to either operate over a minimum load of 30%, or shut down.

(3) The modified model presented results that are much easier to interpret. In office type facility micro-grids, the number of residences at which fuel savings are maximized was found to remain fairly constant. For hotel type facility micro-grids, number of residences was seen to increase with larger facility sizes, but an oddity in this trend appeared after the size increased over a certain threshold.

(4) The variable bounds utilized during simulations were shown to have a large impact on the model's capability of finding a feasible solution, and whether that solution was global or not.

Although no current strategy for finding the appropriate bounds is known, several variable bounds which gave results close the believed global optima were found to exist under certain ranges.

Finally, a discussion section is included which explains the potential benefits that the proposed micro-grid can provide, aside those from pure reductions in energy consumption.

5.7 References

[1] Kashiwagi, T. (2002), Natural Gas Cogeneration Plan/ Design Manual 2002, *Japan Industrial Publishing Co., LTD*, 64-9.

[2] Horie, H. and Hihara, E. (2012). Study on Annual Performance of Room Air Conditioners under Partial Load Condition. *International Refrigeration and Air Conditioning Conference 2012*, Paper 1336.

[3] Department of the New Energy and Industrial Technology Development Organization. (2015). *New Energy and Industrial Technology Development Organization, Meteorological Test Data for Photovoltaic Systems (METPV-11).*

[4] JSA. (2012). Estimation method of generating electric energy by PV power system, *Japanese Standards Associationm* Standard No. JIS C 8907:2005. (In Japanese).

[5] Jensen, J.O., Li, Q. and Bjerrum, N.J. (2010). The Energy Efficiency of Different Hydrogen Storage Techniques. *Energy Efficiency*, Jenny Palm (Ed).

[6] Lamas, J., Shimizu, H., Matsumura, E. and Senda, J. (2013). Fuel consumption analysis of a residential cogeneration system using a solid oxide fuel cell with regulation of heat to power ratio. *International Journal of Hydrogen Energy*, 38, 16338-43.

[7] NEEA. (2015). Northern climate qualified heat pump water heaters. *Northwest Energy Efficiency Alliance*. Retrieved May 1, 2015 from: http://neea.org/docs/default-source/northern-climate-heat-pump-water-heater-specification/qualified-products-list.pdf

[8] El-Sayed, A.G. and Obara, S. (2010). Power Generation Efficiency of Photovoltaics and a SOFC-PEFC Combined Micro-grid with Time Shift Utilization of the SOFC Exhaust Heat. *International Power Electronics Conference 2010*, 2629-36.

[9] Thermax. (2016). Hot water driven chillers, High temperature hot water (2G series). Retrieved May 1, 2016 from http://www.thermaxglobal.com/thermax-absorption-cooling-systems/vapour-absorption-machines/hot-water-driven-chillers/

[10] American Council for an Energy-Efficient Economy. (2015). Replacing your Water Heater. *Smart House*. Retrieved May 1, 2016 from http://smarterhouse.org/water-heating/replacing-your-water-heater

[11] Masahiro O. 2004. *Technology of on-site energy supply*. Japan: Kaibundo publishing: 3-16. (In Japanese).

[12] Marnay, C. Venkataramanan, G., Stadler, M., Siddiqui, A.S., Firestone, R. and Chandran, B. (2008). Optimal Technology Selection and Operation of Commercial-Building Microgrids, *IEEE Transactions on Power Systems*, 23 (3), 975-82.

[13] Calise, F., Palombo, A. and Vanoli, L. (2006). Design and partial load exergy analysis of hybrid SOFC–GT power plant, *Journal of Power Sources*, 158, 225-44.

Chapter 6. Hydrogen supply channels for semi-energy independent micro-grids

6.1 Introduction

In this chapter, a brief overview on hydrogen fuel supply channels is presented. Since hydrogen is not a naturally occurring element, it needs to be generated from other sources, which is done mainly with hydrocarbons or water. Although the current main source of hydrogen is reformation of methane contained in natural gas, efforts to decrease dependence on fossil fuels advocate the use of alternative fuel sources, including waste and renewable energy sources. In Section 6.2, the currently available methods for hydrogen generation and their potential are described. The technologies for hydrogen transport and their safety concerns are presented in Section 6.3. Finally, an overview on currently installed hydrogen pipeline system is given in Section 6.4.

6.2 Hydrogen generation

The concept of hydrogen infrastructure is relatively new, but it has been receiving increased attention recently. As mentioned in the introduction of this paper, there is increasing concern over the availability of fossil fuels and their capacity to cover increasing global energy demands. Therefore, alternative sources of energy that are compatible with the current infrastructure are constantly under research. Hydrogen appears to be the most promising alternative in this regard, as it can be generated from both fossil fuels and renewable energies. Therefore, an energy infrastructure that utilizes hydrogen could be attractive to both consumers and suppliers in the industry, from residential and industrial energy consumption to the transport sector. Furthermore, a reduction in the combustion of fossil fuels is expected to have a positive impact on environmental degradation and air quality, as well as improving energy security by reducing fuel imports. The United States is already recognizing the importance of starting a hydrogen infrastructure in detailed reports that help as guidelines for assessing hydrogen based energy systems [1, 2]. Other reports support the concept of hydrogen infrastructure as a transition between conventional fossil fuel energy systems and the introduction of renewable energies [3, 4]. These reports present the possible paths for converting the actual energy infrastructure into one compatible with hydrogen technologies. This transition is expected to have positive impacts on energy security, environmental protection and economic growth. Currently, over 98% of the global demand for hydrogen is produced through reformation of hydrocarbons (mainly steam reforming of natural gas), and it is mostly consumed only in refineries and ammonia production. As the market for hydrogen fuel expands, natural gas consumption for hydrogen production is expected to increase as well. Therefore, additional sources of hydrogen (e.g., from renewable energies) are to be implemented in order to improve energy security. Midilli and Dincer [5] utilize the global instability ratio and hydrogen based sustainability ratio, developed by Midilli, to evaluate the benefits of hydrogen energy systems. Their report suggests that an increase in non-fossil fuel

hydrogen production is exponentially proportional to increased energy sustainability and lower global energy instability. Additionally, they suggest that a global increase in hydrogen energy utilization could help to improve sustainable development and energy stability values.

For isolated areas with high energy demands that currently rely on diesel powered generators, hydrogen fuel can provide a cleaner and more stable alternative, compared to the installation of large-scale electric storage systems. Isolated areas with high energy demands are those that have an established supply line of fuel, for example, the several islands surrounding the main island in Japan. Japan is not a main producer of oil products, thus the fuel needed to supply the isolated areas needs to be imported from other countries, consuming a high amount of resources and leaving a large carbon footprint in the process. Generating hydrogen in the main island through water electrolysis or reformation of carbohydrates, and using the existing fuel supply lines to transport this fuel, the energy security for these isolated areas could be effectively improved, while reducing carbon emissions due to power generation. However, if isolated areas are to transition into hydrogen based energy supply systems, then additional hydrogen sources that can meet the increased demand need to be explored. Hydrogen generation may be divided into three: non-renewable hydrogen, renewable hydrogen, and hydrogen for energy storage.

6.2.1 Water electrolysis

Supplementary to biomass, hydrogen produced from renewable energy resources may be obtained simultaneously to further decrease the dependence on fossil fuels. Hydrogen from electrolysis can be readily implemented in solar, wind, hydro, and geothermal power systems. For each of these renewable energy sources, a number of additional processes for hydrogen generation are available [6]. Solar energy shows the most diverse range of hydrogen production methods, such as thermolysis, thermochemical water splitting, photo-catalysis, bio-photolysis, artificial photosynthesis. The solar thermochemical water splitting process is further explained by Licht [7]. Besides, electrolysis seems to be the most effective and commercially viable for producing hydrogen from renewable resources [8, 9]. Recent advances in water electrolysis are increasing the efficiency of the process and reducing costs. A Solid Oxide Electrolyzer Cell proposed by Jensen *et al.* [10] showed outstanding results in hydrogen production, and is expected to reduce costs by half compared to conventional alkaline electrolyzers as the technology matures. Hydrogen as a means for energy storage is also possible using both non-renewable and renewable energies. Large-scale power stations, including coal, hydro, geothermal and nuclear power, that generate power at maximum capacity regardless of demand can benefit from water electrolysis to store surplus energy in the form of hydrogen. In the same way, renewable energies that depend on weather conditions, such as wind and solar power, may store energy in the form of hydrogen when the power output exceeds demand.

6.2.2 Hydrocarbon reforming

Currently, the main source for hydrogen is found in hydrocarbons. Hydrocarbons can be separated into H_2 gas and other carbon components through a number of processes. The source of hydrocarbons for hydrogen production is also varied. Methane found in natural gas is currently the main source of non-renewable hydrogen due to its abundance and for having the highest hydrogen content (two molecules of hydrogen gas per atom of carbon) among other hydrocarbons. An efficient and technologically mature process called catalytic steam reforming uses methane (CH_4) and high temperature steam (H_2O) that react over a nickel catalyst to disassociate it into H_2, CO and CO_2 gases. Although this process presents a source of carbon emissions, the catalytic reforming process does not produce NOx or soot emissions as combustion of hydrocarbons does. The steam reforming process may also be used with ethanol, which has the same hydrogen to carbon ratio as methane. Ethanol is in liquid state at standard temperature and pressure, which makes it more convenient to transport compared to natural gas. Ethanol is considered an effective source of energy for low power applications (100 to 1000 W), but for higher power applications it still lacks the infrastructure and logistics for its use [11].

Another source of hydrogen that involves hydrocarbon reforming is biomass. Biomass may be considered a renewable resource depending on the sustainability of its harvesting practices. Balat and Balat [12] list the benefits of bio-hydrogen as fostering the economic sector (sustainability, increased rural jobs, reducing fuel imports), encouraging environmental protection (reducing carbon emissions and air pollution), and improving energy security (domestic targets, reducing fossil fuel consumption). Levin and Chahine [13] have compiled a report on hydrogen production methods using biomass. Biomass has been used as a source of hydrocarbons for several years now, and as such the conventional method of steam reforming may be applied to produce hydrogen. Bio-oil output from biomass is rated above 75 wt%, and further reformation into hydrogen has shown yields of 85% from the total hydrogen content [14]. Hydrogen generation through autothermal reforming of ethanol is also an efficient process with high product purity. Furthermore, ethanol is soluble in water and thus appears to be a suitable fuel for PEMFCs, as they require a high hydration level in the cell stacks [15]. Other processes for hydrogen production using gas are available as well. Gasification of biomass can provide high hydrogen output, if the resulting gases can be separated efficiently. Current research is improving the techniques for gas purification, achieving satisfactory results. Hydrogen is also obtained through photolysis or fermentation using algae, bacteria, or other microorganisms. Fountoulakis and Manios [16] have shown that glycerol addition significantly enhances hydrogen output from anaerobic digestion of municipal solid waste and agro-industrial byproducts. Although these technologies are not yet mature, they appear to have a large output capacity for hydrogen generation.

6.2.3 Industry by-product

In recent years, hydrogen generation through reformation of industrial byproducts has also been receiving attention. Although non-renewable, hydrogen generated from industrial byproducts does not present an additional consumption of resources. Waste products from coke ovens in steelworks plants, mainly coke oven gas and tar, are considered a potential source of hydrogen [17, 18]. Coke oven gas has a hydrogen content of 50-60% and methane content of nearly 25% from which hydrogen may be recovered. A fraction of these waste gases is utilized for other processes in steelworks plants, but often there is excess gas that is not being taken advantage of. If isolated areas adopt hydrogen fuel as a source of energy, then industrial waste gases can be used to reduce fossil fuel imports for hydrogen production. Since these gases are considered waste products, they provide an attractive source of hydrogen with no net CO_2 emissions and lower transportation losses.

Hydrogen also results as a byproduct in caustic soda factories. The chloralkali process disassociates the NaCl salt through electrolysis of brine in a membrane cell, from where products result in chlorine, hydrogen and caustic soda (NaOH). Caustic soda is a commodity with high demand globally, with production surpassing the 45 million tons annually. About half of it is utilized often in general manufacturing, as well as in the manufacture of paper, detergents and drain cleaners. One mole of hydrogen is produced from every two moles of caustic soda, thus annual hydrogen output from this source can be estimated at one million tons of hydrogen. Although global production will most likely not be polled together to supply a few communities, it does remain a viable source of hydrogen fuel in areas near caustic soda factories because the product is essentially waste.

6.3 Hydrogen storage and transport

In addition to hydrogen production, the method for storing hydrogen also needs to be selected with respect to the expected consumption patterns. There are four commercial storage technologies for hydrogen (Table 6.1): compressed gas, liquid hydrogen, metal hydrides, and chemical hydrides [19, 20]. Compressed gas in 200 bar steel cylinders is the most commonly used method. Higher pressures (350 and 700 bar) can be achieved using composite cylinders, although the selection of suitable composite materials is still an issue regarding tank size. Liquid hydrogen is more often used in large-scale transport using tankers, as hydrogen liquefaction has very low efficiency on a small scale. For long-term storage, metal hydride tanks are a better option. Metal hydrides are still expensive, but present diminished losses and improved safety. Chemical hydride technology is still under development, although it presents high energy density for storage. Regarding consumption, it is recommended to use on-site electrolysis and to avoid mid to long-term storage. If consumption is high (over 20 kg/day), on-site reforming of natural gas may be more suitable than electrolysis, mainly due to the costs and operation of the additional components needed for steam reforming [20]. With regard

to safety, hydrogen storage is not considered any riskier than compressed natural gas storage. The minimum fuel to air ratio at which the mixture first becomes flammable is similar between hydrogen and methane, at approximately 5% fuel volume. Furthermore, hydrogen safety standards have been in practice for decades and sufficient knowledge has accumulated to create or improve them, depending on the application [20, 21].

Table 6.1. Summary of hydrogen storage technologies [20].

	Compressed gas			**Liquid hydrogen**	**Metal hydride**	**Chemical hydride**
Technologies	Steel cylinders (200 bar)	Composite Cylinders (350 bar)	Composite Cylinders (700 bar)	N/A	Hydrides of light metals	Hydrides that react with water to produce hydrogen
Energy density	1 wt%H2	6 wt%H2	5 wt%H2	5 wt%H2	1-2 wt%H2	4 wt%H2
Availability	Commonly used	Standard for onboard vehicle tanks	Target for onboard vehicle tanks	Transport by tanker or in large-scale stationary vessels	Still in development	Still in development
Issues	Lowest cost, but low energy density	Low weight composite materials are a challenge		High cost, difficult to scale size down	High cost, yet low energy density	Regenerating the hydride consumes energy

6.4 Hydrogen pipelines

Hydrogen supply through underground pipelines has been achieved in several cases, mainly for its use in petroleum refining processes. Hydrogen pipelines can be usually found operating at pressures below 1000 psi, which is the least needed to transport gas for long distances. However, these pipelines have shown very high safety records, thanks to the ever evolving standards and regulations for hydrogen transport. A large reason for which hydrogen pipelines have not been installed for longer distances is simply the lack of demand. Today with the increasing penetration of fuel cell vehicles in Japan, the US and Europe, hydrogen pipeline infrastructure for wider areas is being considered. Such feat could be achieved by the redesign of existing natural gas pipelines, which are very much entrained in the current energy infrastructure of many countries. To do so, however, several problems concerning hydrogen embrittlement of steel, which in the long term can cause several kinds of faults in the pipes. Studies regarding technical assessment for the installation of hydrogen pipelines can be found in the literature [22]. Hydrogen pipeline costs are currently estimated to be about 68% higher than natural gas pipelines, but as their demand continues to increase, further research is being conducted to reduce these costs. A recent study suggests that costs can be reduced by 31% utilizing currently available technology [23].

6.5 Conclusions

In this chapter, the potential hydrogen supply channels for the semi-independent micro-grid proposed in this thesis are described. Three main sources of hydrogen fuel are identified: water electrolysis, hydrocarbon reforming, and industrial byproducts. Renewable energies are found to be a potential source for hydrogen through water electrolysis (wind, solar and hydroelectric energy) and hydrocarbon reforming (biomass). Although industrial byproducts can be regarded as inexpensive due to the fuel source being waste material, their capacity is limited by the industry's output. Hydrogen safety, storage and transport strategies are discussed as well. It has been found through literature review that hydrogen transport through pipelines is currently possible even without large investments in infrastructure modification.

6.6 References

[1] US Department of Energy. (2002). National Hydrogen Energy Roadmap. *National Hydrogen Energy Roadmap Workshop*, Washington, DC (US).

[2] Levene, J. (2004). Summary of Electrolytic Hydrogen Production-Milestone Completion Report. *National Renewable Energy Laboratory MP-560-36734*, Golden, Colorado (US).

[3] Muradov, N.Z. and T.N. Veziroğlu. (2005). From hydrocarbon to hydrogen-carbon to hydrogen economy. *International Journal of Hydrogen Energy*, 30, 225-37.

[4] Marbán, G. and Valdés-Solís, T. (2007). Towards the hydrogen economy? *International Journal of Hydrogen Energy*, 32, 1625-37.

[5] Midilli, A. and Dincer, I. (2007). Key strategies of hydrogen energy systems for sustainability. *International Journal of Hydrogen Energy*, 32, 511-24.

[6] Dincer, I. (2012). Green methods for hydrogen production. *International Journal of Hydrogen Energy*, 37, 1954-71.

[7] Licht, S. (2003). Solar Water Splitting To Generate Hydrogen Fuel: Photothermal Electrochemical Analysis. *The Journal of Physical Chemistry B*, 107, 4253-60.

[8] Sherif, S.A., Barbir, F. and Veziroglu, T.N. (2005). Wind energy and the hydrogen economy-review of the technology. *Solar Energy*, 78, 647-60.

[9] Fuel Cell Today. (2013). Water Electrolysis & Renewable Energy Systems. *Fuel Cell Today*. Royston, Hertfordshire (UK).

[10] Jensen, J.O., Li, Q. and Bjerrum, N.J. (2010). The Energy Efficiency of Different Hydrogen Storage Techniques. *Energy Efficiency*, Jenny Palm (Ed).

[11] Palo, D.R., Dagle, R.A. and Holladay, J.D. (2007). Methanol steam reforming for hydrogen production. *Chemical Reviews*, 107, 3992-4021.

[12] Balat, M. and Balat, M. (2009). Political, economic and environmental impacts of biomass-based hydrogen. *International Journal of Hydrogen Energy*, 34, 3589-603.

[13] Levin, D.B. and Chahine, R. (2010). Challenges for renewable hydrogen production from biomass. *International Journal of Hydrogen Energy*, 35, 4962-9.

[14] Wang, D., Czernik, S. and Chornet, E. (1998). Production of Hydrogen from Biomass by Catalytic Steam Reforming of Fast Pyrolysis Oils. *Energy & Fuels*, 12, 19-24.

[15] Deluga, G.A., Salge, J.R., Schmidt, L.D. and Verykios, X.E. (2004). Renewable hydrogen from ethanol by autothermal reforming, *Science*, 303, 993-7.

[16] Fountoulakis, M.S. and Manios, T. (2009). Enhanced methane and hydrogen production from municipal solid waste and agro-industrial by-products co-digested with crude glycerol. *Bioresource Technology*, 100, 3043-7.

[17] Onozaki, M., Watanabe, K., Hashimoto, T., Saegusa, H. and Katayama, Y., Hydrogen production by the partial oxidation and steam reforming of tar from hot coke oven gas. *Fuel*, 85, 143-9.

[18] Bermudez, J.M., Fidalgo, B., Arenillas, A. and Menendez, J.A. (2010). Dry reforming of coke oven gases over activated carbon to produce syngas for methanol synthesis. *Fuel*, 89, 2897-902.

[19] Zhou, L. (2005). Progress and problems in hydrogen storage methods. *Renewable and Sustainable Energy Reviews*, 9, 395-408.

[20] HI-Energy. (2014). Hydrogen refuelling and storage infrastructure.

[21] Tchouvelev, A., Hay, R. and Benard, P. (2006). Comparative risk estimation of compressed hydrogen and CNG refueling options. *Center for Hydrogen Safety and Codes & Standards (AVT).*

[22] Gillete, J.L. and Kolpa, R.L. (2007). Overview of interstate hydrogen pipeline systems. *Argonne National Laboratory*, TRN: US0802253.

[23] Fekete, J.R., Sowards, J.W. and Amaro, R.L. (2015). Economic impact of applying high strength steels in hydrogen gas pipelines. *International Journal of Hydrogen Energy*, 40, 10547-58.

Chapter 7. Micro-grid implementation in islands

7.1 Introduction

This chapter is dedicated to the design and economic analysis of an energy supply system for actual implementation in a Japanese island, where current energy costs are exceptionally high and energy security is threatened by the future of oil products. In Section 7.2 of this chapter, the target area for analysis is described, including geography, demographics and current situation regarding energy supply, finalizing with the definition of the input data for optimization analysis for three scenarios with different energy demand patterns. Simulation results are presented and discussed in Section 7.3 Section 7.4 describes the costs for installation, operation and maintenance, part replacement, as well as fuel generation and transport costs, for both the currently installed energy supply system and the proposed micro-grid. In Section 7.5, the cost analysis for three scenarios is presented, with a comparison to the currently installed energy supply system, from where economic viability is addressed. Finally, Section 7.6 summarizes how implementation of the proposed micro-grid should be addressed in the target area.

7.2 Case scenario: Japanese island

Distributed Energy Resource technologies remain to this day with high installation costs, especially when compared to the already installed infrastructure where large scale thermal power plants generate electricity in bulk at low prices. However, such is not the case in isolated areas such as islands. As mentioned in Chapter 1, many Japanese islands rely on a costly energy supply system composed of fuel oil generators that requires constant shipping of fuel. The low generation efficiency of this system and high fuel transport costs result in electricity costs that often surpass twice those of the main islands. Furthermore, the energy security of this area is affected by the limited availability of oil products, which is the main supply line of energy for many islands, as well as the increasing costs of oil products that are forecasted for the following years. In addition, increasing regulations on PM, CO_2 and other greenhouse gas emissions exacerbate the need to minimize dependence on fossil fuels. For this reason, it is believed that DER systems can provide competitive energy costs even at today's technology prices. It is also worth mentioning that there is high risk in not investing on an alternative energy infrastructure before fossil fuels begin to exhibit supply shortages. In this chapter, the micro-grid optimization model developed in Chapter 4 is used to design an energy supply system for a real scenario, representing an isolated Japanese island.

7.2.1 Target area (demographics and economics)

The island of Tokunoshima in the Kagoshima prefecture, Japan has been selected for this case study. This island was selected for being one of the most distant medium-sized islands in Japan. The island of Hachijo, administered by Tokyo, has similar conditions to Tokuhoshima, but it is not addressed in this study. Large-size islands in Japan have currently a reliable energy infrastructure to which the proposed micro-grid may not be able to compete. On the other hand, small-sized islands have such low energy demands that they might benefit from systems using only renewable energies and electric battery storage, as various studies have already proposed. Tokunoshima Island is located about 470 km southwest from the main island of Kyushu. It is part of the Oshima island group of the Kagoshima prefecture, which is composed of the large-sized Amami Island, the medium-sized Tokunoshima Island, and the small-sized Kikai Island. Its location is illustrated in Fig. 7.1.

Figure 7.1. Location of Tokunoshima Island in the Oshima Island group, belonging to the Kagoshima prefecture, Japan.

The 2011 census states that the island has 11,192 households in total, and a population of 25,437 people [1]. Total workforce is estimated at 11,039 people. The island is divided into the Tokunoshima, Amagi and Isen towns. The largest town is Tokunoshima town, with 5,372 households and 11,999 inhabitants. The Amagi and Isen towns are similar in size. Amagi town has 2,792 households with 6,565 inhabitants and the Isen town has 3,028 households with 6,873 inhabitants. People per household are 2.3 on average for all towns. Close to 150 businesses are found in the island [2], and the total income per capita is 2.3 million JPY [3]. Power supply in the island is done mainly through 10 fuel oil generators with a total generation capacity of 30,500 kWh [4]. They are divided into three power stations and connected through a 22 kV transmission line, as illustrated in Fig. 7.2. The largest one is Shintokunoshima power station, in the Amagi town, where four engines with a total generation capacity of 21 MWh are located. The Kametsu station, located in the Tokunoshima town, has four engines and a generation capacity of 7.5 MWh. The Hetono power station is the oldest, located in the Amagi town, where two engines with a total generation capacity of 2 MWh are installed. The oldest engine is located in the Hetono station, installed in 1966, while the newest one is located in the Shintokunoshima town, installed in 2002. A small hydroelectric power plant installed in 1923 with a maximum output of 140 kWh is also part of the current power grid. Total power output for 2011 was 110,530 MWh, with a peak load of 21,650 kWh in the month of July. In 2015, a small solar PV farm was installed in the island totaling a generation capacity of 2,011 kWp with electric battery storage for backup, with plans to further expand capacity to 6,948 kWp at one point in the future.

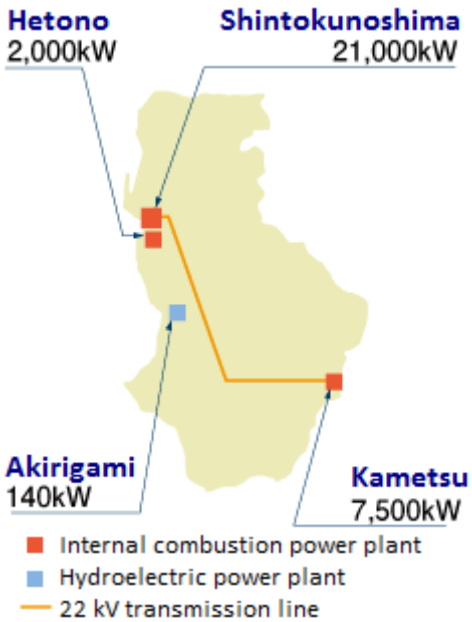

Figure 7.2. Distribution of power stations and transmission lines in Tokunoshima Island [5].

7.2.2 Simulation parameters

The conventional energy supply system currently installed in Tokunoshima is considered to have an electric supply efficiency of 35%, from power generation to end user. Only gas boilers with generation efficiency of 80% are considered for supply hot water, for both residential and non-residential sectors. Electric heat pumps used for air conditioning in all sectors, with an APF of 5.9. Three facility types with different energy demand patterns are considered for this study [6]. Figures 7.3, 7.4 and 7.5 show the electric, hot water, heating, and cooling demands for each facility type. These demands correspond to a total floor area of 1000 m^2 for each facility, and they increase linearly with total floor area. Office type buildings have high electric and air conditioning demands during daytime, decreasing gradually through the evening, while hot water demands are relatively minimal. Hotel type facilities have high electric, air conditioning and hot water demands throughout the day. Store type facilities have high electric, air conditioning and hot water demands during operating hours; after closing time, air conditioning and hot water demands become zero and electric demand becomes minimal. Seasonal characteristics can be observed as well. In the office, hot water demand in winter shows a large spike during a short time period, which does not guarantee the need for a dedicated hot water supply system, but still needs to be covered. The hotel shows both heating and cooling demand in May, which is not seen in other facility types. The store presents nearly identical hot water demands in all seasons.

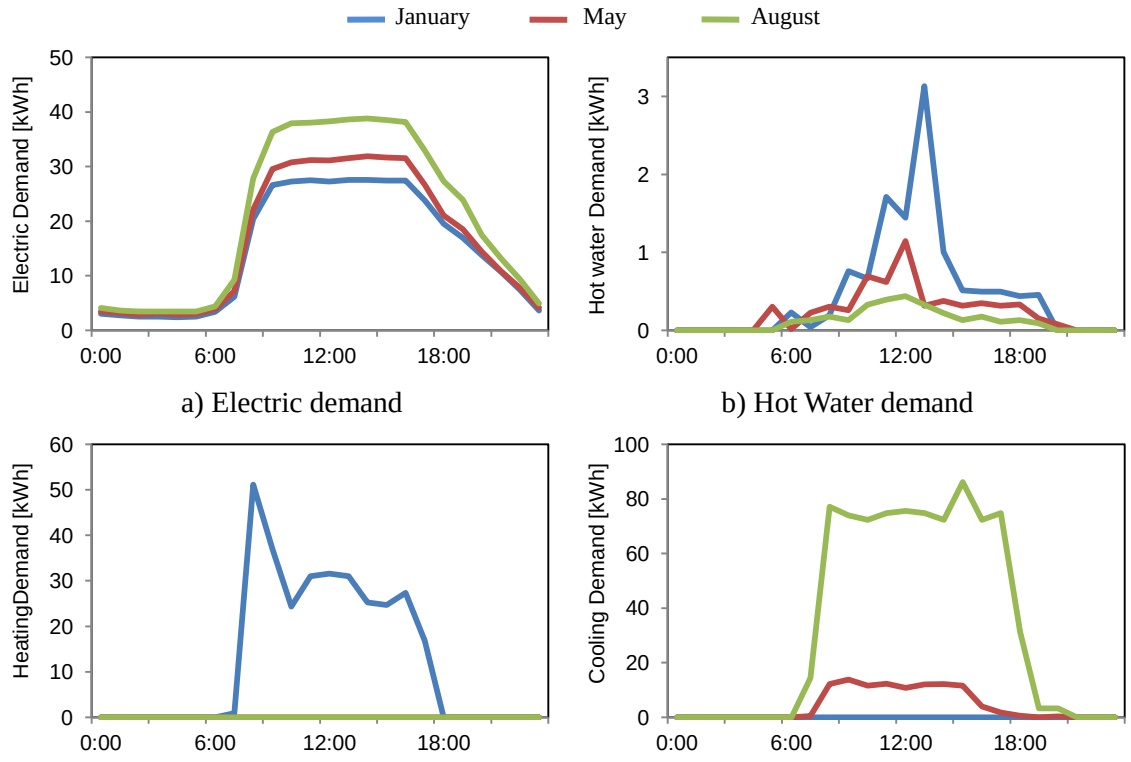

a) Electric demand

b) Hot Water demand

c) Heating demand

d) Cooling demand

Figure 7.3. Average daily electric, hot water, heating and cooling demands of a 1000 m^2 office type building for January, May and August.

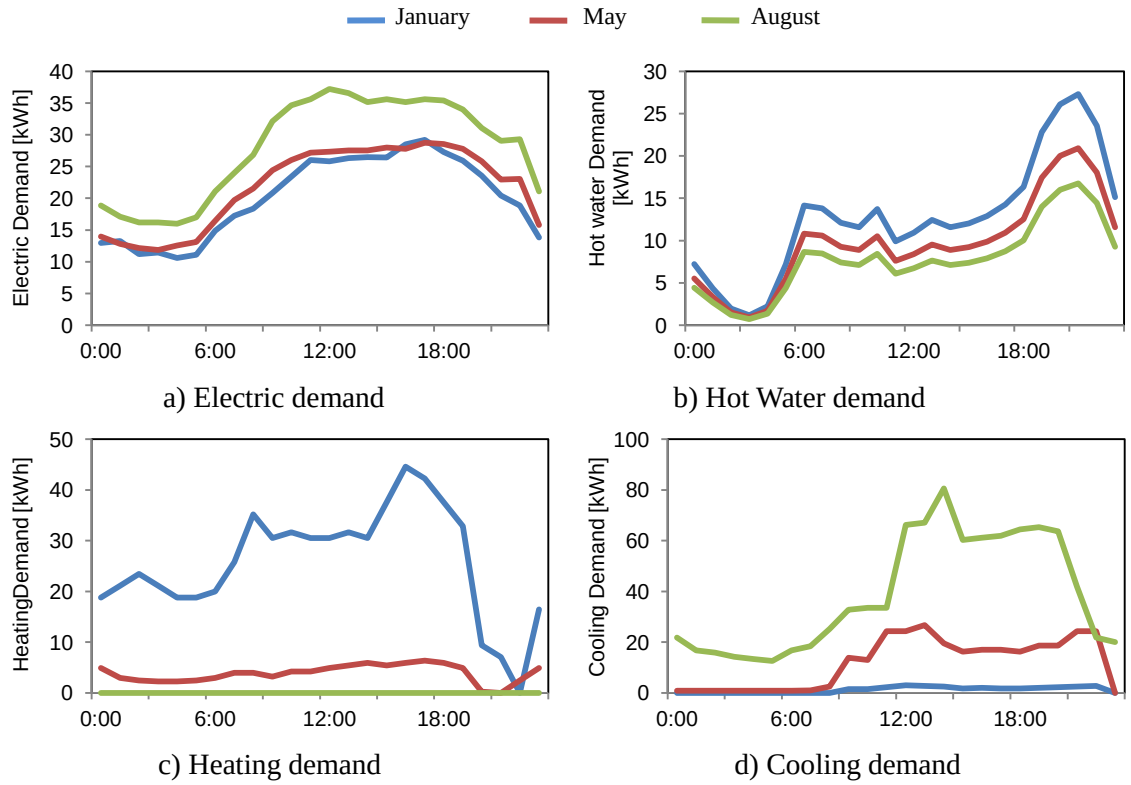

a) Electric demand b) Hot Water demand

c) Heating demand d) Cooling demand

Figure 7.4. Average daily electric, hot water, heating and cooling demands of a 1000 m^2 hotel type building for January, May and August.

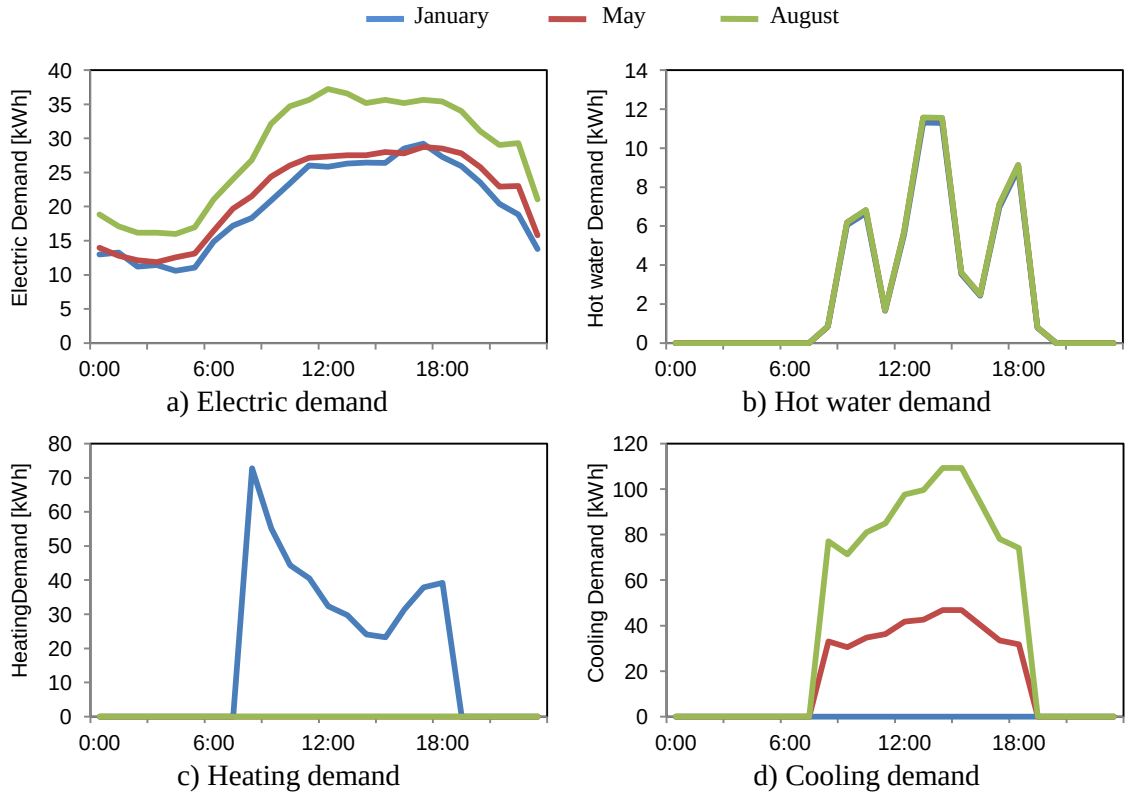

a) Electric demand b) Hot water demand

c) Heating demand d) Cooling demand

Figure 7.5. Average daily electric, hot water, heating and cooling demands of a 1000 m^2 store type building for January, May and August.

Three floor areas were considered for each facility: 1000, 2000 and 3000 m^2 for office and store, and 1000, 3000 and 5000 m^2 for hotel. Residential energy demands are considered identical for all residences, and correspond to a household floor area is at 120 m^2 with three persons per household. All air conditioning is supplied with an electric HP with a 5.9 APF, thus the respective energy demands are included in the electric demand. Residential energy demands for electricity and hot water in Tokunoshima are estimated as shown in Fig. 7.6 [6]. Solar irradiation data (Fig. 7.7) is obtained from [7] for the Kagoshima region.

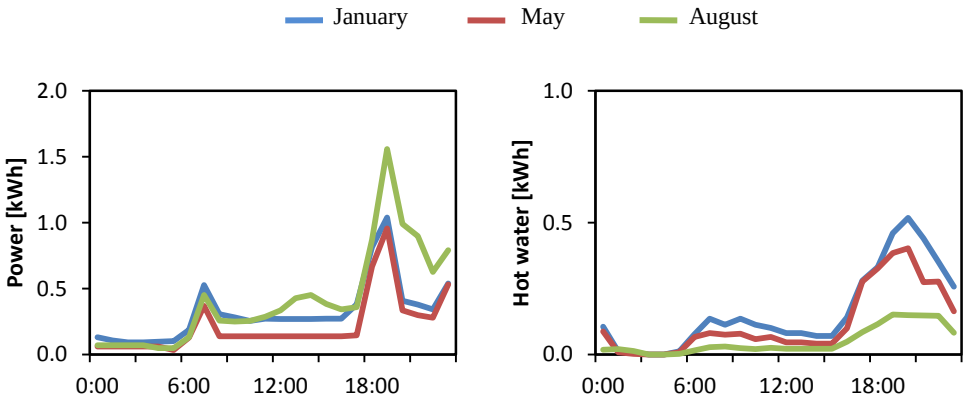

Figure 7.6. Residential power and hot water demands for January, May and August of a 3 person 120 m^2 residence in Tokunoshima.

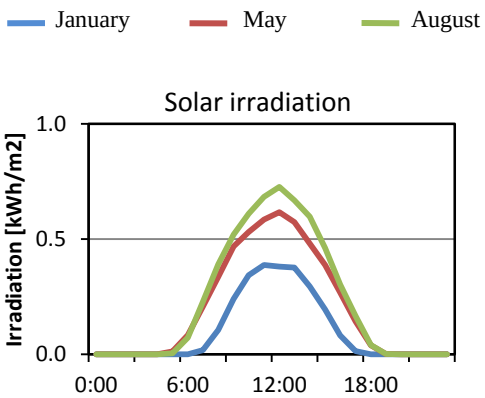

Figure 7.7. Average daily solar irradiation for January, May and August in Tokunoshima.

7.3 Results and discussion

Simulations were carried out utilizing input parameters corresponding to one day for each month. The linear and nonlinear solvers for BARON were CPLEX and MINOS, respectively. Computation time for all feasible solutions was close to one minute. A summary of feasible solutions obtained with the model for each case is given in Table 7.1. All solutions have shown high FSR values for this study case, with different trends for each facility type. Variable bounds used were fairly similar for each

facility type. Number of residences increased with larger facility size for all facility types, while FSR increased with larger facility size for the office type building and decreased for the hotel and store type buildings. SOFC and PEFC size both increase with increasing facility size, and PEFC ratio (*i.e.*, PEFC capacity over total fuel cell capacity) was higher for increasing facility size in the office type building, but lower in the hotel and store type building. This trend is similar to that of FSR. PV area is seen to decrease with larger facility size for all facility types, while HC increases to occupy the 25 m^2 residential roof area. The reason for this is attributed to the increasing number of residences and combined power output from PV. As number of residences increases with larger facility size, the total area covered by PV results in higher power output that needs to be stored during daytime. More residences also equal more electricity consuming HPWHs in the micro-grid. Allowing HCs to cover a larger fraction of the hot water residential demands instead of HPWHs eliminates part of the losses from converting surplus electricity from PV to hydrogen and once again to electricity in the fuel cells. Since energy losses in the hot water tank are smaller, the model is believed to favor HCs for hot water supply in larger micro-grids.

Table 7.1. Simulation results for three facility types of different sizes, and the variable boundaries used in each case.

	Facility size [m^2]	N_R	FSR	SOFC size [kW]	PEFC size [kW]	Area of PV [m^2]	Area of HC [m^2]	N_R upper bound	SOFC size upper bound	PEFC size upper bound
Office	1000	92	44.30%	26	142	25	0	400	500	300
	2000	109	45.64%	27	190	25	0	400	500	300
	3000	144	47.02%	32	264	23	2	400	500	300
Hotel	1000	92	47.18%	30	148	24	1	500	220	400
	3000	116	44.12%	60	222	23	2	500	200	400
	5000	169	40.73%	108	325	19	4	500	200	400
Store	1000	101	51.07%	19	150	24	1	200	300	400
	2000	136	46.44%	38	197	24	1	200	300	400
	3000	180	43.19%	57	258	21	4	400	300	500

The contribution of each micro-grid component to the total supply of energy can be observed in the operation schedule graphs in Figs. 7.8, 7.9 and 7.10 for the Office, Hotel, and Store type facilities, respectively. Only the results for the highest FSR case in each facility are shown here. In the office type building (Fig. 7.8), we see that although PEFC operates at the specified minimum load of 30% during January and May, the small base load covered by the SOFC during the year and the large peak that appears in August justify the large PEFC capacity given by the model. Furthermore, the high solar irradiation in August is able to supply enough power without the PEFC operating, which results in low exhaust heat for the ACH and thus requires that the facility HP operates at the high load seen in Fig. 7.8 (c) in order to cover the facility's air conditioning demands. In fact, the calculated yearly capacity factors for the ACH, from the results in Figs. 7.8-7.10, were 10% for the office case, 11% in

the store case, but were highest at 28% for the hotel case. The calculated capacity factors for other cases were obtained as well. It was seen that ACH capacity factor was higher for cases where FSR was lower. That is because FSR is low when fuel cell operation is high, due to higher fuel consumption, which leads to higher amount of exhaust heat to power the ACH. The lowest FSR was seen for the 3000 m^2 store type facility, where ACH capacity factor was 16%, an increase from the capacity factor in the 2000 m^2 case of 12%, and from 11% in the 1000 m^2 case. A definitive factor in ACH utilization appears to be heating and cooling demand during the day and night, which are nonexistent for the office and store cases. The ACH shows to have the highest contribution to energy supply in the hotel case, where heating and cooling demand are high in all seasons. If ACH operation is only considered with respect to the actual energy demands, and not the available ACH capacity, then the ratio of ACH usage seems more significant. Calculation of the yearly ACH usage in proportion of the air conditioning demands yields 42% for the office, 70% for hotel and 42% for the store type buildings, in the results presented in Figs. 7.8-7.10. Further studies should evaluate whether there is a threshold for ACH usage for which it is better to supply all air conditioning with HP, and utilize instead the fuel cell exhaust heat for other purposes, such as additional power generation using a gas turbine.

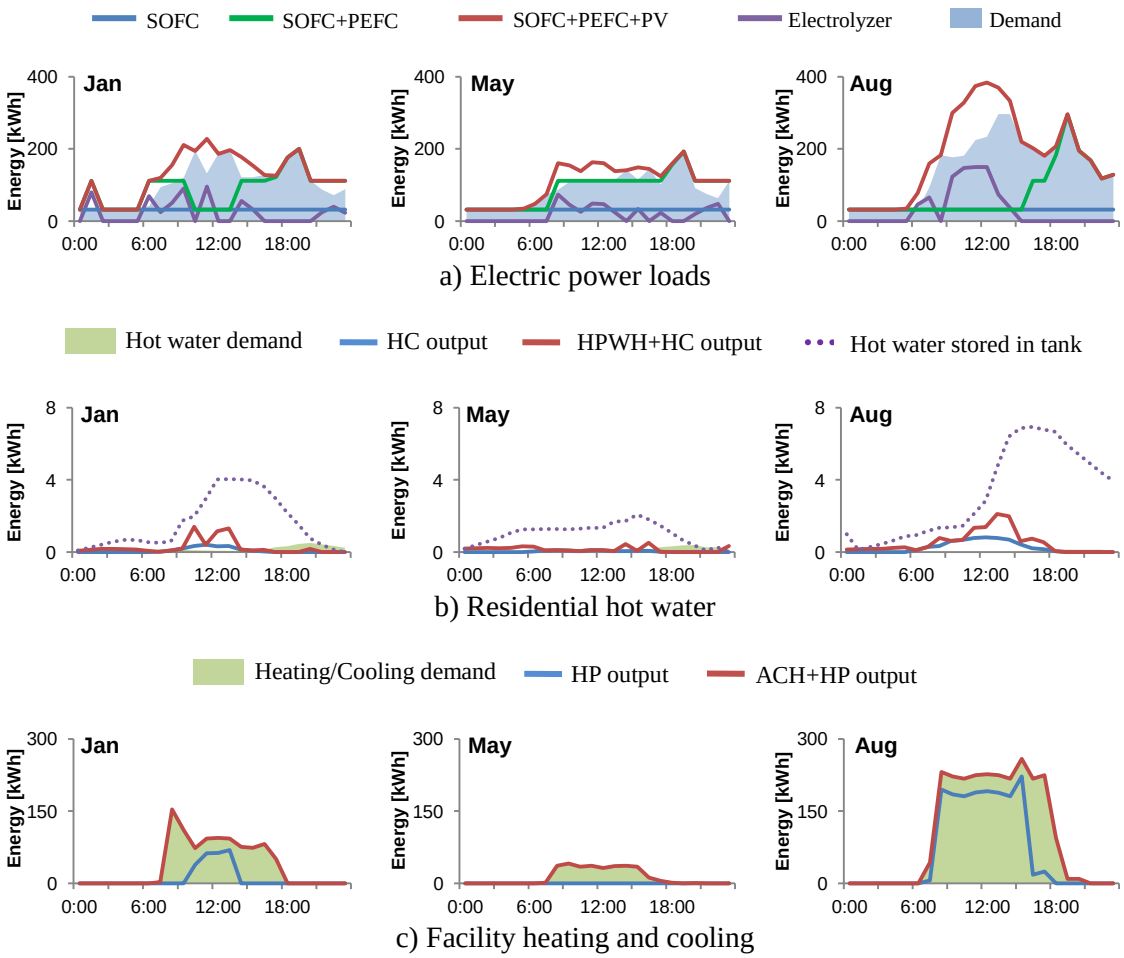

Figure 7.8. Energy demand and supply for a 3000 m^2 Office and 144 residences micro-grid.

Nevertheless, HP plays also an important role in the hotel cases. From Fig. 7.9 (c) we can see the variation in the HP operation in January, while the PEFC is inactive. This is believed to be the model's method for distributing the surplus electricity from solar PV, when otherwise losses in the electrolyzer would be high.

Electrolyzer usage can also be observed in Figs. 7.8-7.10. While its operation is intermittent, yearly capacity factor of the electrolyzer resulted in 22% for the office, 25% for the hotel and 19% for the store type buildings. In the months of August for both the Hotel (Fig. 7.9) and Store (Fig. 7.10) cases, it can be seen that the electrolyzer reaches maximum operation capacity. In these cases, it appears that the model relies on the residential HPWHs for load balance in order to avoid having unused electricity. Since the model's functions were constrained to utilize all electricity, this behavior is expected. And judging by the lack of remaining hot water in the tank at the end of the day, in spite of the high solar HC output, it is evident that the model achieves smart allocation of energy resources. Although electric batteries are not recommended for large scale energy storage, it would also be worth studying if there's a threshold for electrolyzer capacity factor where it would be more effective to utilize battery storage, if this could result in added flexibility for load balancing.

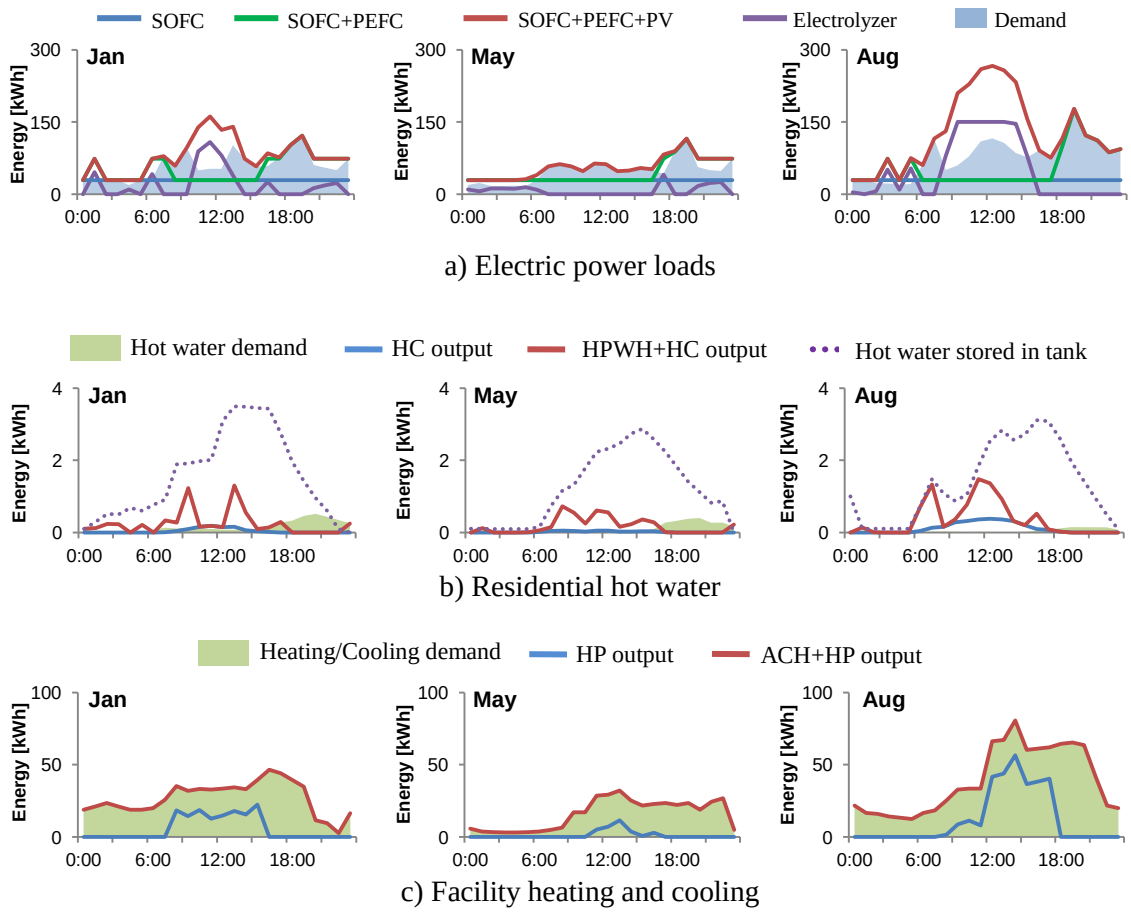

Figure 7.9. Energy demand and supply for a 1000 m^2 Hotel and 92 residences micro-grid.

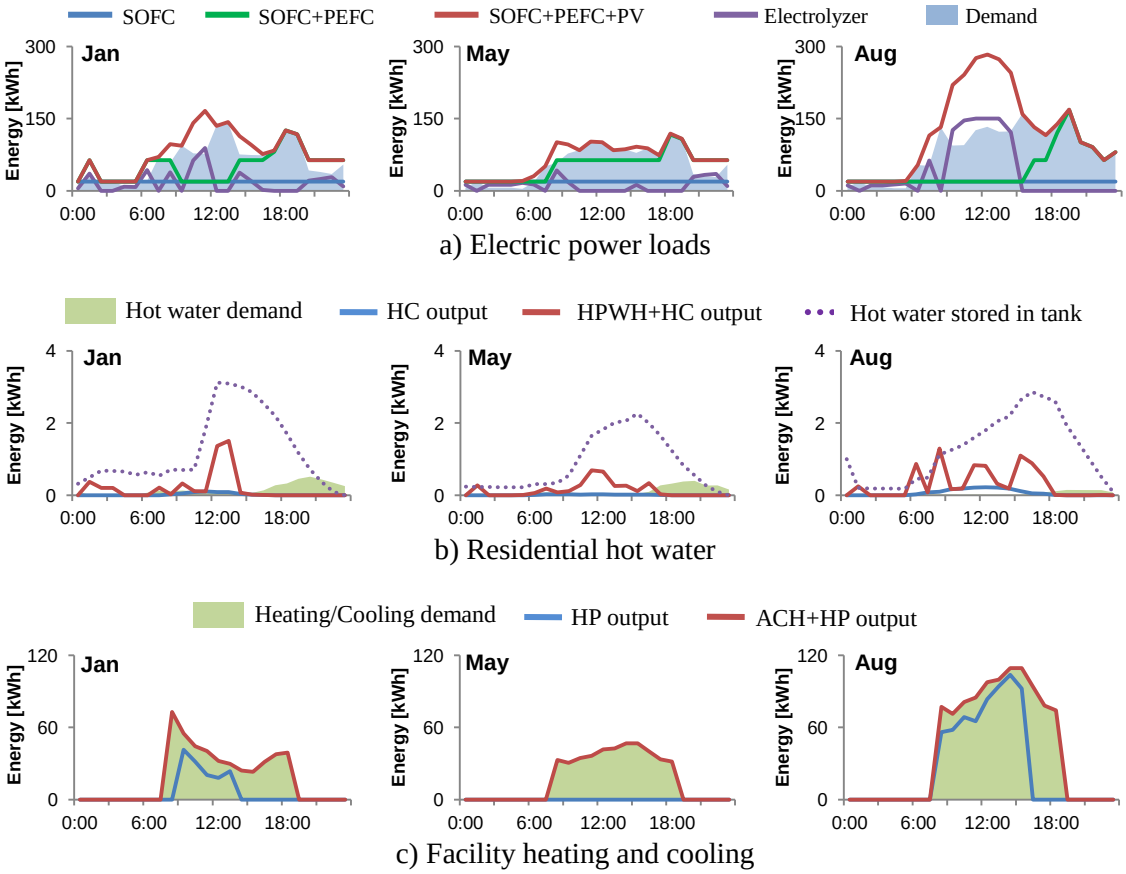

Figure 7.10. Energy demand and supply for a 1000 m^2 Store and 101 residences micro-grid.

7.4 Cost analysis

In order to evaluate the feasibility for implementation of the proposed micro-grid structure in isolated areas, a complete cost analysis is required. Unlike other studies [8-10] that have sought to minimize installation costs and payback period of isolated energy supply systems, the optimization model presented in this thesis utilizes an objective function based primary energy consumption. This is mainly because the proposed micro-grid structure does not operate constantly at full capacity, giving much needed flexibility in energy demands to communities that seek social development. As a result, this micro-grid structure offers power quality and reliability benefits that, although they can be expressed monetarily, are difficult to include in cost based objective functions [11]. Furthermore, DER technologies are relatively new to the market and their costs are expected to decrease during future years. This makes it substantially difficult to analyze which cost baselines are actually needed for the proposed system to be economically feasible, unless optimization simulations are run numerous times. Since the energy demands are less likely to vary drastically during future years, compared to the prices in DER technologies, it seems more worthwhile to perform independent economic analyses after the micro-grid structure has been optimized for primary energy consumption.

To carry out the economic analysis, the costs of technologies are first defined. To calculate the advantages of the proposed system, the costs to continue operating the currently installed energy supply system in the Tokunoshima Island are taken into account as well, including the cost for importing the fuel resources and the transport costs. Then, hydrogen costs need to be addressed as well. Several hydrogen generation strategies are considered and their costs are evaluated together with the grid implementation costs.

7.4.1 Technology costs

The technology costs can be divided into two categories: continuous and discrete. The costs for continuous technologies are considered to be linearly dependent on the installed capacity. Such is the case for solar PV and HC, both fuel cells, and the hydrogen tank. On the other hand, discrete costs consider the components to have a standard capacity, and the total costs depend on the number of units that need to be installed. Installation and annual operation and maintenance costs for the selected technologies are presented in Table 7.2. The capacities described for the discrete technologies correspond to commonly used, commercially available components.

Table 7.2. Technology costs for the components utilized in the micro-grid.

		Costs per kW			Ref.
		Installation	Annual O&M	Lifetime	
Continuous Technologies	Solar Photovoltaics	¥ 364,000	¥ 3,600	20	[12]
	Solar Heat collector	¥ 54,000	¥ 4,000	20	[13]
	Polymer Electrolyte Fuel Cell	¥ 131,400	¥ 1,314	15	[14]
	Solid Oxide Fuel Cell	¥ 131,400	¥ 1,314	15	[14]
	Hydrogen tank	¥ 180,000	¥ 10,800	20	[15]
		Costs per unit			Ref.
		Installation	Annual O&M	Lifetime	
Discrete Technologies	1.5 kW Heat Pump Water Heater	¥ 252,000	¥ 23,760	10	[16]
	4 kW Residential Heat Pump	¥ 136,111	¥ 8,400	10	[17]
	175 kW Absorption Chiller-Heater	¥ 2,551,238	¥ 127,562	15	[17]
	150 kW Water Electrolyzer	¥ 28,224,000	¥ 15,600	10	[15]
	2 kW Facility Heat Pump	¥ 45,376	¥ 2,269	10	[17]

In order to define the total initial costs for implementation of this micro-grid, the total capacity of the components that the optimization model suggests are needed. These values are summarized in Table 7.3, for all facility sizes of each facility type.

Table 7.3 Summary of the component capacities in the micro-grid for each facility type.

		Office			Hotel			Store		
		1000 m^2	2000 m^2	3000 m^2	1000 m^2	3000 m^2	5000 m^2	1000 m^2	2000 m^2	3000 m^2
Continuous Technologies	Solar Photovoltaics [kWp]	319	380	460	310	377	457	346	454	534
	Solar Heat collector [kWh]	9	3	125	37	85	308	24	65	296
	Polymer Electrolyte Fuel Cell [kWh]	142	190	264	148	222	325	150	197	258
	Solid Oxide Fuel Cell [kWh]	26	27	32	30	60	108	19	38	57
	Hydrogen tank [m^3]	2	10	13	7	16	27	8	13	19
Discrete Technologies	1.5 kWh Heat Pump Water Heater [-]	92	109	144	92	116	169	101	136	180
	4 kWh Residential Heat Pump [-]	92	109	144	92	116	169	101	136	180
	175 kWh Absorption Chiller-Heater [-]	1	1	1	1	1	2	1	1	1
	Electrolyzer [kWh]	150	150	150	150	150	150	150	150	150
	2 kWh Facility Heat Pump [-]	100	200	300	100	300	500	100	200	300

The solar PV and HC capacities are defined with respect to the total number of residences and the roof area fraction they occupy. The capacity of the fuel cells was previously reported in Table 7.1. To define the capacity of the hydrogen tank, additional calculations were required. The case of the 3000 m^2 office type facility will be utilized to illustrate this. The maximum and the minimum monthly hydrogen demands were first identified, which were 4,291 kg_{H2} in May and 2,004 kg_{H2} in April, respectively. Then, the number of days that the tank charge should last on average is defined, which is usually considered to be three days, although depending on the frequency on ships that commute to the island, this value may increase. A maximum charge of one week's supply is considered later for comparison. The tank's capacity is then defined as the average of the monthly maximum and minimum hydrogen demand, multiplied by 30 (*i.e.*, the days in one month) and divided by the number of days that the tank's charge is expected to last in the case that no hydrogen fuel is added to the tank. The tank's capacity calculated this way is expressed in kilograms, so the density of compressed hydrogen at 700 bar is used to calculate the volumetric value, which for this case results in 13 m^3. Although the volume of this storage system is considerable, it corresponds to only 0.09 m^3 per residence, which is considered to be enough to justify its size. In comparison, a tank that can last for a week's worth of charge would require a volumetric capacity of 33 m^3, or 0.23 m^3 per residence. The hydrogen tank's costs represent a very large fraction of the total installation cost of the micro-grid, so large tank capacities are not recommended unless shipping frequency is severely limited.

7.4.2 Fuel supply costs

7.4.2.1 Fuel oil and LPG costs

As explained in Section 7.2.1, energy supply in Tokunoshima Island is currently obtained mainly through fuel oil generators and gas boilers utilizing LPG. To calculate the economic feasibility of the proposed micro-grid, the costs of the current energy supply system are used for comparison. Global oil prices saw a dramatic decrease in price in 2014, from an average of 110 USD (12,110 JPY)[1] to 50 USD (5,504 JPY) per barrel. A decrease in oil prices was seen between 2008 and 2009 as well,

[1] All currency exchange in 2016 JPY (1 USD = 110.10 JPY)

where prices fell from 140 USD (15,411 JPY) to 40 USD (4,403 JPY) per barrel [18]. This price drop was followed by a steep increase of prices during the following three years, where it reached prices of 120 USD/barrel. The volatility in oil prices is a major concern for island communities, and as we see from previous trends, the recent drop in oil prices will most likely be followed by an increase in prices. In Chapter 1 of this thesis, the forecast of oil prices up to the year 2040 shows that prices may even increase up to 250 USD (27,522 JPY) per barrel in the worst case scenario, but still consider a barrel price near 150 USD (16,513 JPY) in 2040 for the reference scenario. In Japan, about 80% of the total oil product imports come from countries in the Middle East. Fuel oil used in electric generators is generally economic, but it has reached prices of 131 JPY/L in Japan [19]. This economic analysis parts from this point with the hypothesis that hydrogen fueled micro-grids will be economically feasible as oil prices surpass this value.

Prices for LPG have not seen high variations compared to oil, and thus their price is considered to remain fairly constant. The price of LPG in Japan is considered to be 230 JPY/m^3 [20].

7.4.2.2 Hydrogen costs

Various hydrogen fuel sources were described in Chapter 6. In this section, five hydrogen generation methods are considered for fuel supply to Tokunoshima Island. They are divided into Off-site and On-site generation. Off-site generation includes SMR, coke-oven gas reforming, and water electrolysis using nighttime power electricity. For On-site generation, only biomass gasification, and water electrolysis utilizing wind power are considered.

Off-site generation:

- Steam Methane Reforming (SMR): Natural gas is currently the main source of hydrogen globally, which accounts for nearly 98% of the total hydrogen supply. Natural gas is an important commodity in today's energy infrastructure, and thus it is relatively easy to find suppliers of this resource. Extensive analyses are available regarding hydrogen production costs using SMR. Considering the costs for natural gas, and including compression, storage and dispensing, hydrogen production costs using this method have been estimated at 409 JPY/kg_{H2} [21].
- Coke-oven gas (COG) reforming: Exhaust gases from coke ovens used in steelworks factories have a high hydrogen content that can be recovered. Previous methodologies for this process involved cooling the exhaust gases before treatment, which presented an estimated cost of 13 JPY/Nm^3 of hydrogen. New research sees the possibility of saving costs by utilizing hot COG in the reforming process, which results in an estimated cost of 9.30 JPY/Nm^3 of hydrogen [22].

- Water electrolysis utilizing nighttime power: To maximize efficiency, base load power plants need to operate at a constant load. Power demands usually decrease during the night, affecting the generating efficiency of these power plants. To avoid this, electric companies in Japan offer reduced prices of electricity during low demand hours, with discounts that range from 10% to 15% [23]. Nevertheless, this marketing strategy does not guarantee that the base-load power plants reach maximum load operation, as it is still subject to variations in the demand. If customers were to find the electricity price attractive, a scenario where energy demand increases over the base-load capacity may be considered, which would require additional power generators to begin operating to cover this demand. On the other hand, for seasons where nighttime electricity does not increase even with the strategy implemented, the base-load would continue operating at non-optimal efficiency. Therefore, a hydrogen production plant that utilizes nighttime power exclusively to balance the base-load to max capacity could be implemented. By guaranteeing that all surplus electricity will be consumed, a lower electricity price may be negotiated. In this study, current prices for nighttime electricity of 7.22 JPY/kWh are considered to be reduced to 6 JPY/kWh. To run this plant, eight hours of electricity are used to power a 300 kWh electrolyzer plant with a 20 year lifetime and 80% generation efficiency, resulting in a hydrogen fuel cost of 7.51 JPY/L.

Off-site generation:

- Biomass gasification: hydrogen generation using biomass gasification has been extensively researched [24]. Hydrogen production costs using this method depend heavily on the plant capacity and the cost of feedstock to generate biomass. The highest costs are seen when gasification plants are first implemented. As they progress through the learning curve, further plants can be installed with less capital expenses. Early stage suppliers of biomass feedstock also exhibit prices, as they are unable to supply the feedstock with reliability and in high quantities. A study has estimated costs for hydrogen production at 626 JPY/kg_{H2} using an early stage plant supplied by low cost feedstock, while a late stage plant with low cost feedstock would result in costs as low as 271 JPY/kg_{H2}. Biomass gasification plants have been successfully installed in various places in Japan, and the technology continues to improve. Transmitting this technology to Tokunoshima Island is then considered to represent a late stage gasification plant. However, a feedstock infrastructure is not yet available and thus costs are expected to be high. For this study, the hydrogen cost of biomass gasification is considered as 405 JPY/kg_{H2}, corresponding to a late stage plant with high feedstock costs.
- Water electrolysis utilizing wind power: wind power has been considered for power generation in islands in various cases. This study seeks to find a balance between the residential sector and the commercial and public sectors. This is achieved by entrusting the

residences with solar power generation by making use of their spatial distribution, while using a non-residential facility to house the main power generation system. For this reason, wind power has not been considered a part of the optimization problem. Instead, electricity obtained from wind power farms is regarded as a source for hydrogen, which can supply the cogeneration fuel systems installed in the central facilities. Additional power obtained from wind energy may also be used to power the infrastructure that is not covered by the proposed micro-grid structure, such as road lighting and water supply. Wind energy costs have been decreasing in the past years, and have reached a levelized cost of energy of 3 JPY/kWh [25]. Considering an average capacity factor of 25% and the electrolyzers already installed in the facilities, hydrogen costs using this method are considered as 15 JPY/L in this study.

7.4.3 Fuel transport costs

Hydrogen generated off-site needs to be transported to the island for consumption. Fuel transport costs for islands in Japan depend on the distribution method, which corresponds to the demand size. Low demands require more resource consuming distribution channels. Current fuel transport costs are 0.06 USD/L for large islands, 0.08 USD/L for medium islands, and 0.12 USD/L for small islands [26]. Tokunoshima Island is considered a medium-sized island, and thus fuel transport costs are 0.08 USD/L. To compare the economic viability of the proposed micro-grid, the costs to continue operating the conventional system using fuel oil and natural gas are analyzed. Despite the 2016 price drop in oil, EIA estimates that oil prices will continue to escalate during following years. Oil barrel costs are expected to remain in the 100-150 USD/barrel range until 2040 in the reference case, or 150-200 USD/barrel in the high oil price case [27].

7.5 Cost comparison

The different shares of sources to supply the hydrogen micro-grid have been grouped into seven hydrogen source share scenarios for this study. It is worth noting that energy security is proportional to the number of available primary energy sources and their share of the total energy supply [28]. This is represented with the Shannon-Wiener Diversity Index *SWDI*, given in Eq. (7.1), where p_i is the share of primary energy source *i* in the total primary energy supply.

$$SWDI = -\sum_i (p_i \cdot \ln(p_i)) \quad (7.1)$$

By definition, an energy supply system with 100% dependence on one source of primary energy has a *SWDI* of zero, and thus has the highest vulnerability with regard to energy security. The seven

scenarios considered are presented in Table 7.4, where the total share of each hydrogen source and the corresponding *SWDI* are shown.

Table 7.4. Hydrogen source share scenarios and respective Shannon-Wiener Diversity Index.

	Only imports	COG+SMR	Bio+NP	SMR+Bio	No imports	COG+Wind	COG+Bio
Natural gas (CH4)	0%	20%	0%	20%	0%	0%	0%
COG gasification	80%	80%	0%	0%	0%	75%	50%
Night power	20%	0%	20%	0%	0%	0%	0%
Biomass gasification	0%	0%	80%	80%	75%	0%	50%
Wind power	0%	0%	0%	0%	25%	25%	0%
SWDI	50%	50%	50%	50%	56%	56%	69%

Scenario "*Only imports",* assumes that all hydrogen is generated off-site, with 80% of the demand supplied by COG reforming and 20% by nighttime power electrolysis. In scenario "*COG+SMR"*, COG reforming covers 80% of the demand and 20% comes from natural gas reforming. In scenario "*Bio+NP"*, natural gas is not utilized and instead biomass generates 80% of the demand and 20% comes from nighttime power electrolysis. Scenario "*Bio+SMR"* considers the use mainly of biomass gasification with an 80% share, and 20% backup share of natural gas reforming. "*No imports"* scenario eliminates fuel transports and all hydrogen is generated on-site, with a 75% wind share and 25% biomass gasification share. "*COG+Wind"* scenario considers a 75% share of COG reforming, while 25% of the demand is generated on-site using wind power. "*COG+Bio"* scenario utilizes the waste reforming technologies for COG and biomass gases, with equal shares of 50%. Utilization of more than two hydrogen sources per micro-grid is considered to bring in additional costs regarding logistics during initial stages, thus only two sources are considered in the described scenarios.

Using these scenarios, the total installation and running costs for different facility types are evaluated. Analysis period was 20 years, corresponding to the longest lifetime found in the micro-grid components. Those components with shorter lifetimes are replaced as needed during the analysis period. The energy costs per kilowatt-hour for each facility type and size are presented in Fig. 7.11, for all hydrogen share scenarios. Scenarios were rearranged from lowest to highest cost in this figure.

Overall, the office type buildings showed the highest costs, and the hotel type building the lowest. Smaller facilities also showed higher costs in general, which may be partly attributed to the oversized ACH, since its capacity was considered constant for all cases at 175 kWh. For the 1000 m^2 office, no scenario gave lower costs than the conventional system. For the 2000 and 3000 m^2 offices, as well as all hotel and store sizes, the proposed micro-grid presented lower energy costs compared to the conventional system in all scenarios.

The *COG-Bio* scenario did not only show the lowest energy cost for all facility sizes, but also the highest index for energy security. However, neither biomass nor COG alone can guarantee low costs

as seen in the *Bio+SMR* and *COG+SMR* scenarios, which showed the highest costs for all cases. The four scenarios in which wind or nighttime power is considered showed almost no difference in energy costs. This facilitates the decision of which scenario to apply during initial implementation of the proposed micro-grids, depending on the availability of wind and nighttime power resources. Furthermore, if the hydrogen output from COG reforming is limited or not available, the *Bio+NP* and *No imports* scenarios offer both viable solutions.

If the final target is to eliminate fuel transports, *Bio+NP* or *COG+Bio* scenarios can be implemented before investing in wind turbines. Similarly, *COG+Wind* may be implemented first before the biomass gasification plant is running. Although *COG+Bio* presented the lowest cost, the output capacity from each of these hydrogen sources would need to be considered as well, if several micro-grids are going to utilize the same hydrogen source scenario. The small difference in cost between the *No imports* and *Only imports* scenarios also shows that fuel transport costs can be offset by using low cost hydrogen sources such as industrial waste.

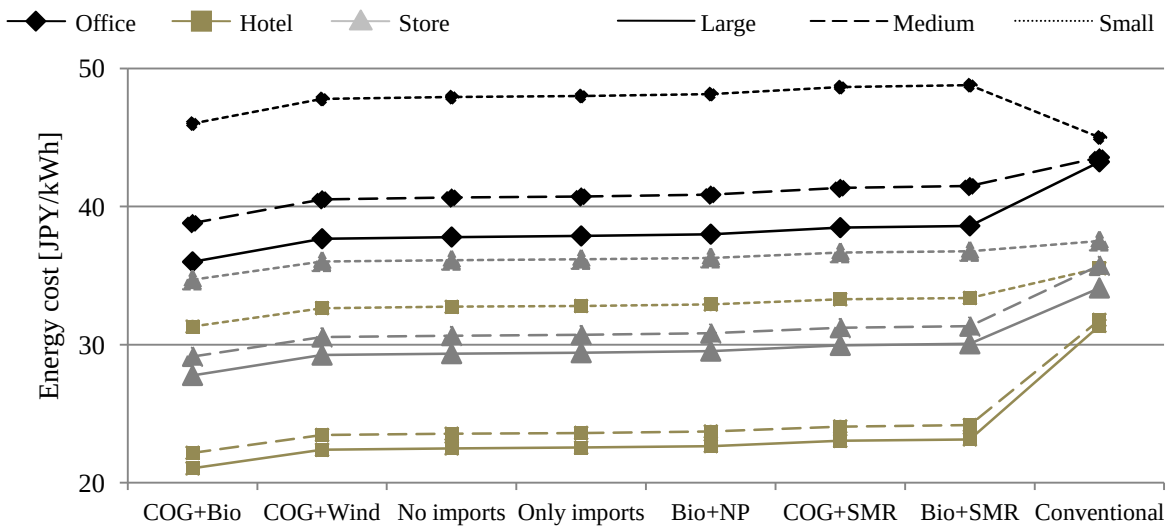

Figure 7.11. Final energy costs for implementation of the proposed micro-grid during a 20 year period, compared to the costs for continuing to operate the conventional system. Each color represents a type of facility, and the line style represents the different sizes of each facility type.

Considering the lowest energy costs corresponding to the hydrogen share scenario *COG+Bio*, the return on investment is calculated for different oil prices. Four oil price trends are selected for comparison, one corresponding to constant oil prices during the following 20 years, and three trends considering a yearly increase in oil prices of 2%, 4% and 6%. Again, only the cases with the highest FSR for each facility type will be addressed here.

Figure 7.12 shows the return on investment for the 3000 m^2 office case. The points at which the lines suddenly decrease represent component replacement costs. It is clear that with increasing oil

prices, complete return on investment is achieved earlier. Even if oil prices remain constant, return on investment can be achieved within the specified period of 20 years for the 3000 m^2 office type facility case. Complete return on investment may be achieved in 13, 10 or 9 years if oil prices have a yearly increase of 2%, 4% or 6%, respectively. The small difference between these two last cases suggests that it might be difficult to achieve shorter payback periods than 10 years, which even so represents an economically feasible scenario.

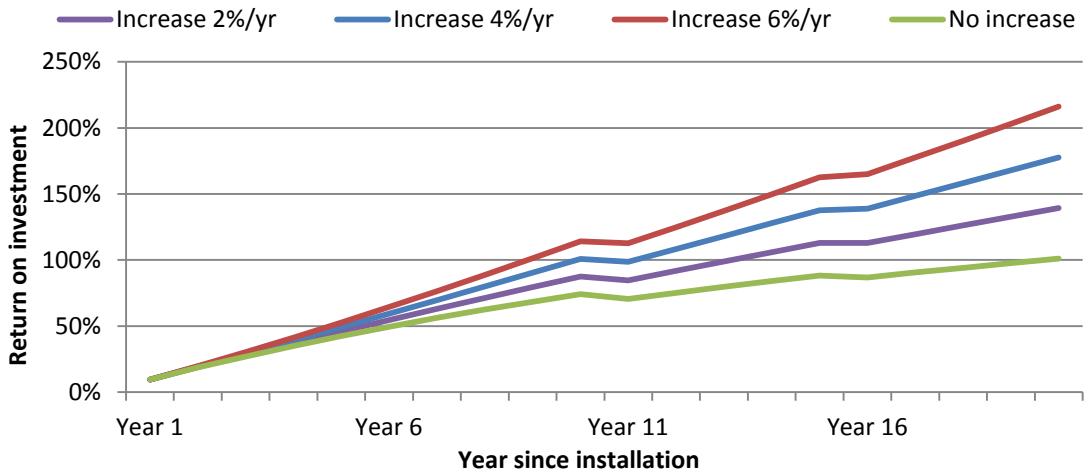

Figure 7.12. Return on investment for the 3000 m^2 office type facility case for different oil price scenarios.

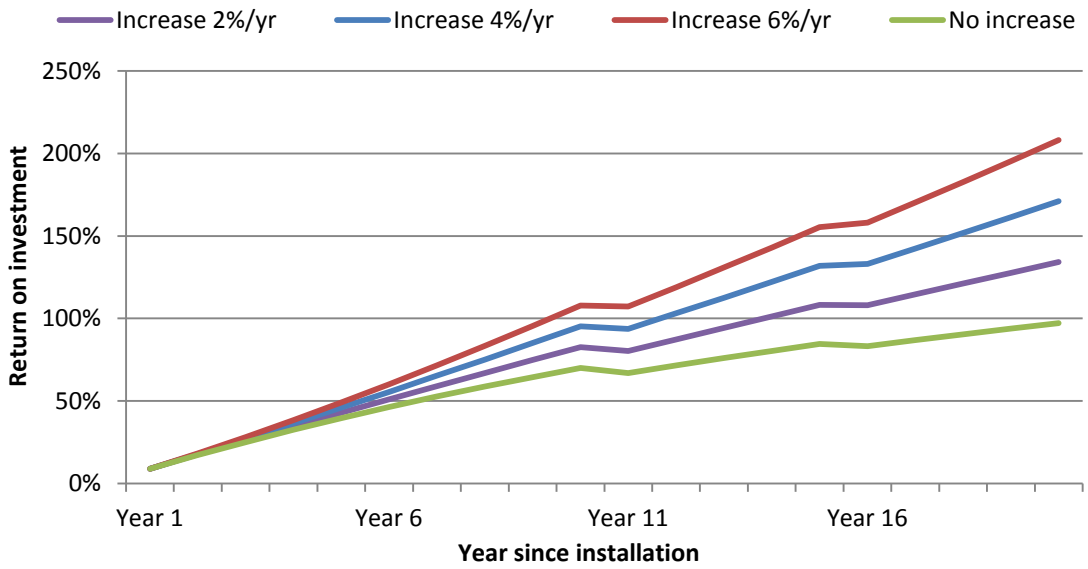

Figure 7.13. Return on investment for the 1000 m^2 hotel type facility case for different oil price scenarios.

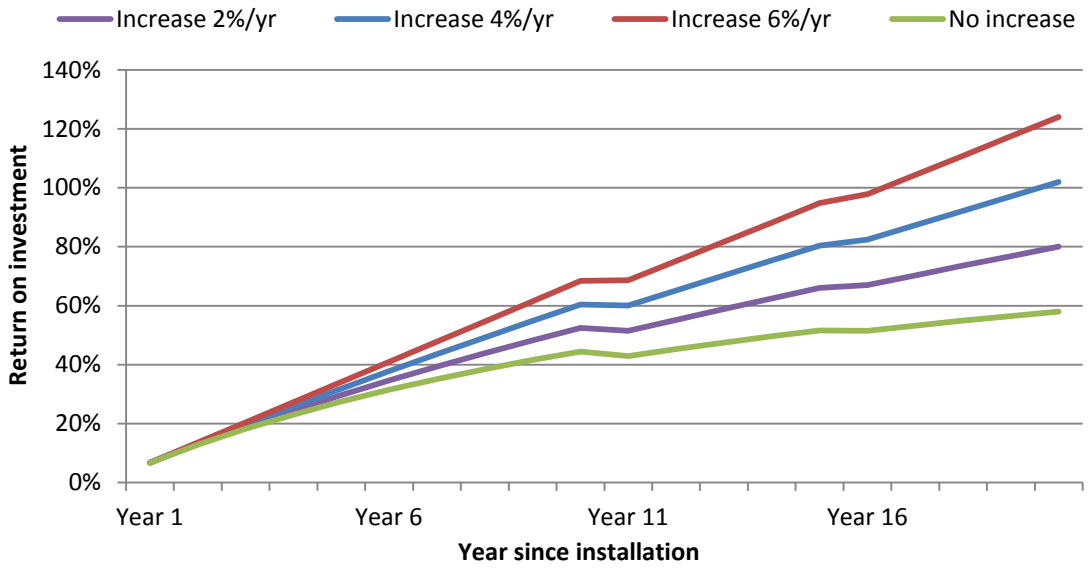

Figure 7.14. Return on investment for the 1000 m^2 store type facility case for different oil price scenarios.

Return on investment for the hotel type facility was not achieved during the 20 year analysis period for the oil price scenario for no increase, while for the 2% yearly increase scenario it was on year 14, year 12 for the 4% yearly increase scenario, and year 10 for the 6% yearly increase scenario. In the store type facility, complete return on investment was also not observed for the case where oil price does not increase, while for the 2%, 4% and 6% yearly increase scenarios, return on investment occurred on the year 15, 13 and 10, respectively.

As suggested by Fig. 7.11, the lower FSR values that appeared on the largest facility size for the hotel and store cases did not lead to lower economic feasibility. For the 3000 m^2 store type facility case, complete return on investment was observed for all oil price scenarios. From the no increase, 2%, 4% and 6% increase scenarios respectively, return on investment was observed at years 18, 13, 10 and year nine. These values were more impressive on the 5000 m^2 hotel type facility case, where complete return on investment was achieved on year 13 on the scenario without increase in oil price. Scenarios with 2%, 4% and 6% yearly increase in oil price resulted in complete return of investment at years nine, eight and seven, respectively. For the office type facility case however, the lowest FSR corresponding to the smallest facility size did not result in better economic feasibility. The results suggest thus that as the micro-grid energy demands increase, economic feasibility improves and return on investment can be achieved earlier. It is worth noting that since the hydrogen tank has a significant impact on the total cost of the micro-grid, the objective function based on maximization of FSR does consequently help in improving economic feasibility of the grid.

7.6 Micro-grid expansion and limitations

All studied cases except for the 1000 m^2 office type facility showed economic feasibility. Complete penetration of the proposed micro-grid into the Tokunoshima Island is regarded as viable. To achieve this, the strategy described in Chapter 3, Section 3.5.2 is utilized. This strategy is divided into six stages.

1. Initial trial.
2. Household integration.
3. Independent operation.
4. Additional trials.
5. Widespread implementation.
6. Transition into hydrogen pipelines.

Since the micro-grid structure allows for gradual implementation, only one town should be considered for initial trials. The Tokunoshima town hall is considered to be a viable choice for this. This three story building has a total floor area close to 3000 m^2, with the demands of an office type building. One such case has been analyzed in this chapter and regarded to be economically feasible. Furthermore, as a public facility it has the budget to make the large investment needed, while acting as an effort from the government to promote sustainable energy systems. The town hall is located about one kilometer away from the Tokunoshima town port, having thus good access to the hydrogen supply that will be needed at first. The town hall is found in a densely populated area, thus connection to other households does not require large changes in infrastructure. Implementation of this micro-grid will cover stages one through three.

In stage four, additional trials, a hotel is considered for implementation of the second micro-grid. In particular, the hotel Grand Ocean Resort is considered to be a promising target. It is a seven story building with a total floor area close to 5000 m^2. An analysis of such a facility has been presented in this study as well, showing economic feasibility. A store type building with an area close to 1000 m^2 in which a third micro-grid can be implemented can be located in the Nishimuta home center, which is composed of two 500 m^2 buildings. The definition of a central facility only requires that energy demands are similar, and that the area occupied by the facility is compact enough for the ACH to supply air conditioning without substantial heat losses due to long transmission pipes. Both the suggested hotel and store are located near the Tokunoshima port as well.

As stage four is successfully implemented, other facilities with large energy demands in the island would be worth considering for installation of the proposed micro-grid, such as hospitals and schools. Stage five, widespread implementation, is suggested to take place only in the Tokunoshima town, which covers about half of the total area in the island, on the east side. As seen in Fig. 7.2, the

7.5 MWh Kametsu power station is located in this area. As micro-grid penetration increases, this power station would ideally shut down, while the remaining two power stations on the west side of the island continue to supply electricity to the Isen and Amagi towns. Around this stage is where implementation of hydrogen pipelines should be addressed. Since the majority of the large scale facilities are located near the Tokunoshima port, hydrogen pipelines are believed to be a viable option for hydrogen fuel distribution. However, the northern area of the island has not been yet studied and pipeline interconnection between that area and the southern port area may not be possible. Only after the micro-grids in the Tokunoshima town can be fully interconnected into a single group of individually operating systems, should implementation of micro-grids begin in the remaining communities. Figure 7.15 shows the map of how this strategy may be followed.

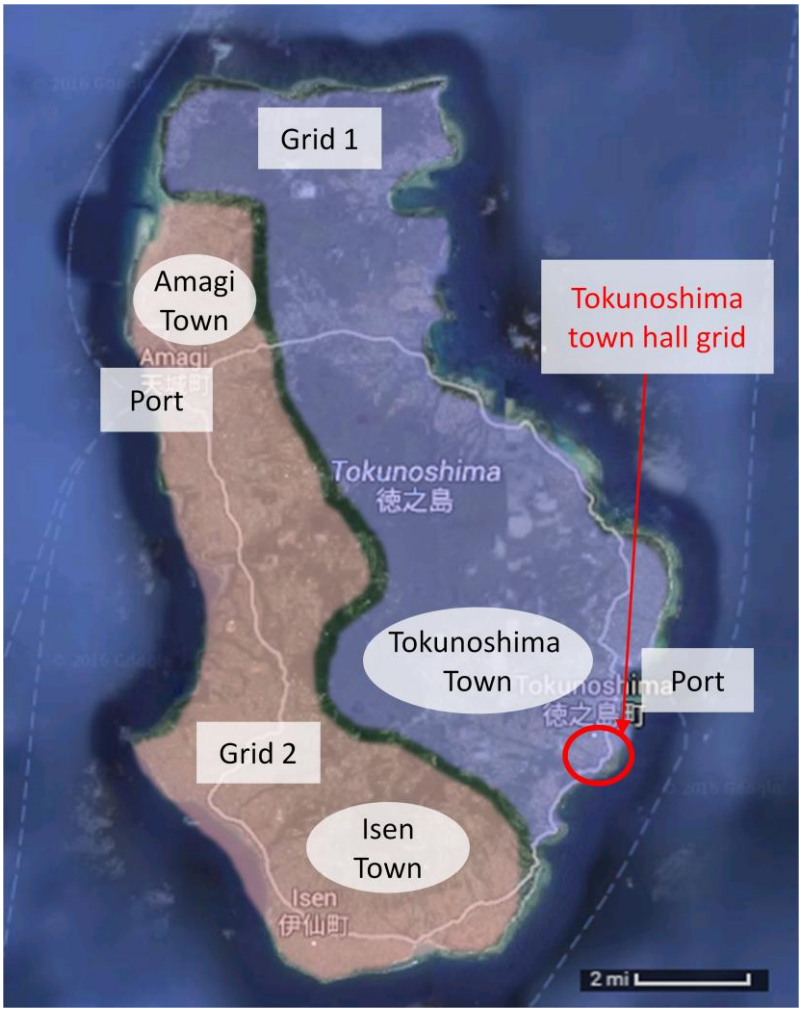

Figure 7.15. Implementation strategy of the proposed micro-grids into the Tokunoshima Island.

Looking back at the demographic statistics in Section 7.2.1, the available number of facilities should be in good proportion to the number of households. The analysis presented in this chapter suggested micro-grids with a number of residences ranging from 90 to 180. The residence to facility ratio in Tokunoshima Island lays currently around 72. This, however, does not take into account

public facilities or businesses that share a single building. Furthermore, since several of the registered facilities in the island are relatively small, it would be worth analyzing the possibility of grouping them into clusters that can act as a central facility. If energy demands are as low as those seen in the analysis for a 1000 m^2 office type facility, economic feasibility may not be guaranteed. Further research regarding the achievable output capacity for hydrogen fuel needs to be carried out as well. It is common to see large agricultural sectors in island communities, and Tokunoshima is such a case. Although biomass feedstock appears to be available in the selected area, the actual output capacity from initial implementation to future years has not been yet calculated.

7.7 Conclusions

In this chapter, the optimization model for semi-independent hydrogen micro-grids proposed in this thesis is applied to a real scenario. The target area is the Japanese island of Tokunoshima, where current energy infrastructure presents energy costs more than twice of those seen in the main Japanese Islands. The optimization model is applied to three different facility types, of sizes corresponding to those commonly seen in islands. The following conclusions are drawn from this study:

(1) The optimization model was able to find solutions with high fuel savings for all studied cases. The solutions were found using similar variable bounds for each facility type, and computation time was around one minute using data corresponding to one day per month, which was regarded as an acceptable time. Larger data input can be solved under acceptable times with higher processor speeds.

(2) The model found different management strategies for each micro-grid component when different energy demand patterns were given as input, corresponding to the different types of central facilities.

(3) Different scenarios for hydrogen source share were proposed and an economic analysis for the obtained feasible solutions was performed. It was found that fuel savings is not always correlated with lower energy costs. On the other hand, hydrogen storage costs represented a large share of the total energy costs. Therefore it is believed that maximizing fuel savings does indeed contribute to lower energy costs by minimizing the need for storage.

(4) All facility types and sizes, with the exception of small offices, were found to be economically feasible under the specified conditions, and payback periods were found to increase substantially as oil prices increase.

(5) The proposed micro-grid appears to be an economically feasible alternative to the current energy supply system in Japanese islands. The optimized micro-grid size seems to be appropriate to the number of households in the selected region. A strategy from initial to full implementation of the micro-grid in the selected region is discussed as well.

7.8 References

[1] Kyushu Regional Agricultural Administration Office. (2008). Tokunoshima outline. (In Japanese). Retrieved May 1, 2016 from http://www.maff.go.jp/kyusyu/seibibu/kokuei/14/gaikyou/

[2] Ullet-keishin. Ullet 2010. (In Japanese). Retrieved May 1, 2016 from http://keishin.ullet.com/search/city/46530/pref/46.html#pref/46/city/46530

[3] Amami Islands regional office union. (2010). Basic plan and implementation plan (first term). *Amami Islands growth strategy vision*. (In Japanese). Retrieved May 1, 2016 from http://www.amami.or.jp/kouiki/vision/vision_keikaku.pdf

[4] Kyushu Electric Power Co. (2014). Manual on interconnection of electric generation equipment using renewable energies in Tokunoshima. (In Japanese). Retrieved May 1, 2016 from http://www.kyuden.co.jp/library/pdf/press/2014/toi9g9wku.pdf

[5] Kyushu Electric Power Co. (2016). Main power plants: Tokunoshima. (In Japanese). Retrieved May 1, 2016 from http://www.kyuden.co.jp/company_outline_branch_kagoshima_initiative_institution_tokunoshima.html

[6] Kashiwagi, T. (2002), Natural Gas Cogeneration Plan/ Design Manual 2002, *Japan Industrial Publishing Co., LTD*, 64-9. (In Japanese).

[7] NEDO. (2015). New Energy and Industrial Technology Development Organization, Meteorological Test Data for Photovoltaic Systems (METPV-11). *Department of the New Energy and Industrial Technology Development Organization.*

[8] Kyriakarakos, G., Dounis, A.I., Rozakis, S., Arvanitis, K.G. and Papadakis, G. (2011). Polygeneration microgrids: A viable solution in remote areas for supplying power, potable water and hydrogen as transportation fuel. *Applied Energy*, 88, 4517-26.

[9] Abbey, C. and Joos, G. (2009). A stochastic optimization approach to rating of energy storage systems in wind-diesel isolated grids. *IEEE Transactions on power systems*, 24, 418-26.

[10] Moghaddam, A.A., Seifi, A., Niknam, T. and Alizadeh Pahlavani, M.R. (2011). Multi-objective operation management of a renewable MG (micro-grid) with back-up micro-turbine/fuel cell/battery hybrid power source. *Energy*, 36, 6490-507.

[11] Stadler, M., Marnay, C., Siddiqui, A.S., Lai, J., Coffey, B. and Aki, H. (2009). Effect of Heat and Electricity Storage and Reliability on Microgrid Viability - A Study of Commercial Buildings in California and New York States. *Lawrence Berkley National Laboratory*.

[12]METI. (2016). Recent trends on renewable energy markets. *Agency for Natural Resources and Energy.* (In Japanese). Retrieved May 1, 2016 from: http://www.meti.go.jp/committee/chotatsu_kakaku/pdf/016_01_00.pdf

[13] Agency for Natural Resources and Energy. (2016). Verification of implementing solar heat collectors. *Consideration guidelines for implementation of commercial use solar heat systems*. (In Japanese). Retrieved May 1, 2016 from: http://www.enecho.meti.go.jp/category/ saving_and_new/attaka_eco/reference/

[14] European Comission. (2016). Technical background. *Fuel cells and hydrogen.* Retrieved May 1, 2016 from: http://ec.europa.eu/research/energy/eu/index_en.cfm?pg=research-fch-background

[15] Chang., P. L., Hsu, C.W., Hsiung, C.M. and Lin, C.Y. (2013). Constructing an innovative Bio-Hydrogen Integrated Renewable Energy System. *International Journal of Hydrogen Energy*, 38, 15660-9.

[16] SMUD. (2016). HPWH vs. ERWH (U.S. Government EnergyGuide Labels). Sacramento Municipal Utility District. Retrieved May 1, 2016 from: http://www.smud-heatpumph2o.org/calc.php.

[17] Nakayama, R., Saito, A., Matsumura, E. and Senda, J. (2015). Optimum design for energy supply system based on the minimum life cycle cost in business facility. *Proceedings of the International Conference on Power Engineering-15, Yokohama, Japan*, Paper ID: ICOPE-15-1046. (In Japanese).

[18] EIA. (2016). What drives crude oil prices? *Energy & Financial Markets*. US Energy Information Administration.

[19] METI. (2016). Oil products price survey: Prices for industrial use (diesel/fuel oil A). *Agency for Natural Resources and Energy*. (In Japanese).

[20] METI. (2013). International energy costs comparison. *2012 Annual report regarding energy*. (In Japanese).

[21] Dillich, S., Ramsden, T. and Melaina, M. (2012). Hydrogen Production Cost Using Low-Cost Natural Gas. *DOE Hydrogen and Fuel Cells Program Record*, Record #12024.

[22] Onozaki, M., Watanabe, K., Hashimoto, T., Saegusa, H. and Katayama, Y., Hydrogen production by the partial oxidation and steam reforming of tar from hot coke oven gas. *Fuel*, 85, 143-9.

[23] Kyushu Electric Power Co. Inc. (2016). New tariffs plan, Select night electrification. (In Japanese). Retrieved May 1, 2015. http://www.kyuden.co.jp/menu_new-plan.html

[24] NREL. (2011). Hydrogen Production Cost Estimate Using Biomass Gasification. *National Renewable Energy Laboratory*, NREL/BK-6A10-51726.

[25] Lawrence Berkley National Laboratory. (2015). 2014 Wind Technologies Market Report Highlights. *US Department of Energy*.

[26] METI. (2014). Current situation and problems regarding oil transport. *Agency for Natural Resources and Energy*. (In Japanese).Retrieved May 1, 2015 from: http://www.meti.go.jp/committee/sougouenergy/shigen_nenryo/sekiyu_gas/pdf/005_02_01.pdf

[27] US Energy Information Administration. (2015). *Annual energy outlook 2015.*

[28] Takeshita, T. (2014). Energy and Climate Change. *The Routledge Handbook of Environmental Economics in Asia.* Routledge.

Chapter 8. Conclusions

8.1 Conclusions

For years, the world has pursued the inclusion of renewable energies into the main power share and to this day the goal is far from achieved. One of the main reasons for this is that it is difficult to implement backup power systems that do not depend on fossil fuels, which are needed to stabilize the power output of intermittent renewable energies like solar and wind in different scales. Unless true independent systems are developed, the world is likely to preserve its existing energy supply infrastructures based on combustion of fossil fuels. Although the technology for independent systems is available, the majority of customers are not willing to give up their liberty of purchasing power from the grid at convenience. Furthermore, power supplying companies may not be willing to support the introduction of energy independent systems that will result in market losses. This, among many other issues, makes the problem of energy independence not only a technical one but a social one as well. Therefore it is important to consider semi-energy independent systems as a transition to reduce fossil fuel dependence.

In this thesis, two possible pathways to the implementation of high energy independence systems have been proposed. The first one involves fuel cell and solar PV residential systems that are virtually independent from the grid, but still utilize natural gas as a primary energy source. This system addresses the previously described problems in a way that, the fuel cell is not limited to a certain storage capacity and can produce as much electricity as needed within its rated load, but the system still integrates into the existing natural gas infrastructure and continues to play a role in its market. Since power transmission and generation losses are avoided, the system is able to operate with a substantial reduction in primary energy consumption as well. Because the natural gas infrastructure of accounts for a large portion of the total energy share in many developed countries, residential fuel cell systems are expected to viable choice for high penetration of energy independent systems (in this case, independence from the electrical grid is achieved). The second pathway is the implementation of systems that are not connected to any existing energy infrastructure, but instead create a new market of hydrogen supply, to which existing power companies and fuel providers can easily integrate. Newly constructed residential areas, and existing communities without access to the main power grid such as islands, now have the option to establish their own energy supply systems instead of pursuing integration into the existing infrastructures. Doing so reduces the need of installing costly electric towers and transmission lines that continue to add fluctuations in demand loads to existing power plants, and for isolated areas, it reduces the need for constant shipping of oil products with high price fluctuations that threaten their energy security. Instead, existing power plants may wish to focus on reaching their existing rated capacity with the production of hydrogen to supply the hydrogen micro-grids presented in this study. In the same way, natural gas suppliers can contribute to the total

hydrogen fuel output, while select industries provide low cost fuel generated from waste gases and byproducts at a limited capacity. Since the required hydrogen infrastructure does not exist to this day, isolated hydrogen micro-grids are expected to be a viable choice for low penetration but high performance in regards of cost and energy independence (in this case, independence from the conventional energy infrastructure is completely achieved by the introduction of a new hydrogen fuel market).

The major findings of the present thesis are briefly summarized as follows. In Chapter 3, a residential fuel cell cogeneration system using solar PV and hydrogen storage is proposed as an alternative to common solar PV and rechargeable battery systems. The proposed system achieved nearly 97% independent operation from the power grid, while the alternative system's independence ratio is only 64%. The proposed system also achieved lower primary energy consumption than the alternative system during most of the year. Although initial investments for the fuel cell system were slightly higher, the benefits from higher grid independence are discussed and they are believed to provide an advantage during following years, especially as the prices for fuel cell technologies decrease compared to the already mature technology of rechargeable batteries.

Subsequently, a micro-grid structure for complete grid independence is analyzed in Chapter 5. The micro-grid is designed to fully meet the energy demands of one building in the commercial or public sector, defined as the central facility, and a number of interconnected residences. An optimization model is designed to calculate the capacity of micro-grid components and their daily operation that can minimize primary hydrogen consumption. After addressing areas of improvement in the model and the possible sources of hydrogen supply, a case study in a remote Japanese island is presented in Chapter 7. The results suggest that the proposed micro-grid can operate consistently without energy shortages and with high reductions in primary energy consumption (i.e., hydrogen fuel) with respect to the currently installed energy supply system. Several types and sizes of the central facility were analyzed, and with the exception of small scale office type buildings, all study cases showed promising results. An economic analysis also shows that competitive energy prices and high energy security index values can be achieved depending on the selected sources of hydrogen.

Implementation strategies for the proposed system were discussed as well, although a more focused study in the fields of infrastructure and civil engineering would be needed to identify the limitations and resources needed for actual installation of the proposed systems. The models and analyses presented in this thesis have a mainly technical approach regarding reliable operation and minimization of primary energy consumption. Although basic economic analyses have been presented in this thesis, further research into the economic viability of the proposed systems is strongly suggested.

Publications related to the present study

- **Journal papers**

(1) J. Lamas, H. Shimizu, E. Matsumura, J. Senda, "Fuel consumption analysis of a residential cogeneration system using a solid oxide fuel cell with regulation of heat to power ratio", International Journal of Hydrogen Energy, Vol. 38, pp. 16338-16343, (Oct. 2013).

(2) J. E. Lamas, T. Inui, K. Nakamura, X. Wang, T. Zhang, M. Taketani, N. Nishi et al., "Reconstruction of Syria's Electric Power Infrastructure using Renewable Energies", Global Resource Management, Vol. 1, pp. 111-121, (Mar. 2014).

(3) X. Wang, J. E. Lamas, T. Zhang and K. Nakamura, "Electricity Supply to a Local/Isolated Area by Means of Renewable Energy", Global Resource Management, Vol. 1, pp. 123-131, (Mar. 2014).

(4) J. Lamas, H. Shimizu, S. Nakamura, E. Matsumura, J. Senda, "Study on developing the energy independence of residence with the distributed energy system composed of photovoltaic power generation and fuel cell driven by hydrogen (1st report : Evaluation of energy-saving effect of the system using heat-to-power ratio controllable SOFC)", Transactions of The Japan Society of Mechanical Engineers, Vol. 81, No. 826. Paper 14-00160, (Jun. 2015).

(5) H. Shimizu, J. Lamas, E. Matsumura, J. Senda, "Study on developing the energy independence of residence with the distributed energy system composed of photovoltaic power generation and fuel cell driven by hydrogen (2nd report : Differences in performance of energy saving and cost between methods of electricity storage)", Transactions of The Japan Society of Mechanical Engineers, Vol. 81, No. 826. Paper 14-00164,
(Jun. 2015).

(6) J. Lamas, "Energy supply in isolated areas: an outline of the current situation and the potential of hydrogen technologies for distributed power generation", Global Resource Management, Vol. 2, pp.31-53, (Mar. 2016).

- **Proceedings (Full Paper, peer reviewed)**

(1) J. Lamas, H. Shimizu, E. Matsumura, J. Senda, "Case Study of the Viability of a Residential Combined Heat and Power System using Solar Energy and a Solid Oxide Fuel Cell", Proceedings of The 5th International Workshop of Energy Conversion, pp. 156-160, (Oct. 2013).

(2) J. Lamas, E. Matsumura, J. Senda, "Optimization model for hydrogen fueled micro-grids in isolated areas", Proceedings of the International Conference on Power Engineering-15, Paper ID: ICOPE-15- 1011, (Dec. 2015).

(3) S. Sawaki, J. Lamas, E. Matsumura, J. Senda, "Optimization model for minimizing hydrogen consumption in hydrogen micro-grids for isolated areas", The JSME Kansai Branch AY2014 Graduation Research Presentation Meeting, Paper ID: 11A21, (Mar. 2015).

(4) J. Lamas, E. Matsumura, J. Senda, "Conceptual study on fuel cell and solar energy micro-grid systems for energy supply in japanese islands", Proceedings of The 6th International Workshop of Energy Conversion, pp. 45-53, (Mar. 2016).

- **Oral presentations**

(1) J. Lamas, H. Shimizu, E. Matsumura, J. Senda, “Case Study of the Viability of a Residential Combined Heat and Power System using Solar Energy and a Solid Oxide Fuel Cell”, The 5th International Workshop of Energy Conversion, (Nov. 2013)

(2) J. E. Lamas, T. Inui, K. Nakamura, X. Wang, T. Zhang, M. Taketani, N. Nishi et al., “Reconstruction of Syrian Electric Power Infrastructures by Renewable Energies”, International Workshop on Renewable Energy, (Oct. 2013)

(3) X. Wang, J. E. Lamas, T. Zhang and K. Nakamura, “Electricity Supply to a Local/Isolated Area by Means of Renewable Energy”, International Workshop on Renewable Energy, (Oct. 2013)

(4) J. Lamas, H. Shimizu, E. Matsumura, J. Senda, “Effect of subsidies on energy cost for residential heat and power cogeneration systems in the Kansai region, Japan” , Biennial Conference on Sustainable Business, Energy and Development in Asia, (Mar. 2014).

(5) J. Lamas, H. Shimizu, E. Matsumura, J. Senda, “Performance Analysis of a Residential Heat and Power Cogeneration System Using Solar Energy and a Fuel Cell”, International Conference of PM2.5 & Energy Security, (Mar. 2014).

(6) S. Sawaki, J. Lamas, E. Matsumura, J. Senda, “Optimization model for minimizing hydrogen consumption in hydrogen micro-grids for isolated areas”, The JSME Kansai Branch AY2014 Graduation Research Presentation Meeting, (Mar. 2015).

(7) J. Lamas, E. Matsumura, J. Senda, “Conceptual Study on Combined PV and Fuel Cell Systems for Co-generation Applications in Isolated Areas Using Hydrogen Fuel”, The 9th Doshisha University-Chonnam National University Joint Symposium, (Nov. 2015).

(8) J. Lamas, E. Matsumura, J. Senda, “Optimization model for hydrogen fueled micro-grids in isolated areas”, International Conference on Power Engineering-15, (Dec. 2015).

(9) J. Lamas, E. Matsumura, J. Senda, “Conceptual study on fuel cell and solar energy micro-grid systems for energy supply in japanese islands”, The 6th International Workshop of Energy Conversion, (Mar. 2016).

(10) J. Lamas, E. Matsumura, J. Senda, “Strengthening the energy security of Japanese islands through hydrogen infrastructure”, Institute for Technology, Enterprise and Competitiveness Workshop 2016, (Mar. 2016).

Acknowledgements

I would like to show my most sincere thanks to Professor Jiro Senda and Professor Eriko Matsumura from the Mechanical Engineering Department in Doshisha University, as well as Professor Emeritus Hajime Fujimoto, for their valuable guidance and constant patience that led to the finalization of this research.

I would also like to show my infinite gratitude to the Japanese Ministry of Education, Culture, Science and Technology for their generosity in granting me the scholarship to perform my studies in Japan, for without it

Also, I would like to thank everyone that closely collaborated in this study, especially Hirotoshi Shimizu, Minoru Hanasaki, Ryo Nakayama, Shinsuke Sawaki, as well as other alumni with whom I began my studies. Also, I want to show my appreciation to Horiba, Ltd., for accepting me into their internship program and helping me shape my career.

Additionally, I would like to thank all the Professors and staff at Doshisha University's Global Resource Management Program. It was because their guidance and support that led me to take the approach in this thesis. In particular, I want to thank Professor Emeritus Akihiro Ametani, and Professors Motoi Wada and Masanori Naito for creating the self motivating environment of the program. I also want to thank Professor Nathaniel Agola for willing to discuss my ideas and helping me see beyond the pure technical aspect into the actual value for society that this research can bring. Also, I want to thank my colleagues in the Global Resource Management Program for their constant inspiration and support.

Lastly, I want to give my infinite gratitude to my parents and family, for their immeasurable support and encouragement even through my studies abroad, and most importantly, to Kayo Tokiwa, for her constant and unconditional support, love and encouragement.

May 19, 2016

Jorge Eduardo Lamas De Anda

APPENDIX A. Micro-grid optimization program modeled in GAMS

```
*The demand data are prepared to be imported from a file called Microgrid_Input_Data.xlsx.
*File should have 3 sheets called: Residential demands, Facility demands, and Solar irradiation
*The scalar values and variable bounds written in this text should be adjusted as needed

$onecho > Data_in.txt
par=IRR             rng=Irradiation!C3 Rdim=1 Cdim=1
par=R_DEM_E         rng=Residence!C3 Rdim=1 Cdim=1
par=R_DEM_W         rng=Residence!Q3 Rdim=1 Cdim=1

*IMPORTANT: data should be for a 1000m2 facility
par=F_DEM_E         rng=Facility!C3 Rdim=1 Cdim=1
par=F_DEM_H         rng=Facility!Q3 Rdim=1 Cdim=1
par=F_DEM_C         rng=Facility!AE3 Rdim=1 Cdim=1
par=F_DEM_W         rng=Facility!AS3 Rdim=1 Cdim=1
par=KC_PV           rng=Irradiation!Q3 Rdim=1

$offecho
$call GDXXRW Microgrid_Input_Data.xlsx @Data_in.txt
$gdxin Microgrid_Input_Data.gdx


**Hours in 1 ~ 7 days: 24, 48, 72, 96, 120, 144, 168

SETS
     h          Hours per month /1*24/
     ht         Set of hours to calculate tank charge /2*24/
     m          Months  /Jan, Feb, Mar, Apr, May, Jun, Jul, Aug, Sep, Oct, Nov, Dec/;

PARAMETERS
     IRR(*,*)           Annual hourly irradiation for h-m
     R_DEM_E(*,*)       Residential electric demand for h
     R_DEM_W(*,*)       Residential hot water demand for h
     F_DEM_E(*,*)       Facility electric demand for h
     F_DEM_H(*,*)       Facility heat demand for h
     F_DEM_C(*,*)       Facility cooling demand for h
     F_DEM_W(*,*)       Facility hot water demand for h
     KC_PV(*)           Correction factor for photovoltaics

$load  IRR R_DEM_E R_DEM_W F_DEM_E F_DEM_H F_DEM_C F_DEM_W KC_PV

SCALARS
     A_ROOF             Total roof area of the residence [m2] /25/
     ELZ_EFF            Electrolyzer efficiency /0.8/
     ELZ_CAP            Electrolyzer capacity [kWh] /150/
     H2_TK_EFF          Efficiency of hydrogen storage /0.9/
     ACH_EFF            Absorption chiller efficiency /1.45/
     ACH_CAP            Absorption chiller capacity /350/
     APF                Annual performance factor for heating&cooling /5.9/
     HEX_EFF            Heat exchanger efficiency for the fuel cells /0.9/
     HPHW_EFF           Heat pump hot water heater efficiency /2.2/
     BOILER_EFF         Efficiency of boiler in conventional systems /0.8/
     DG_EFF             Diesel generator efficiency in conventional system /0.35/
```

*Residential hot water tank

HW_TK_EFF	Hot water tank decay rate /0.01/
H_outeff	Heat storage discharge efficiency /1/
H_ineff	Heat storage charge efficiency /0.9/
RHW_max_in	Heat storage max charge rate /0.25/
RHW_max_out	Heat storage max discharge rate /0.25/
RHW_Size	Heat storage capacity /20/

*Solar PV and HC constants

KD_PV	Power density of photovoltaics [kW m-2] /0.14/
KD_HC	Energy density of heat collectors [-] /0.44/
SOFC_EFF_E	Efficiency is scalar because SOFC operates constantly /0.45/
SOFC_EFF_H	Efficiency is scalar because SOFC operates constantly /0.40/
PEFC_EFF_E	Taken as constant in this case /0.35/
PEFC_EFF_H	Taken as constant in this case /0.55/

*Define facility size and N_RES
*Add or remove N_RES and FAC_SIZE if it is variable (there are 6 lines)

FAC_SIZE	for a constant facility size of /5000/;
* N_RES	for a number of residences of /150/;

VARIABLES
*scalars
*Add or remove N_RES and FAC_SIZE if it is variable (2/6)

N_RES	Total number of residences in the grid
A_PV	Roof area covered by photovoltaics
A_HC	Roof area covered by heat collectors
SOFC_SIZE	Maximum capacity of the solid oxide fuel cell
PEFC_SIZE	Maximum capacity of the polymer electrolyte fuel cell
CONV_SUM	Energy consumption of sums of conv minus grid

*Vectors

W_PV(h,m)	Phtovoltaics output
Q_HC(*,m)	Heat collectors output
TE_DEM(h,m)	Total electric demand

*Residential hot water tank

RHW_TK(*,m)	Residential hot water tank charge
HPHW_OUT(*,m)	Residential heat pump hot water heater output
HPHW_W(h,m)	Residential heat pump hot water heater input
H_PROV(h,m)	Heat provided by the system
H_fromTK(h,m)	Heat to be obtained from the tank
H_OUT(*,m)	Heat removed from the tank
H_IN(*,m)	Heat input into the tank
H_Loss(*,m)	Heat losses
H_forTK(h,m)	Heat to be stored into the tank
H_consumed(h,m)	Sum of demand and heat to be stored into the tank

*Fuel cells

W_PEFC(h,m)	PEFC variable output
V_SOFC(h,m)	Amount of fuel used by the SOFC
V_PEFC(h,m)	Amount of fuel used by the PEFC
PEFC_SW(h,m)	PEFC On-Off switch
QR_SOFC(h,m)	SOFC heat recovery
QR_PEFC(h,m)	PEFC heat recovery
QR_FC(h,m)	Total heat recovered from Fuel cells

*Facility heat demands

FHW_OUT(h,m)	Facility hourly hot water output
ACH_OUT(h,m)	Absorption chiller output
FAC_OUT(h,m)	Facility air conditioning output
EXH(h,m)	FC heat exhaust not used for ACH nor FHW
HP_OUT(h,m)	Shortage in air conditioning supplied by a Heat Pump
HP_W(h,m)	Energy needed by the Heat Pump

*Surplus energy

W_GRID(h,m)	Total power in grid
W_SUR(h,m)	Electricity surplus
V_H2(h,m)	Amount of hydrogen generated by the electrolyzer
CONV_Q(h,m)	Conventional system's total energy consumption
GAS(h,m)	Energy needed from gas
DIESEL(h,m)	Energy needed from diesel

*Objective variables

H2_BOUGHT	Hourly amount of hydrogen that needs to be imported
FSR	Total amount of hydrogen that needs to be imported;

POSITIVE VARIABLES

*Add or remove N_RES and FAC_SIZE if it is variable (3/6)

N_RES,A_PV,A_HC,SOFC_SIZE,PEFC_SIZE,W_PV(h,m),Q_HC(*,m),TE_DEM(h,m),
RHW_TK(*,m),HPHW_OUT(*,m),HPHW_W(h,m),H_PROV(h,m),H_fromTK(h,m),
H_OUT(*,m),H_IN(*,m),H_Loss(*,m),H_forTK(h,m),H_consumed(h,m),
W_PEFC(h,m),V_SOFC(h,m),V_PEFC(h,m),
QR_SOFC(h,m),QR_PEFC(h,m),QR_FC(h,m),FHW_OUT(h,m),ACH_OUT(h,m),EXH(h,m),
FAC_OUT(h,m),HP_OUT(h,m),HP_W(h,m),W_GRID(h,m),W_SUR(h,m),V_H2(h,m),
CONV_SUM,CONV_Q(h,m),GAS(h,m),DIESEL(h,m);

FREE VARIABLES

H2_BOUGHT;

BINARY VARIABLES

PEFC_SW(h,m);

EQUATIONS

TOTAL_CONV(h,m)	Total energy consumption for the conventional grid
AREA_RST	Roof area restriction for PV and HC
PV_CALC(h,m)	Calculation of PV output
HC_CALC(h,m)	Calculation of HC output
RHW_SUP(h,m)	Residential hot water supply
RHW_REM(ht,m)	Residential hot water remaining
H_available(h,m)	Heat supplied by the system
H_balance(h,m)	Heat supplied is equal to heat consumed
H_TKsupply(h,m)	Heat that is obtained from the tank
H_totank(h,m)	Heat that goes into the tank
H_decay(ht,m)	Heat losses from the tank
H_MaxIn(ht,m)	Max charge rate
H_MaxOut(h,m)	Max discharge rate
HPHW_ELEC(h,m)	Electricity needed for the Heat Pump Water Heater
SUM_E_DEM(h,m)	Sum of electric demands
FC_SIZING	The sum of both fuel cells is higher than the demand
PEFC_CAP(h,m)	PEFC output is lower than its capacity
PEFC_MIN(h,m)	PEFC output is at least 15% of its rated load

PEFC_OUT(h,m) Calculate the current output of the PEFC
SOFC_FUEL(h,m) Calculate fuel used by SOFC
PEFC_FUEL(h,m) Calculate fuel used by PEFC

SOFC_HREC(h,m) Calculate heat recovered by SOFC
PEFC_HREC(h,m) Calculate heat recovered by PEFC
SUM_HREC(h,m) Total heat recovered

FC_HREC_SUP(h,m) Facility heat recovery supply (hot water and ACH)
FHW_SUP(h,m) Facility how water supply

FAC_SUP(h,m) Facility air conditioning supply
FC_TO_ACH(h,m) Calculate the heat available for the Absorption chiller
ACH_MAX(h,m) Absorption chiller output must not exceed its capacity
HP_ELEC(h,m) Calculate the electricity needed from the Aux Heat Pump

E_DEM_RST(h,m) Electric output must be higher than demand
SURP_TO_ELZ(h,m) Surplus electricity to be used in the electrolyzer
H2_LIM(h,m) Limit h2 output to electrolyzer capacity
H2_PROD(h,m) Calculate the generated hydrogen
H2_SUP(h,m) Hydrogen supplied to the fuel cells

SUM_ADD sum of conventional system's energy consumption

GAS_ONLY(h,m) Energy needed from gas
DIESEL_ONLY(h,m) Energy needed from diesel

H2_IMPORT Into objective function: total hydrogen that must be imported;

```
*conventional system energy consumption
TOTAL_CONV(h,m).. CONV_Q(h,m) =e=
    (F_DEM_W(h,m)/BOILER_EFF+(F_DEM_E(h,m)+(F_DEM_H(h,m)+F_DEM_C(h,m))/APF)/
    DG_EFF)*FAC_SIZE/1000+(R_DEM_E(h,m)/DG_EFF+R_DEM_W(h,m)/BOILER_EFF)*N_R
    ES;
GAS_ONLY(h,m).. GAS(h,m) =e= (F_DEM_W(h,m)/BOILER_EFF)*FAC_SIZE/1000 +
    (R_DEM_W(h,m)/BOILER_EFF)*N_RES;
DIESEL_ONLY(h,m).. DIESEL(h,m) =e=
    ((F_DEM_E(h,m)+(F_DEM_H(h,m)+F_DEM_C(h,m))/APF)/DG_EFF)*FAC_SIZE/1000 +
    (R_DEM_E(h,m)/DG_EFF)*N_RES;

*Solar power output
AREA_RST.. A_PV+A_HC =l= A_ROOF;
PV_CALC(h,m).. W_PV(h,m) =e= KC_PV(m)*KD_PV*A_PV*IRR(h,m);
HC_CALC(h,m).. Q_HC(h,m) =e= KD_HC*A_HC*IRR(h,m);

*Total electric demand
SUM_E_DEM(h,m).. TE_DEM(h,m) =e=
    (R_DEM_E(h,m)+HPHW_W(h,m))*N_RES+F_DEM_E(h,m)*FAC_SIZE/1000+HP_W(h,m);
FC_SIZING(h,m).. SOFC_SIZE+PEFC_SIZE =g= TE_DEM(h,m);
PEFC_CAP(h,m).. W_PEFC(h,m) =l= PEFC_SIZE;
```

```
*PEFC part load operation limited to 30%
PEFC_MIN(h,m)..      W_PEFC(h,m)    =g=  PEFC_SIZE*0.3;
PEFC_OUT(h,m)..      W_PEFC(h,m)*PEFC_SW(h,m)  =g=  TE_DEM(h,m)-SOFC_SIZE-
    W_PV(h,m)*N_RES;
SOFC_FUEL(h,m)..     V_SOFC(h,m)    =e=  SOFC_SIZE/SOFC_EFF_E;
PEFC_FUEL(h,m)..     V_PEFC(h,m)    =e=  (W_PEFC(h,m)/PEFC_EFF_E)*PEFC_SW(h,m);

*Residential hot water demand
RHW_SUP(h,m)..       H_PROV(h,m)    =e=  Q_HC(h,m)+HPHW_OUT(h,m)+H_fromTK(h,m);
RHW_REM(ht,m)..      RHW_TK(ht,m)   =e=  RHW_TK(ht-1,m)+H_IN(ht,m)-H_OUT(ht,m)-
    H_Loss(ht,m);
H_available(h,m)..   H_consumed(h,m) =e=  R_DEM_W(h,m)+H_forTK(h,m);
H_balance(h,m)..     H_consumed(h,m) =e=  H_PROV(h,m);
H_TKsupply(h,m)..    H_fromTK(h,m)  =e=  H_OUT(h,m)*H_outeff;
H_totank(h,m)..      H_IN(h,m)      =e=  H_forTK(h,m)*H_ineff;
H_decay(ht,m)..      H_Loss(ht,m)   =e=  RHW_TK(ht-1,m)*HW_TK_EFF;
H_MaxIn(ht,m)..      RHW_TK(ht,m)   =l=  RHW_TK(ht-1,m)+ RHW_Size*RHW_max_in;
H_MaxOut(h,m)..      H_OUT(h,m)     =l=  RHW_Size*RHW_max_out;
HPHW_ELEC(h,m)..     HPHW_W(h,m)    =e=  HPHW_OUT(h,m)/HPHW_EFF;

*SOFC heat recovery
SOFC_HREC(h,m)..     QR_SOFC(h,m)   =e=  V_SOFC(h,m)*SOFC_EFF_H;
PEFC_HREC(h,m)..     QR_PEFC(h,m)   =e=  V_PEFC(h,m)*PEFC_EFF_H;
SUM_HREC(h,m)..      QR_FC(h,m)     =e=  (QR_SOFC(h,m)+QR_PEFC(h,m))*HEX_EFF;

*Facility hot water demand
FHW_SUP(h,m)..       FHW_OUT(h,m)   =e=  F_DEM_W(h,m)*FAC_SIZE/1000;
FC_HREC_SUP(h,m).. QR_FC(h,m)     =e=  FHW_OUT(h,m)+ACH_OUT(h,m)+EXH(h,m);

*Facility air conditioning demand
FAC_SUP(h,m)..       FAC_OUT(h,m)   =e=
    (F_DEM_H(h,m)+F_DEM_C(h,m))*FAC_SIZE/1000;
FC_TO_ACH(h,m)..     FAC_OUT(h,m)   =e=  ACH_OUT(h,m)*ACH_EFF+HP_OUT(h,m);
ACH_MAX(h,m)..       ACH_OUT(h,m)   =l=  ACH_CAP/ACH_EFF;
HP_ELEC(h,m)..       HP_W(h,m)      =e=  HP_OUT(h,m)/APF;

*Hydrogen production
E_DEM_RST(h,m)..     W_GRID(h,m)    =e=
    SOFC_SIZE+W_PEFC(h,m)*PEFC_SW(h,m)+W_PV(h,m)*N_RES;
SURP_TO_ELZ(h,m).. W_GRID(h,m)    =e=  TE_DEM(h,m)+W_SUR(h,m);
H2_LIM(h,m)..        W_SUR(h,m)     =l=  ELZ_CAP;
H2_PROD(h,m)..       V_H2(h,m)      =e=  W_SUR(h,m)*ELZ_EFF*H2_TK_EFF;
H2_SUP(h,m)..        H2_BOUGHT(h,m) =e=  V_SOFC(h,m)+V_PEFC(h,m)-V_H2(h,m);
SUM_ADD..            CONV_SUM       =e=  sum((h,m),CONV_Q(h,m))-
    sum((h,m),H2_BOUGHT(h,m));

*Bounds are set
*Add or remove N_RES.L and FAC_SIZE.L if it is variable (4/6)
N_RES.lo  =    10;
N_RES.up  =    500;
A_PV.up   =    25;
A_HC.up   =    25;
RHW_TK.lo(h,m) =    0.1;
*Tank capacity 300 L at 80 C
RHW_TK.up(h,m) =    20;
```

```
HPHW_OUT.up(h,m)= 1.5;
SOFC_SIZE.up =    200;
PEFC_SIZE.up =    400;

*Objective function
H2_IMPORT..       FSR   =e=   CONV_SUM/sum((h,m),CONV_Q(h,m));

Model Isolated_Grid_FSR /all/;

Isolated_Grid_FSR.workspace = 3000;

Option MINLP = BARON;
$onecho > baron.opt
LPSol 3 # select  CPLEX as the LP solver
NLPSol 2 # select MINOS as the NLP solver
MaxTime  259200
EpsA 1e+1
EpsR 1e-1
$offecho

Option NLP = MINOS;
$onecho > minos.opt
Linsearch tolerance 0.1
Pivot Tolerance 1e-11
$offecho

Option LP = CPLEX;
$onecho > cplex.opt
advind =1
epmrk = 0.1
writelp
writemps
writemst
writeord
writeparam
quality = yes
simdisplay = 1
$offecho

option Bratio = 1;
option SysOut = on;

Isolated_Grid_FSR.OptFile = 1;

Solve Isolated_Grid_FSR using MINLP maximizing FSR;

*Add or remove N_RES.L and FAC_SIZE.L if it is variable (5/6)
execute_unload "Isolated_Grid_FSR.gdx" N_RES.L,A_PV.L, A_HC.L,
            SOFC_SIZE.L, PEFC_SIZE.L,
            TE_DEM.L, W_GRID.L, W_PV.L, W_PEFC.L,
            Q_HC.L, RHW_TK.L, FHW_OUT.L, HPHW_W.L, H_IN.L, CONV_SUM.L,
            ACH_OUT.L, HP_OUT.L, PEFC_SW.L,
            W_SUR.L, V_SOFC.L, V_PEFC.L,
            FSR.L, H2_BOUGHT.L, CONV_Q.L, GAS.L, DIESEL.L;
```

```
*******************************************
*Results are exported to EXCEL using 'execute'
*Add or remove N_RES and FAC_SIZE if it is variable (6/6)
execute  'gdxxrw.exe Isolated_Grid_FSR.gdx Squeeze = N o=Isolated_Grid_FSR.xlsx var=N_RES.L
     rng=Sheet1!B1';
execute  'gdxxrw.exe Isolated_Grid_FSR.gdx Squeeze = N o=Isolated_Grid_FSR.xlsx var=A_PV.L
     rng=Sheet1!B2';
execute  'gdxxrw.exe Isolated_Grid_FSR.gdx Squeeze = N o=Isolated_Grid_FSR.xlsx var=A_HC.L
     rng=Sheet1!B3';
execute  'gdxxrw.exe Isolated_Grid_FSR.gdx Squeeze = N o=Isolated_Grid_FSR.xlsx
     var=SOFC_SIZE.L rng=Sheet1!B5';
execute  'gdxxrw.exe Isolated_Grid_FSR.gdx Squeeze = N o=Isolated_Grid_FSR.xlsx
     var=PEFC_SIZE.L rng=Sheet1!B6';
*execute  'gdxxrw.exe Isolated_Grid_FSR.gdx Squeeze = N o=Isolated_Grid_FSR.xlsx
     var=FAC_SIZE.L rng=Sheet1!B7';
execute  'gdxxrw.exe Isolated_Grid_FSR.gdx Squeeze = N o=Isolated_Grid_FSR.xlsx var=FSR.L
     rng=Sheet1!B8';

execute  'gdxxrw.exe Isolated_Grid_FSR.gdx Squeeze = N o=Isolated_Grid_FSR.xlsx
     var=H2_BOUGHT.L rng=Sheet1!A13';
execute  'gdxxrw.exe Isolated_Grid_FSR.gdx Squeeze = N o=Isolated_Grid_FSR.xlsx
     var=CONV_Q.L rng=Sheet1!A186';
execute  'gdxxrw.exe Isolated_Grid_FSR.gdx Squeeze = N o=Isolated_Grid_FSR.xlsx var=GAS.L
     rng=Sheet1!A216';
execute  'gdxxrw.exe Isolated_Grid_FSR.gdx Squeeze = N o=Isolated_Grid_FSR.xlsx var=DIESEL.L
     rng=Sheet1!A246';

execute  'gdxxrw.exe Isolated_Grid_FSR.gdx Squeeze = N o=Isolated_Grid_FSR.xlsx
     var=TE_DEM.L rng=Sheet2!C3';
execute  'gdxxrw.exe Isolated_Grid_FSR.gdx Squeeze = N o=Isolated_Grid_FSR.xlsx
     var=W_GRID.L rng=Sheet2!C176';
execute  'gdxxrw.exe Isolated_Grid_FSR.gdx Squeeze = N o=Isolated_Grid_FSR.xlsx var=W_PV.L
     rng=Sheet2!C349';
execute  'gdxxrw.exe Isolated_Grid_FSR.gdx Squeeze = N o=Isolated_Grid_FSR.xlsx
     var=W_PEFC.L rng=Sheet2!C522';

execute  'gdxxrw.exe Isolated_Grid_FSR.gdx Squeeze = N o=Isolated_Grid_FSR.xlsx var=Q_HC.L
     rng=Sheet3!C3';
execute  'gdxxrw.exe Isolated_Grid_FSR.gdx Squeeze = N o=Isolated_Grid_FSR.xlsx
     var=RHW_TK.L rng=Sheet3!C176';
execute  'gdxxrw.exe Isolated_Grid_FSR.gdx Squeeze = N o=Isolated_Grid_FSR.xlsx
     var=FHW_OUT.L rng=Sheet3!C349';
execute  'gdxxrw.exe Isolated_Grid_FSR.gdx Squeeze = N o=Isolated_Grid_FSR.xlsx
     var=HPHW_W.L rng=Sheet3!C522';
execute  'gdxxrw.exe Isolated_Grid_FSR.gdx Squeeze = N o=Isolated_Grid_FSR.xlsx var=H_IN.L
     rng=Sheet3!C695';

execute  'gdxxrw.exe Isolated_Grid_FSR.gdx Squeeze = N o=Isolated_Grid_FSR.xlsx
     var=ACH_OUT.L rng=Sheet4!C3';
execute  'gdxxrw.exe Isolated_Grid_FSR.gdx Squeeze = N o=Isolated_Grid_FSR.xlsx
     var=HP_OUT.L rng=Sheet4!C176';
execute  'gdxxrw.exe Isolated_Grid_FSR.gdx Squeeze = N o=Isolated_Grid_FSR.xlsx
     var=PEFC_SW.L rng=Sheet4!C349';
```

```
execute  'gdxxrw.exe Isolated_Grid_FSR.gdx Squeeze = N o=Isolated_Grid_FSR.xlsx var=W_SUR.L
     rng=Sheet5!C3';
execute  'gdxxrw.exe Isolated_Grid_FSR.gdx Squeeze = N o=Isolated_Grid_FSR.xlsx
     var=V_SOFC.L rng=Sheet5!C176';
execute  'gdxxrw.exe Isolated_Grid_FSR.gdx Squeeze = N o=Isolated_Grid_FSR.xlsx
     var=V_PEFC.L rng=Sheet5!C349';

*Format the excel sheet to explain each variable
$onecho > File_Header_IG.txt
text="Number of houses" rng=Sheet1!a1
text="Area of Photovoltaics" rng=Sheet1!a2
text="Area of Heat collectors" rng=Sheet1!a3
text="SOFC size" rng=Sheet1!a5
text="PEFC size" rng=Sheet1!a6
text="Facility size" rng=Sheet1!a7
text="FSR" rng=Sheet1!a8
text="Hourly H2 Bought" rng=Sheet1!a12
text="Conventional Energy bought" rng=Sheet1!a185
text="Energy needed from gas" rng=Sheet1!a215
text="Energy needed from diesel" rng=Sheet1!a245

text="Total electric demand" rng=Sheet2!c1
text="Electricity in grid" rng=Sheet2!c174
text="Electricity from photovoltaics" rng=Sheet2!c347
text="Calculated PEFC output" rng=Sheet2!c520

text="Hot Water from heat collectors" rng=Sheet3!c1
text="Hot Water in residential tank" rng=Sheet3!c174
text="Hot Water from fuel cells" rng=Sheet3!c347
text="Electricity needed from Heat Pump Water Heater" rng=Sheet3!c520
text="Hot Water into the tank" rng=Sheet3!c693

text="Output from Absorption chiller" rng=Sheet4!c1
text="Output from Heat Pump" rng=Sheet4!c174
text="PEFC switch" rng=Sheet4!c347
text="PEFC_SW*PEFC_W" rng=Sheet4!c520

text="Surplus electricity" rng=Sheet5!c1
text="SOFC Fuel consumption" rng=Sheet5!c174
text="PEFC Fuel consumption" rng=Sheet5!c347

*****************************************
$offecho
execute 'gdxxrw.exe Isolated_Grid_FSR.gdx o=Isolated_Grid_FSR.xlsx @File_Header_IG.txt';

*Output file with results will be called Isolated_Grid_FSR.xlsx
```